VARIANCE ESTIMATION IN MULTISENSOR FUSION ALGORITHM

Zhong Chong-quan, Dong Xi-lu, Zhang Li-yong, Cao Yang

School of Electronics and Information Engineering,
Dalian University of Technology, Dalian 116024, China

Abstract: In weighted fusion algorithm for multisensor, the weights are only determined by noise variance and the precision of the variance estimation will affect the performance of the fusion algorithm. An approach of variance estimation for multisensor is presented and proves unbiased in this paper. The recurrence formula for the algorithm is also proposed, and moreover, there is no need for initial values, for which the approach is adaptive and can be used in real-time estimation. A numerical example is given to show the usefulness of the approach.

Keywords: multisensor integration, data fusion, variance, estimation theory, Gaussian noise.

1. INTRODUCTION

Modern industry adopts a great variety of sensors to monitor and control production in order to obtain a satisfactory control performance of the industrial process (Yang and Yuzo, 2000), and thus some appropriate methods are required. Multisensor data fusion is defined as the process of integrating information from multiple sources to produce the most specific and comprehensive unified data about an entity, activity or event (Raol and Girija, 2002). The process is supposed to achieve improved accuracy and more specific inferences than could be achieved by the use of a single sensor alone. In the field of measurement, weighted fusion algorithm is widely used for multisensor fusion process. The weight of each sensor is determined only by its own variance (Ling, et al., 2000; Yifeng and Leung, 1997). The precision of the variance estimation will affect the performance of the fusion algorithm seriously and the accuracy of the fusing results as well.

The variance of sensor is determined by both internal noise and environmental interference. Most of the

variance estimation methods used in weighted fusion algorithm are based on experience or the sensor's variance parameter and the environmental noise is not included in consideration, which results in the distortion of the variance and the imprecision of the fusing results (Zhong, et al., 2002).

An algorithm of variance estimation for multisensor is presented and proves unbiased in this paper. No *a priori* information about each sensor and environment noise is needed in this algorithm and the real-time variance estimation can be achieved only by the observations of sensors. Simulated data given in this paper indicate the usefulness of the algorithm.

2. WEIGHTED FUSION ALGORITHM FOR MULTISENSOR

The observation of state can be modeled by using the linear system (Zhong, et al., 2002):

$$Y = Hx + e \tag{1}$$

where Y is the (n, 1) observation vector with $Y = [y_1 \quad y_2 \quad \cdots \quad y_n]^T$, x is the (1, 1) state, H is a known (n, 1) vector with $H = [1 \quad 1 \quad \cdots \quad 1]^T$, and e is the (n, 1) vector of measurement error (noise, including internal and environmental) with $e = [e_1 \quad e_2 \quad \cdots \quad e_n]^T$, a zero-mean Gaussian white noise sequence and independent of each other. It is also assumed that the noise sequence is a stationary process with ergodic property. Therefore,

$$E(e_i) = E(y_i - x) = 0$$

$$i = 1,2,\cdots,n \tag{2}$$

$$E(e_i^2) = E[(y_i - x)^2] = R_i$$

$$i = 1,2,\cdots,n \tag{3}$$

where $E(\cdot)$ is the expected value operator, and R_i denotes the noise variance of sensor i. According to the result (Gao, et al., 1999; Yifeng and Leung, 1997), The estimate of the state is:

$$\hat{x} = (H^T W^{-1} H)^{-1} H^T W^{-1} Y = \frac{\sum_{i=1}^{n} \frac{y_i}{R_i}}{\sum_{i=1}^{n} \frac{1}{R_i}} \tag{4}$$

The state estimation variance (Ling, et al., 2000) is

$$E[(x - \hat{x})^2] = \frac{1}{\sum_{i=1}^{n} \frac{1}{R_i}} \tag{5}$$

From the foregoing, it can be seen that the weight of each sensor is determined only by its own variance. The accuracy of the results obtained from data fusion process will be determined by the precision of the variance estimation directly.

3. VARIANCE ESTIMATION FOR MULTISENSOR

The mean of measurements from n sensors is:

$$\bar{y} = \frac{1}{n} \sum_{k=1}^{n} y_k \tag{6}$$

where $\bar{y}$ is the unbiased estimation of x obviously. From (3), the variance of sensor j is:

$$R_j = D(y_j - x) = E[(y_j - x)^2]$$

$$j = 1,2,\cdots,n \tag{7}$$

where $D(\cdot)$ is the variance operator. In fact, it is impossible to obtain the actual state x. Here let $\bar{y}$, the unbiased estimation of x, replace x in form, then the following form can be obtained:

$$E(y_j - \bar{y}) = 0 \tag{8}$$

$$R_j' = D(y_j - \bar{y}) = D\left(y_j - \frac{1}{n} \sum_{k=1}^{n} y_k \right)$$

$$= D\left[\frac{(n-1) y_j - \sum_{\substack{k=1 \\ k \neq j}}^{n} y_k}{n} \right]$$

$$= D\left[\frac{(n-1)e_j - \sum_{\substack{k=1 \\ k\neq j}}^{n} e_k}{n}\right]$$

$$= \frac{(n-1)^2}{n^2} R_j + \frac{1}{n^2}\sum_{\substack{k=1 \\ k\neq j}}^{n} R_k$$

$$j = 1,2,\cdots,n \tag{9}$$

R'_j denotes the variance of the difference between the measurement from sensor j and the mean of the measurements from n sensors. The relation between R'_j and R_k （$k = 1,2,\cdots,n$）is given in （9）. Sum up R'_j （$j = 1,2,\cdots,n$）:

$$\sum_{j=1}^{n} R'_j = \sum_{j=1}^{n}\left[\frac{(n-1)^2}{n^2} R_j\right] + \sum_{j=1}^{n}\left(\frac{1}{n^2}\sum_{\substack{k=1 \\ k\neq j}}^{n} R_k\right)$$

$$= \frac{(n-1)^2}{n^2}\sum_{j=1}^{n} R_j + \frac{n-1}{n^2}\sum_{j=1}^{n} R_j$$

$$= \frac{n-1}{n}\sum_{j=1}^{n} R_j \tag{10}$$

According to (9) and (10), the following form of the variance of sensor j is obtained:

$$R_j = \frac{n}{n-2}\left[R'_j - \frac{1}{n(n-1)}\sum_{k=1}^{n} R'_k\right] \tag{11}$$

Considering the condition of measuring N times by using n sensors, y_{ij} is the i-th measurement from sensor j and e_{ij} is the error. Based on the ergodic property of stochastic process，incorporation of (8) and (9) gives the estimation of R'_j:

$$\hat{R}'_j = \frac{1}{N}\sum_{i=1}^{N}(y_{ij} - \bar{y}_i)^2$$

$$= \frac{1}{N}\sum_{i=1}^{N}\left(y_{ij} - \frac{1}{n}\sum_{k=1}^{n} y_{ik}\right)^2 \tag{12}$$

By using (11), the variance estimation of sensor j is:

$$\hat{R}_j = \frac{n}{n-2}\left[\hat{R}'_j - \frac{1}{n(n-1)}\sum_{k=1}^{n}\hat{R}'_k\right] \tag{13}$$

What should be given attention to is that the foregoing algorithm is invalid when measuring with only two sensors because of the lack of the redundant information. The method of variance estimation is applicable when the number of sensors is larger than 2.

4. THE UNBIAS OF VARIANCE ESTIMATION

Based on the assumption of noise and (12), the following equation is obtained:

$$E(\hat{R}'_j) = E\left[\frac{1}{N}\sum_{i=1}^{N}\left(y_{ij} - \frac{1}{n}\sum_{k=1}^{n} y_{ik}\right)^2\right]$$

$$= \frac{1}{N}\sum_{i=1}^{N} E\left(y_{ij} - \frac{1}{n}\sum_{k=1}^{n} y_{ik}\right)^2$$

$$= \frac{1}{Nn^2}\sum_{i=1}^{N} E\left(\sum_{k=1}^{n}(y_{ij} - y_{ik})\right)^2$$

$$= \frac{1}{Nn^2}\sum_{i=1}^{N}\left\{\sum_{k=1}^{n}\sum_{m=1}^{n} E[(y_{ij} - y_{ik})(y_{ij} - y_{im})]\right\}$$

$$= \frac{1}{Nn^2}\sum_{i=1}^{N}\left\{\sum_{k=1}^{n}\sum_{m=1}^{n} E[(e_{ij} - e_{ik})(e_{ij} - e_{im})]\right\}$$

$$= \frac{1}{Nn^2}\sum_{i=1}^{N}[(n-1)^2 \cdot R_j + \sum_{\substack{k=1 \\ k\neq j}}^{n} R_k]$$

$$= \frac{(n-1)^2}{n^2} R_j + \frac{1}{n^2}\sum_{\substack{k=1 \\ k\neq j}}^{n} R_k \tag{14}$$

Considering (9) and (14), the conclusion that $\hat{R}'_j$ is the unbiased estimation of R'_j can be reached. By using (13), R_j also proves to be unbiased.

5. IMPLEMENTATION OF ALGORITHM AND THE SIMULATED INSTANCE

5.1 Implementation of algorithm

Assume that $\hat{R}'_{ij}$ denotes the variance estimation of the i-th measurement from sensor j, then (12) can be described by the following recursion:

$$\hat{R}'_{ij} = \begin{cases} 0 & i=0 \\ \frac{1}{i}\left[(i-1)\cdot \hat{R}'_{(i-1)j} + (y_{ij} - \frac{1}{n}\sum_{k=1}^{n} y_{ik})^2\right] & i=1,2,\cdots \end{cases} \tag{15}$$

Using (15) in (13), the variance estimation of each sensor based on i times sampling is obtained. However, a smaller number of sampling times than needed will lead to an inaccurate estimation and even results in the negative variance estimation. In order to ensure that the variance estimation is strictly positive, (13) is reformed as follows:

$$\hat{R}_j = \frac{n}{n-2}\left|\hat{R}'_j - \frac{1}{n(n-1)}\sum_{k=1}^{n}\hat{R}'_k\right| \tag{16}$$

In practice, (15) and (16) are used to estimate the variance of each sensor.

The algorithm of variance estimation presented in this paper can be used in real-time estimation because of its small amount of calculations by using recursive algorithm. In the mean time, it is also an adaptive algorithm and there is no need to set its initial value. With sample size increasing, the variance estimation of each sensor tends to be stable and approaches the true variance gradually.

5.2 Simulated Instance

Consider a system with 8 sensors. It is assumed the noise of each sensor is composed of internal noise and environmental noise and the noise is independent of each other. Suppose that the internal noise of each sensor is zero-mean white Gaussian noise with standard deviation 0.10, 0.20, 0.05, 0.40, 0.50, 0.30, 0.24 and 0.10 respectively and environmental interference zero-mean white Gaussian noise with standard deviation 1.0, 0.8, 1.5, 2.0, 0.8, 2.5, 3.0 and 1.3 respectively. In Table 1, algorithm 1 refers to the algorithm presented in this paper. The algorithm in which the weight is determined only by the sensor's own variance is algorithm 2, and the algorithm of averaging measurement is algorithm 3. In algorithm 4, each sensor's weight is determined by its true variance. Based on the foregoing assumption, the state modeled by $y(t)=t$ is sampled 2000 times, with the sampling interval T=1. The simulation results are shown in Figure 1, Table 1, and Table 2.

As can be seen from Figure 1, the estimated variance of each sensor gradually approaches its true variance as the sampling times increasing in algorithm 1. Data given in Table 1 and Table 2 indicate that algorithm 1 is better than algorithms 2 and algorithm 3. Algorithm 1 is a little inferior to algorithm 4 which is the optimal algorithm theoretically (see Table 1). Mean of estimation errors in each sampling range given in Table 2 can be regarded as the state estimation variance of each algorithm. According to (5), the optimal estimated variance is 0.1951. Data given in Table 2 show that mean of the square of state estimation errors approaches the true value as the sampling times increase.

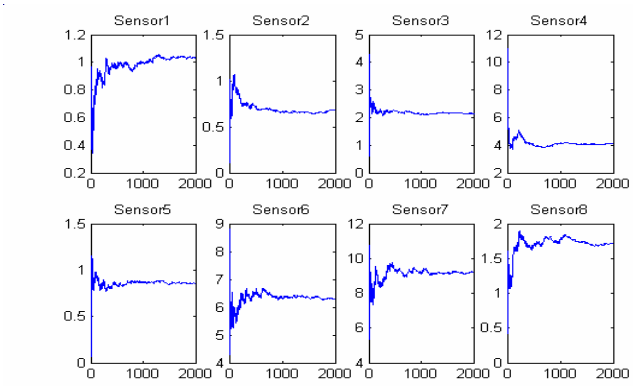

Fig. 1 The curve of sensors' variance estimation. As can be seen from the figure, the estimates of the variance converge to the actual values gradually.

Table 1 The absolute value distribution of estimation error

Error Rang	Algorithm 1	Algorithm 2	Algorithm 3	Algorithm 4
0-0.1	360	171	229	364
0.1-0.3	653	325	485	645
0.3-0.7	747	597	725	749
0.7-1.5	236	681	519	238
1.5-3	4	221	42	4
>3	0	5	0	0

Table 2 The mean square error of state estimation

Sampling Rang	Algorithm 1	Algorithm 2	Algorithm 3	Algorithm 4
1-50	0.3059	1.0778	0.3947	0.2190
51-500	0.2106	0.9094	0.3926	0.2090
501-2000	0.1954	0.9052	0.4266	0.1952

6. CONCLUSION

The algorithm of variance estimation for multisensor is discussed in this paper and proves unbiased. The approach is adaptive and can be used in real-time estimation due to the presentation of the recurrence formula. A numerical example is given to illustrate the results and to show the usefulness of the approach.

REFERENCES

Ling L., Li Z., Chen C., Gu Y. and Li C. (2000). Optimal weight distribution principle used in the fusion of multisensor data. *Journal of Chinese Inertial Technology*, **8**, 36-39.

Raol, J.R. and Girija, G. (2002). Sensor data fusion algorithms using square-root information filtering. *IEE Proceedings-Radar, Sonar and Navigation*, **149**, 89-96.

Yang D. and Yuzo, Y. (2000). Multi-sensor data fusion and its application to industrial control. *Proceedings of the 39th SICE Annual Conference*, 215-220.

Yifeng Zhou and Leung, H (1997). Minimum entropy approach for multisensor data fusion. *Proceedings of the IEEE Signal Processing Workshop on Higher-Order Statistics*, 336-339.

Zhong C., Zhang L., Yang S. and Zhao W. (2002). Study of grouping weighted fusion algorithm for multi-sensor. *Journal of Dalian University of Technology*, **42**, 242-245.

RESPIROMETR ESTIMATIONS BASED MONITORING OF BIO OGICA WASTEWATER TREATMENT PROCESSES

uan D h ng [2] Fan i ing [2] u Hai in

y I t tut Aut t C A y y
P C y
Aut t t t y I t tut C y y
P C y y

Abstract: A method is presented to monitor wastewater treatment processes by incorporating multivariable principal component analysis (PCA) with the knowledge of respirometry estimations. Respirometry is the measurement of an activated sludge respiration which reflects the oxygen rate consumed by biomass, and can be estimated from dissolved oxygen concentrations. Because dissolved oxygen concentrations which are available at most plants have the quick response time and easy maintenance, respirometry estimations based monitoring strategy has advantages for the fault detection. The improvement of some fault detection indexes are demonstrated through IWA s Benchmark simulations. *Copyright 2003 IFAC*

Keywords: Waste treatment, Monitoring, Estimation, Water pollution, Environment engineering.

1. INTRODUCTION

Process monitoring is implemented to ensure that process outputs comply with requirements on product quality, operation safety and efficient use of resources. With the enforcement of even stricter rules on discharges and applications of computer data-collection systems, it is interested in operation monitoring of wastewater treatment plants (WWTP) in recent years. Difficulties such as variably operating conditions, correlation, non-linearity, multi-time scale are often encountered when engineers deal with these data of wastewater treatment plants.

Process monitoring, that is fault detection, isolation and diagnosis, have gained successful applications in petrochemical industry (Kourti and MacGregor, 1996; enkatasubramanian, 2001). Rosen (1998) and Rosen and Olsson (1998) summarized the data pretreatment methods, multivariable principal component analysis (PCA) and partial least squares (PLS) algorithm for monitoring of WWTP. Rosen and Lennox (2001) presented a methodology that is Bakshi s (1998) wavelet multi-scale analysis in combination with

multivariable principal component analysis. Lennox and Rosen (2002) worked further, which an adaptive PCA method is adopted for the changing mean and deviation of process variables or disturbances. Teppola et al (1998) focused on monitoring of paper s wastewater treatment plants.

Analysis instruments are often installed at the entrance and the exit of wastewater because of restriction of investments and operation costs, and the assay time interval of other variables is about 1-2 hour(s). The insufficient of sampling data and the multi-scale sampling times is a challenge problem for WWTP monitoring. The practical usability of analysis instruments is not considered adequately (Lennox, 2002). So for on-line fault detection and diagnoses, more effective process monitoring methods are needed. On the other hand, it is noticed that dissolved oxygen sensors are used widely with sampling times in seconds. By measuring dissolved oxygen (DO) concentrations and further numerical computations, respirometry can be estimated. Respirometry can not only reflect the consumption rate of oxygen in activated sludge, but also is an indication of substrate degradation extent and the ability of microorganism metabolism. Because DO sensors have advantages in stability, quickness and low cost, hence on-line process monitoring based on respirometry (Spanjers, et al, 1998) or respirometric-titrimetric (Gernaey, et al, 2001) may be more practical.

In this work, respirometry measure principles are introduced. Then by making a general of mass balance and numerical differential, respirometry is estimated and combined with conventional data matrix of PCA to form one kind of hybrid PCA model. More mechanism information is added to PCA model and it is helpful to establish economical and quick on-line process monitoring strategies. Finally the approach to monitoring Benchmark of biological wastewater treatment processes is given and the improvement of some fault detection indexes is demonstrated.

2. RESPIROMETRY MEASUREMENT PRINCIPLES

Respirometry is the measurement of the respiration and interpretation of the biological oxygen consumption rate under well-defined experimental conditions. Although the principle of the respirometry measurement is simple, the restriction of some uncertain factors, such as the phase where oxygen concentration is measured and whether or not there is input and output of liquid and gas must be take into account carefully. The respiration rate is calculated by making a general mass balance for oxygen over the liquid phase as follows.

$$\frac{dS_O}{dt} = \frac{Q_{in}}{}(S_{o,in} - S_O) + K_L a(S_O^0 - S_O) - r_O \quad (1)$$

Where S_0 is the dissolved oxygen concentration in liquid phase (mg/l), Q_{in} is flow rate of liquid entering the system (l/min), $S_{o,in}$ is dissolved oxygen concentration entered into the liquid phase, K_La is oxygen transfer coefficient (l/min), S^0 is saturated dissolved oxygen concentration, r_o is oxygen uptake rate (OUR) (mg/l·min), is liquid volume of the respirometer. There are many kinds of methods to calculate respirometry in literatures.

3. RESPIROMETRY ESTIMATIONS

Besides using a respirometer to measure respirometry, theoretically, in virtue of measuring dissolved oxygen concentrations in liquid, then Eq.1 based to calculate consuming rate of oxygen is an alternative approach. Here the differential estimation value of S_o needs to be constructed by the numerical differential based on the measured values of S_o. The simplest method is to calculate with backward differential. In this work, three point numerical differentiation formula is used to calculate the differential value of S_o

$$\begin{cases} \dfrac{dS_O(t-\Delta t)}{dt} = \dfrac{1}{2\Delta t}(-3S_O(t-\Delta t) + 4S_O(t) - S_O(t+\Delta t)) \\ \dfrac{dS_O(t)}{dt} = \dfrac{1}{2\Delta t}(-S_O(t-\Delta t) + S_O(t+\Delta t)) \\ \dfrac{dS_O(t+\Delta t)}{dt} = \dfrac{1}{2\Delta t}(S_O(t-\Delta t) - 4S_O(t) + 3S_O(t+\Delta t)) \end{cases} \quad (2)$$

Noticed this numerical differential needs to be dealt with for on-line monitoring strategies. When a new measured point is added, together with the former two measured values, three differential values can be obtained according to Eq.2. Since every measured value has been cited three times during recursive computations, there are three corresponded differential estimation values at every interval time. Theoretically, it is difficult to select one from three. Since this research aims at fault diagnosis, selecting the minimum at every point is as estimations of the numerical differential.

4. PCA INCORPORATING WITH E TERNAL INFORMATION

There are three approaches to fault detection and isolation based on a first principle model, a data-driven empirical modeling and the knowledge inference. In the aspect of fault detection, the multivariable statistical analysis approach is proved very valid. For complicated processes, because of fault coupling and propagation, it is difficult to isolate the source of faults. Model based is the direct description of common-causal variations. When used in fault diagnosis, the main problem is that development of model, especially modeling the plant-wide needs large cost. Intuitively, combined partial relations such as mass balances and reaction dynamics with PCA model, though such knowledge may be not complete, it is possible to enhance some functions of FDI (Yoon and MacGregor, 2001).

Given the data matrix (n m), the data obtained from other equations can be appended to some rows or some columns of .

$$= H^T + H^T + C + E \quad (3)$$

Here, G(n p) represents observed information matrix, augmented p columns in data matrix; H (m q) represents variable information matrix, augmented q rows in data matrix; E is error matrix, coefficient matrix M, B, C have corresponding dimensionality, and need to be estimated, the detailed derivation can refer to Yoon and MacGregor (2001). In this paper, it is based on mass balance relationship to predication new estimated variables that is augmenting column in the data matrix. For example, at some observation time, the measured data matrix $_m$(n m) has been obtained, for the data matrix $_e$ (n m_1, m_1 m) gained by mechanism relationship estimation, it can be constructed as follows:

$$= [\ m \quad e\ ] \quad (4)$$

For the augmented matrix , various PCA modeling can be carried through. Also the output data matrix Y can be augmented in PLS.

$$= [\ m \quad e\ ] \quad (5)$$

If it is PCA model originally, that is there is no output data matrix Y_m, when the output data matrix Y_e is augmented, PCA problem is converted into PLS. A key step is if such data matrix $_e$ or Y_e can be found to improve some specific index of PCA or PLS.

5. PCA MODEL OF BENCHMARK

The Benchmark WWTP (Alex, et al, 1999) designed by IWA and COST 624 has proven very useful for the evaluation of control strategies developed for N removal wastewater treatment plants. Biological reactor with a total volume of 5999 m^3 is subdivided into five well-mixed compartments in series with a 10-layer secondary settling tank which volume is 4000 m^3. Denitrification takes place in former two anoxic reactors, while later three aerated reactors serve for carbon removal and nitrification. Tuning airflow can control dissolved oxygen concentrations of aerated tanks. IWA s Activated Sludge Model No.1 (ASM1) (Henze, et al, 1987) and the double exponential setting velocity function (Tak cs, et al, 1991) are chosen as a representation of reactors and settling processes separately.

The Benchmark contains 145 state variables. There are 13 component variables which are (1) readily biodegradable soluble substrate S_S, (2) biodegradable particulate material $_S$, (3) slowly biodegradable soluble material S_I, (4) slowly biodegradable particulate material $_p$, (5) slowly biodegradable inert material $_I$, (6) heterotrophic biomass $_{BH}$, (7) autotrophic biomass $_{BA}$, (8)oxygen S_o, (9) NH_4 NH_3 nitrogen S_{NH}, (10) soluble biodegradable organic nitrogen S_{ND}, (11) particulate biodegradable organic nitrogen $_{ND}$, (12) nitrate and nitrite nitrogen S_{NO}, and (13) Alkalinity S_{ALK}. In these components, S_{NH}, S_{NO}, S_o, and S_{ALK} are measurable known at present. Others can not be measured directly. Although there are so many variables, that used for monitoring are a few. In the secondary settler, what can be considered are only those state variables physically measurable and relating with effluent. In Lennox s (2002) study, the following variables were chosen to form PCA model: (1) NH_4 concentration of influent, NH_{4i}, (2) influent wastewater flow, Q_i, (3) total solid suspended matter in reactor 3, TSS_3, (4) effluent NH_4 concentration, NH_{4e}, (5) effluent nitrate concentration, NO_{3e}, (6) total suspended solids of effluent, TSS_e (7) Alkalinity in effluent, S_{ALKe}; (8) total suspended solids of return sludge, TSS_u (9-12) oxygen in reactors 1-4, S_{o1-4}. When TSS_3 and NO_{3e} cannot be measured online, it is needed to develop the new monitoring methodology.

As described in introduction, the consumption of oxygen is related to the degradation extent to the substrate. Using the oxygen concentration and respirometry estimation inside reactors as monitoring variables to form PCA model may have more advantages in quickness and applicability. Simulations given in next section verified such ideas. In this study, following practical measurable variables are chosen to form PCA model: (1-4) oxygen in reactors 1-4 S_{o1-4}, (5-8) respirometry estimations in reactors 1-4, r_{o1-4}, (9) influent flow, Q_i, (10) influent NH_4 concentration, NH_{4i}, (11) effluent NH_4 concentration, NH_{4e}. Three principal components are retained to represent about 90 percent data variances.

6. SIMULATIONS

Components of the influent are time-varied and various. It cost high to monitor by the online analysis and assay. After abnormal influent to the process, biological reacts are not only complicated in mechanism, but also the main biochemical index, such as biochemical oxygen demand (BOD), changed slowly. Once the living environment suitable for biomass is disturbed, the effluent quality will be affected in a long time. So, to monitor and discover various abnormalities come from inlet looks very important. Here two abnormal states are evaluated, that is: (1) the normal operation is impacted by violent variations in influent flow Q_0 caused by rain event; (2) Metabolism of autotrophic biomass in activated sludge reactors is impacted by the toxin pulse in influent. It can be described by amendment to μ_A in ASM1:

$$\mu_A = \begin{cases} \mu_A & \text{other time} \\ 0.2\mu_A & 216.667 \le t < 216.667 + 6 \quad \text{hr} \end{cases} \tag{6}$$

(1) Monitoring the abnormal of influent flow Q_0.

Thought the storm event do not emerge constantly, great influences on WWTP operations are observed. Storm will directly force influent flow and components to vary drastically. Thought the control system can give corresponding action, or the operator can take some measures to keep away, however when attack is serious and the duration is long, it is needed to predict automatically as soon as possible, so as to maintain stationary operating. Results are shown in Fig.1. PI controller at reactor 5 controls DO concentration at the set-point, $S_{o,sp}$=2.0g/m^3.

(2) Monitoring toxin pulses of influent

Toxin pulse lasts 6 hours. The variation of μ_A would affect the activity of autotrophic biomass directly. Because of the control action and mass cycle, states variations observed practically were not so remarkable. From figures (Lennox, 2002), only S_{NO} varied evidently. So, when nitrate-measuring device is not installed in the outlet, it is not easy to diagnose the latent influence of toxin pulse using process monitoring strategies based on common PCA. It will be valid to combined PCA approach with other process knowledge. The results of diagnosing toxin

pulse emergence using the PCA model proposed in this paper are shown in Fig.2. 48 minutes after toxin pulse emerged, the predicted error square index SPE and *Hotelling* T^2 statistics performance were all exceed their confidence interval, bar chart showed the predicted errors of 11 variables in PCA model at this time. It not only need nitrate-measuring device by means of conventional approach, but the toxin pulse emergence can be diagnosed only after 4.5 hours.

7. CONCLUSION

On-line monitoring strategy incorporated respirometry estimation knowledge with multivariable principal component model is presented for WWTP. Respirometry estimations only need to measure dissolved oxygen concentrations inside activated sludge reactors and some related flow signals. Because DO consumption is related to the activity of biomass and the extent of substrate degradation, moreover it is universal to install dissolved oxygen concentration devices and flow meters which have quick response, stable operation, and easy maintenance at wastewater treatment plants, so it has advantages in the efficiency of fault detection and practicability to form the process monitoring strategy based on respirometry estimations. Using this new strategy for monitoring benchmark of IWA, some statistics index varied significantly and diagnosis could be given timely when two typical abnormal conditions on flow variation caused by rain event and toxin pulse of influent. It is the further work to estimate respirometry and oxygen transfer coefficients at the same time.

REFERENCES

Alex J., et al (1999). Benchmark for evaluating control strategies in wastewater treatment plant. In: ECC99 , Karlsruhe, Germany.

Bakshi B. R. (1998). Multiscale PCA with application to multivariate statistical process monitoring. AIChE J., **44**(7), 1596-1610.

Gernaey A., et al (2001). Activated sludge monitoring with combined respirometric- titrimetric measurements. Water Research, **35**(5), 1280-1294.

Henze M., et al (1987). Activated Sludge Model No.1, IAWPRC Task group on Mathematical Modeling for Design and Operation of Biological WWTP, Scientific and Technical Reports No.1, IAWPRC, London.

Kourti T. and J.F. MacGregor (1996). Multivariate statistical process control methods for monitoring and diagnosing process and product performance, J. Quality Tech., **2** , 409-428.

Lennox J. and C. Rosen (2002). Adaptive multiscale principal component analysis for online monitoring of wastewater treatments, Water Science Technology, **45** (4-5), 227-236.

Lennox J. (2002). Multivariate subspaces for fault detection and isolation: with applications to the wastewater treatment process, PhD thesis, University of Queensland, Australia.

Rosen C. (1998). Monitoring wastewater treatment systems, Lic. Thesis, Lund Institute of Technology.

Rosen C. and G. Olsson (1998). Disturbance detection in wastewater treatment systems, Water Science Technology, **37**(12), 197-205.

Rosen C. and J. Lennox (2001). Multivariate and multiscale monitoring of wastewater treatment operation, Water Research, **35**(14), 3402-3410

Spanjers H., et al (1998). Respirometry in control of the activated sludge process, principles, Scientific and Technical Report No. 7. IAWQ, London, UK.

Tak cs I., Patry, G. G. and Nolasco D. (1991). A dynamic model of the clarification thickening process, Water Research, **25**(10), 1263-1271.

Teppola, P., et al. (1998). Principal component analysis, contribution plots and feature weights in the monitoring of sequential process data from a paper machine wet end. Chemometrics Intell. Lab. Syst., **44**, 307-317.

enkatasubramanian . (2001). Process fault detections and diagnosis: past, present and future. IFAC (ChemFas-4) conference, Chejudo, Korea.

Yoon, S. and J. F. MacGregor (2001). Incorporating external information into multivariate statistical models, IFAC (ChemFas-4) conference, Korea.

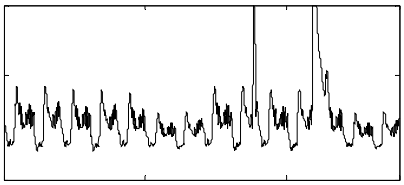
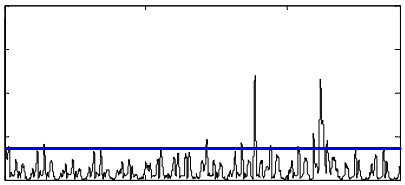
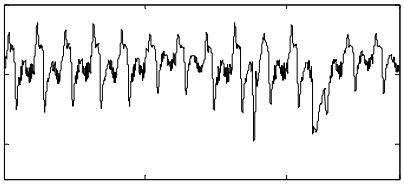
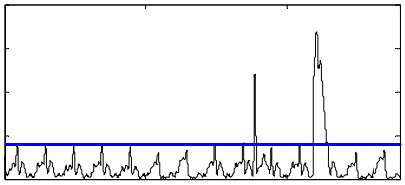
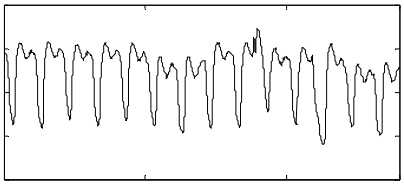
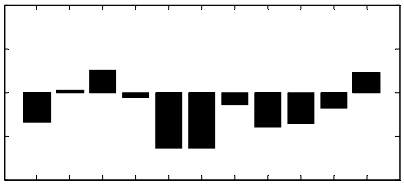
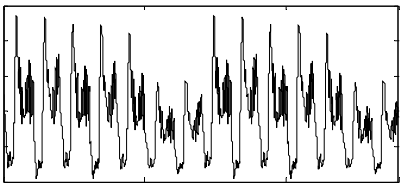
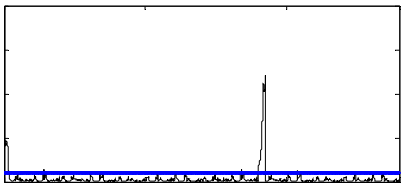
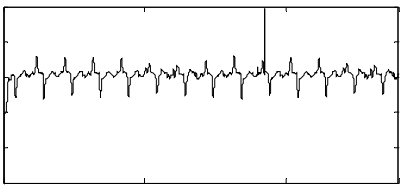
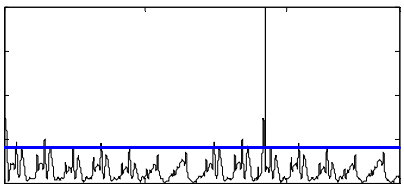
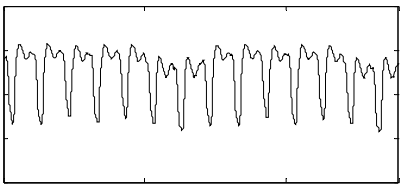
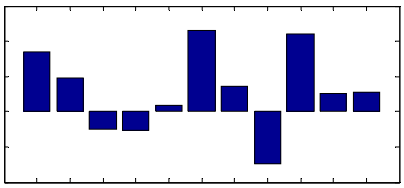

WAVELET PACKET IMAGES MATCHING APPLIED TO NOISE FAULTS DIAGNOSIS

Lu Chen[1], Wang GuiZeng[1], Qiu QingGang[2]

1.Dept. of Automation, Tsinghua University, Beijing, China (100084)
2.Dept. of Power Engineering, Dalian University of Technology, China
E-MAIL: luchen@mail.tsinghua.edu.cn

Abstract: In order to avoid the difficulty of installing vibration sensors and extracting characteristic frequency vectors on the traditional vibration-based abrasion faults diagnosis of main bearing of diesel engine, this paper presents a new approach based on the noise signal of diesel engine and wavelet packet images processing. Based on that, the standard time-frequency distribution images of all fault conditions, including the gap abrasion information of main bearing, can be defined. Correspondingly, a gap abrasion fault diagnosis model of main bearing with images matching is set up. Through comparing the Euclid Distance values between standard fault images and the test image, the model can recognize the gap abrasion condition. The result shows that this method is simple and effective, and makes the best use of fault information.

Keyword: Fault Diagnosis, Gap Measurements, Images Processing, Images Matching, Noise, Time-Frequency

1. INTRODUCTION

Nowadays, there are many diesel engines used in chemical process industry. The fault diagnosis & monitoring of diesel engine is very difficult due to its complex structure. The main bearing is the important part of reciprocating engine, and its extreme abrasion can affect the normal operation of diesel engine. The gap measurements of main bearing are very significant. Faults diagnosis and conditions monitoring of most parts of a diesel engine (including piston, valve and so on) often base on the vibration signal. Vibration sensor is easy to approach those parts and sensitive to their

abrasion faults. But the main bearing locates in the interior of diesel engine, so diesel engine has to be disassembled for installing a vibration sensor near main bearing; but it will result in a lot of troubles. If using noise measurements in the exterior of diesel engine to realize the faults diagnosis and monitoring of main bearing, it will bring very important meanings. In addition, the variety of gap condition of main bearing does not cause the obvious variety of vibration & noise signals; the work processing of diesel engine is a non-stationary shock processing, its energy has a wide distribution in frequency domain, and from the ordinary spectrum figure, it is very difficult to find its fault characteristics similar to those of rotating machinery. In references (Liu Shiyuan, et al., 1999; Geng Zhongxing, Qu Liangsheng, 1994; Xu Min, 1998), wavelet packet and wavelet analysis are used to extract signal characteristics from time domain and some special frequency domain of vibration signal, and these methods all have a satisfactory result. However, all above methods does not make the best use of time-frequency information included in vibration signal; in addition, those methods are based on vibration signal, and not use the noise-based approach that is more easier and effective for fault monitoring of main bearing. Based on that, this paper presents a new fault diagnosis method based on wavelet packet images processing and noise signal.

2.EXPERIMENT AND EXPERIMENT CONDITION

In order to research the relationship between noise signals and the gap abrasion conditions of main bearing, the test equipment is set up specially, as shown in Fig.1. This test diesel engine is a 2100 diesel engine, connected with a waterpower loadometer that can adjust the output power. A ND2 acoustic detector is used to sample the noise signals of diesel, the capacitor microphone of it should be located on the same horizontal level with the main bearing of diesel, so its distance to the engine is 0.8m, its height to the ground is 0.75m. The noise of diesel is usually relatively stronger in some directions and weaker in other directions. So the first step is to scan the surface of diesel for a best measuring position, which can assure the best radiation direction of sound energy, see (Xu Min, 1998; Lu Chen, 2002).

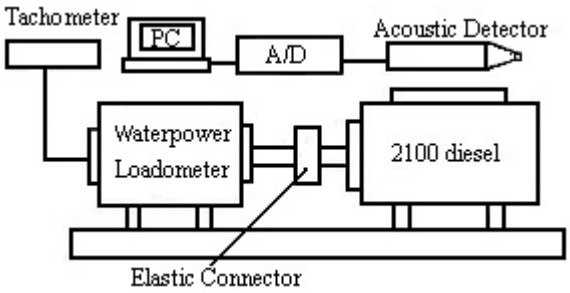

Fig.1. Sketch map of test equipment

In order to obtain measurement result exactly, it is necessary to simulate four conditions of gap abrasion of the main bearing (0.12mm, 0.20mm, 0.26mm, 0.30mm). The limited maximum gap abrasion of the test main bearing is 0.25mm, so the above four conditions of testing gap include basically all work conditions from normal gap to serious abrasion. In addition, rotating speed: 1200r/min, output power: 80%, sample rate: 10.8KHz, sample length: 8192 points.

In order to obtain a highest precision, it is also necessary to mark the noise signal sample. Firstly, need to measure the pressure signal in the interior of cylinder by installing a pulse sensor near the camshaft. The angle range is from -360° to 360° during a work cycle of diesel. During the course of test, record each maximum pressure value while breaking off oils and regard it as 0°. Through the above method, it can be assured that the length of noise signal is integral multiple of a work cycle of diesel.

3.WAVELET ANALYSIS OF NOISE SIGNAL

In our previous research, wavelet analysis was applied to the fault diagnosis of gap abrasion. This method uses wavelet analysis to extract the high

frequency band of noise signal, and then uses Hilbert transform to extract the envelope of the high frequency band. Finally, FFT spectrum of the envelope can be obtained. As a result, it is found that the amplitude values of 0.5× rotating speed and 2× rotating speed frequency are very sensitive to gap abrasion of main bearing, and increase along with the increment of gap abrasion, see (Lu Chen, 2002).

Wavelet analysis can judge the gap abrasion conditions of main bearing, but it does not make the best of the information included in noise signals. Wavelet packet analysis has no redundant results and does not damage the any information of signal. It can also process a detailed decomposition for both low frequency band and high frequency band. Therefore, it is very fit for the analysis of non-stationary random signal, like the vibration & noise signal of diesel engine.

4. WAVELET PACKET ANALYSIS OF NOISE SIGNAL AND IMAGES PROCESSING

4.1 The Principle Of Wavelet Packet

The basic idea of wavelet analysis is to use a cluster of wavelet functions to express a signal. It has a high time-frequency resolution in low frequency bands, a high time resolution and low frequency resolution in high frequency bands. The main information of discrete wavelet transform locates in low frequency domain. The above characteristic is just the shortcomings of discrete orthogonal wavelet. However, the theory of wavelet packet imports a best-basis rule on the base of wavelet theory. It can reflect the characteristic of signal more effectively, and process a more detailed decomposition for high frequency bands. As a result, the decomposition sequence has a high time-frequency resolution and same bandwidth in the whole time-frequency domain. Due to the limit of pages, more detailed theory about wavelet packet, please see the relevant reference, see (Hu Changhua, and Zhang Junbo, 1999; Mallat S.A, 1989; Coifman R.R and Wickerhauser M V., 1992; Geng Zhongxing, Qu Liangsheng, 1994).

4.2 Time-Frequency Phase Plane Express Of Noise Signal And Images Processing

Phase plane is a two-dimension plane composed by time axis and frequency axis. It is not a function relationship, but a state expression and a real expression of signal. If sample length of signal is N, then the result of wavelet decomposition can be expressed by N adjacent rectangles (the area of each rectangle is $\Delta t \times \Delta f$). Δt and Δf represent the resolution of time axis and frequency axis respectively. The different gray color value in each rectangle just represents the amplitude value. So the time-frequency characteristics of signal can be clearly expressed on time-frequency phase plane. The different gap conditions of main bearing will lead to the change of time-frequency distribution of noise signal, see (Geng Zhongxing and Qu Liangsheng, 1994).

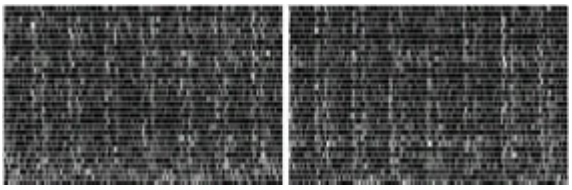

(a) (b)

Fig.2 Time-frequency distribution images of two gap conditions (a: 0.30mm; b: 0.20mm)

The gray values of image can be decided by the following method: firstly, normalize each level of coefficients after wavelet packet decomposition; then get corresponding gray values from these coefficients multiplied by 255, and the level length of decomposition is 5. Through our analysis, it can be found that each different gap of main bearing corresponds to one different time-frequency distribution figure. Even the time-frequency distribution figures of noise signals under the same gap condition from different starting time of sample are also little different from each other. It shows that the wavy behavior always exists in different work

cycles of diesel; in other words, time domain noise waveforms of different work cycles are little different from each other. Simultaneously, on the time-frequency distribution images of different work cycles under the same gap condition, the gray values of some pixels at those corresponding frequency bands are also different from each other. Therefore, the time-frequency distribution image can include all information reflecting the work condition of diesel and give the extent of amplitude value of any time point and frequency band. In order to restrain the disturbance of noise and stand out fault characteristics, the method of images average processing is presented in this paper. It is consistent with the method of parameters average.

The image is formed by software method: firstly, processing wavelet packet decomposition for noise signal, then its time-frequency distribution image will be displayed on computer screen. Through programming, the position coordinates and gray values of all pixel points can be obtained, then save these data as an image file format. Finally, the time-frequency distribution images under different gap conditions can also be obtained. In our experiment, the size of image is 481×386, the range of gray value is 0~255. Certainly, the wider range of gray value can enhance the resolution of image, and reflect more details of wavelet packet decomposition.

5. FAULT DIAGNOSIS MODEL OF INTERNAL COMBUSTION ENGINE BASED ON IMAGES MATCHING

5.1 Images Average Processing

From the above discussion, it is known that, there exists wavy phenomenon among different work cycles of diesel, and also in the interior of each work cycle, so the differences of time-frequency distribution of different cycles under the same work and gap condition should not be neglected. If only use one single noise signal sample as the base of the abrasion fault diagnosis of main bearing, it will lack of correctness. Therefore, it is necessary to process an average for all time-frequency distribution images of one work and gap condition, so as to lessen the wavy effect and stand out the fault information. In our experiment, select respectively 10 time-frequency distribution images to average for 4 types of gap conditions of main bearing, then get four “standard” images representing 4 types of gap conditions. In order to verify the validity, it needs to use 10 images to average for obtaining “standard” images, and five images to average for processing fault diagnosis of main bearing, see (Cheng Guiming and Zhang Mingzhao, 2000). Certainly, the number of images to be averaged can also be larger than 10 or 5. Moreover, the larger number can improve the precision of fault diagnosis.

If, an images cluster $A_k(i,j)$,k=0,1,2,…N. The gray value of the (i, j) pixel unit in $A_k(i,j)$ is $G_k(i,j)$. (i is row, j is column), then after the average processing, the gray value of the (i, j) pixel unit in the standard image (averaged) of any gap condition of main bearing is below:

$$SG_m(i,j)=\frac{1}{N}\sum_{k=1}^{k=N}G_k(i,j) \quad (1)$$

In equation (1): m=1,2,3,4; i=1,2,…,N_L, j=1, 2,…,N_S; N_L is the row count of image pixels. N_S is the column count of image pixels. Let N in equation (1) be 10 as computing each “standard image”, and be 5 as processing fault diagnosis (computing “test image”). The Euclid Distance between two images is defined as equation (2).

In equation (2): $N=N_L\times N_S$, it is just the total count of image pixels; A(i,j) is the gray value of the (i, j) pixel in test image, $SG_m(i,j)$ is the gray value of the (i, j) pixel in m-th “standard image”. The length of noise signal used to produce each standard/test image is integral multiple of a work cycle of diesel. Certainly, for any gap condition, 10 noise signal samples of standard image are all from the same

time series, and the same to 5 noise signal samples of test image.

$$D_m = \sqrt{\frac{1}{M}\sum_{i=1}^{i=N_L}\sum_{j=1}^{j=N_S}[A(i,j) - SG_m(i,j)]^2}$$

m=1,2,3,4 (2)

5.2 The Decision Of Threshold Value

During the process of fault diagnosis, for any image A(i,j) (test image) after the average of 5 images, according to equation (2), compute each Euclid Distance value D_m between four "standard" images and test image (m=1,2,3,4). $D_{min}=\min\{D_m\}$, define the difference between any one of four Euclid Distance values and D_{min} as below:

$$C_m=|D_m-D_{min}| \quad (3)$$

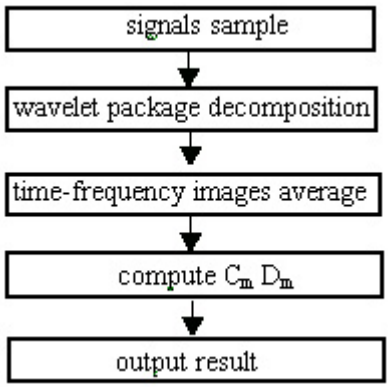

Fig.3 Process of diagnosis

Through test analysis, a diagnosis threshold value can be set V_d=5. For any test image, if there is only one $C_m<V_d$, then the gap abrasion condition of main bearing is just the one which this C_m corresponds to. Whereas, if there are more than one $C_m<V_d$, then it is no way to judge.

6. DIAGNOSTIC EXAMPLE

In Fig.4, each on the left side is the standard image, which represents one of four gap conditions of main bearing, and the right ones are test images. From top to bottom, it is 0.12mm, 0.20mm, 0.26mm and 0.30mm respectively.

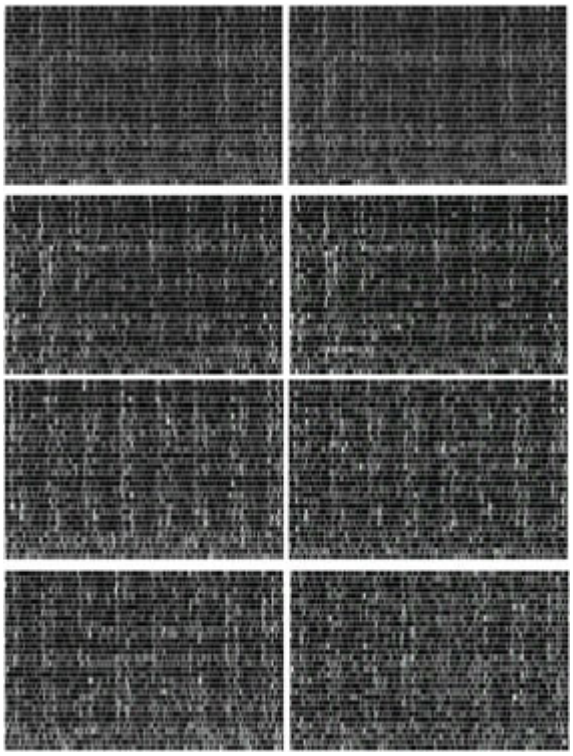

Fig.4 Standard images and test images

In Fig.4, it shows that, there are differences among the four "standard" images. Simultaneously, each "standard" image is quite similar to its corresponding diagnosed image under the same gap condition; it is because the processing of images average can extract the characteristics of images and restrain the noises. According to the steps shown in Fig.3, for each gap condition, selecting two averaged images to diagnose. The result is shown in Table 1.

In Tab.1, SI represents standard image, S1~S8 are test images, D1~D4 are the Euclid Distance values between the standard images and the test images, R represents result, and Gap1~Gap4 represent the diagnostic results of gap conditions.

In our experiment, 30 test images are analyzed by the above method in our experiment, only one image can be not classified, and all the others can be classified correctly. The rate of recognition can reach to 95%.

Tab.1 Euclid distance between standard images and test images

	SI D1	SI D2	SI D3	SI D4	R
S1	15.3	65.7	56.7	52.1	Gap1
S2	63.6	29.3	66.1	58.7	Gap2
S3	57.4	69.3	27.7	62.5	Gap3
S4	54.1	62.3	61.7	16.5	Gap4
S5	17.2	67.9	58.1	53.3	Gap1
S6	60.4	26.1	63.8	56.7	Gap2
S7	55.5	67.5	25.5	57.4	Gap3
S8	53.9	61.6	63.2	17.6	Gap4

7.CONCLUSIONS

From Tab.1, a conclusion can be deduced that, if using images matching model based on Euclid Distance to diagnose the gap condition, then the differences of D_m between the test image sample and each of "standard" images are very distinguished. The essence of this method is, on the time-frequency phase plane, the similar extent of positions and amplitude values of all frequency bands is expressed by Euclid Distance between two time-frequency images. The average method can be used to reduce the wavy effect and noise disturbance, but not solve this problem radically. Certainly, the number of images to be averaged can also affect D_m.

Through wavelet packet analysis, the detailed information of each time domain and frequency band can be obtained. The noise signal of diesel has the characteristic of non-stationary and includes abundant condition information of diesel, so wavelet packet is suitable for analyzing it. Through the test result, it shows that the abrasion fault diagnosis model based on images matching has a strong practicability and feasibility, and the noise signal based method is also feasible. In addition, the threshold value is mainly decided by experience, so far, there is not a quantitive analysis method, it need to be improved in future research.

8.ACKNOWLEDGEMENT

This research is supported by both National Natural Science Fund and the 863 Program of China.

9. REFERENCES

Cheng Guiming and Zhang Mingzhao (2000). *Apply MATLAB Language on Digital Signal and Digital Image*, 255~270. Science Publishing House, Beijing.

Geng Zhongxing and Qu Liangsheng (1994). The Principle of Wavelet Packet and Application on Machinery Fault Diagnosis. *Signal Processing*. **10(4)**, 244~249.

Hu Changhua and Zhang Jubo (1999). *System Analysis and Design Based on MATLAB—Wavelet Analysis*, 6~23. Xi An University of Electronic Technology, Xi An.

Xu Min (1998). *The Handbook of Equipment Fault Diagnosis*, 171~187. Xi An JiaoTong University, Xi An.

Lu Chen (2002). *Condition Monitoring and Fault Diagnosis of Main Bearing of I.C.E. Based on Noise Analysis*, 58~69. Dalian University of Technology, Dalian.

Mallat S.A (1989). A Theory for multiresolution Signal Decomposition: The Wavelet Respresentation. *IEEE Trans on Pattern Analysis and Machine Intell*. **11(7)**, 674~693

Coifman R.R and Wickerhauser M V. (1992). Entroy-Based Algorithms for Best Basis Selection. *IEEE Tran.on Information Theory*, **38(2),** 713

Liu Shiyuan, Du Runsheng and Yang Shuzi (1999). Engine Diagnosis by Wavelet Packets Decomposition of Vibration Signal Measured on Cylinder Head. *Journal of Huangzhong Univ. of Science and Technology*. **27(8),** 7~9

PERFORMANCE MONITORING BASED ON CHARACTERISTIC SUBSPACE

Ming Guo Shuqing Wang

National Key Laboratory of Industrial Control Technology

Zhejiang University, Hangzhou, 310027, P.R.China

Abstract： In the operation and control of chemical process, automatic data logging systems produce large volumes of data. It is important for supervising daily operation that how to exploit the valuable information about normal and abnormal operation, significant disturbance and changes in operational and control strategies. In this paper, principal component analysis (PCA) is clarified its essence from the view of space, and every different subspace represents different operational mode and process performance. Based on that, distance between two subspaces is calculated to evaluate the difference between them. The method is illustrated by a case study of a fluid catalytic cracking unit (FCCU) reactor-regenerator system. *Copyright © 2003 IFAC*

Keywords： Principal component analysis, statistical process control, space distance, process performance monitoring, FCCU.

1. INTRODUCTION

Advances in computer technology and application of advanced control theory have resulted in routine collection and storage of large volumes of data in chemical plant. Massive amounts of stored data can be used for analysis of the process operation and previous occurrences of abnormal situation. Principal component analysis (PCA) can extract valuable information from large historical database. Notable applications of PCA in chemical engineering have been in process monitoring (Nomikos and MacGregor, 1995; Kresta, *et al.,* 1991), disturbance detection (Ku and Storer, 1995), sensor fault diagnosis (Wang and Song, 2002) and process fault diagnosis (Kano, *et al.,*2001; Dunia and Qin,1998; Zhang, *et al.*,1996).

As far as process fault diagnosis is concerned, statistical process monitoring via PCA involves the use of Hotelling T^2 and Q (also known as Square Prediction Error or SPE) charts. Fault is identified with contributions of process variables to SPE. It is only valid for simple fault situation, and difficult to identify the root causes. Zhang and Martin (1996) proposed fault direction to identify different fault. Fault diagnosis is achieved by comparing the direction of the current on-line measurements with those of a database of known trajectories of identified faults. This method based on angle measurement does not make full use of principal component information of faults, and only the first loading

vector is used. Dunia and Qin (1998) analyze the detectability, identifiability and reconstructability of faults using subspace approach. But they assume that the fault effect is not propagated into the other variables, which restricts its application. Kano, *et al.* (2001) proposed a novel statistical process monitoring method based on changes in the subspace which is spanned by several principal components. The method makes use of principal component information sufficiently, and has better monitoring performance than conventional PCA based on Hotelling T^2 and Q charts. In essence, the method proposed in this paper is similar to the one proposed by Kano, *et al.*. Their work is not dealt with fault identification, while our approach goes beyond the fault detection task. Once a fault is detected, we have proposed a method based on subspace distance to identity the type of fault.

The paper is structured as follows: the second section gives a more strict procedure of deduction for PCA based on subspace distance, and proposes a method of fault identification according to historical database. The third section presents an application of the approach to FCCU reactor-regenerator system. The final section summarizes the approach.

2. PCA BASED SUBSPACE

2.1 Spacial Signification of PCA

PCA decomposes a normalized sample vector into two portions,

$$\boldsymbol{x} = \hat{x} + \tilde{x}\,, \tag{1}$$

where $\boldsymbol{x} \in \Re^m$ is the sample vector normalized to zero mean and unit variance. The vector $\hat{\boldsymbol{x}}$ is the projection on the principal component subspace S:

$$\hat{\boldsymbol{x}} = \boldsymbol{P}\boldsymbol{P}^T\boldsymbol{x} = \boldsymbol{C}\boldsymbol{x} \tag{2}$$

where $\boldsymbol{P} \in \Re^{m\times k}$ is the PCA loading matrix, and $k \geqslant 1$ is the number of PCs retained in the PCA model. The matrix $\boldsymbol{C} = \boldsymbol{P}\boldsymbol{P}^T$ is projection operator on the principal component subspace S, $\hat{\boldsymbol{x}} \in S \subseteq \Re^m$, with $\dim(S)=k$. The columns of the loading matrix $\boldsymbol{P}$ are the eigenvectors of the correlation matrix associated with the k largest eigenvalues.

Similarly, the residual $\tilde{\boldsymbol{x}}$ satisfies

$$\tilde{\boldsymbol{x}} = (\boldsymbol{I} - \boldsymbol{C})\boldsymbol{x} = \tilde{\boldsymbol{C}}\boldsymbol{x} \in \tilde{S} \subset \Re^m\,, \tag{3}$$

where $\tilde{\boldsymbol{C}}$ is projection operator on the residual subspace $\tilde{S}$, with $\dim(\tilde{S}) = m - k$. From the view of space, PCA divides the measurement space S_{m} ($\dim(S_{\mathrm{m}})=m$) into two orthogonal subspaces, a principal component subspace and a residual subspace. That is,

$$S_m = S \oplus \tilde{S} \tag{4}$$

Principal component subspace primarily characterizes the measurement subspace. When a change in variable correlation occurs, that is, space S_{m} has a change, the bases of principal component subspace also produce corresponding changes. We call principal component subspace S as characteristic subspace.

For a certain chemical process, we can define fault set $\{F_i\}_{i=1}^n$ according to the data recorded in historical database and technologic information. We denote S_i, S_j as the characteristic subspace of fault F_i, F_j respectively. They are spanned by the corresponding loading vectors, respectively, that is,

$$S_i = span(\boldsymbol{u}_1, \boldsymbol{u}_2, \mathrm{L}\ , \boldsymbol{u}_r) \tag{5}$$

$$S_j = span(\boldsymbol{v}_1, \boldsymbol{v}_2, \mathrm{L}\ , \boldsymbol{v}_s) \tag{6}$$

where $\dim(S_i)=r$, $\dim(S_j)=s$. Without loss of generality, suppose $s \leq r$. The dimensions of subspace S_i, S_j can be determined by the percent of contribution to the accumulative variances. The difference between F_i and F_j can be reflected by the difference of bases of their characteristic subspace. In order to identify different fault, the distance between two subspaces is used to measure the difference. Let matrix

$\boldsymbol{U} = [\boldsymbol{u}_1, \boldsymbol{u}_2, \mathrm{L}\ \boldsymbol{u}_r]$, $\boldsymbol{V} = [\boldsymbol{v}_1, \boldsymbol{v}_2, \mathrm{L}\ \boldsymbol{v}_s]$, with $\boldsymbol{U}^T\boldsymbol{U} = \boldsymbol{I}$, $\boldsymbol{V}^T\boldsymbol{V} = \boldsymbol{I}$. The projection operator from subspace S_j onto subspace S_i can be represented as

$$\boldsymbol{C} = \boldsymbol{U}\boldsymbol{U}^T \tag{7}$$

For any unit vector $\boldsymbol{y} \in S_j$, that is, $\|\boldsymbol{y}\|_2 = 1$, its projection on subspace S_i is written as $\hat{\boldsymbol{y}} = \boldsymbol{C}\boldsymbol{y}$. Now, the distance between two subspaces is defined as

$$d_{i,j} = \max_{\boldsymbol{y}} \|\boldsymbol{y} - \hat{\boldsymbol{y}}\|_2 \tag{8}$$

subject to $$\|\boldsymbol{y}\|_2 = 1 \tag{9}$$

Since $\boldsymbol{y}$ is a unit vector in S_j, it can be represented as

$$\boldsymbol{y} = \boldsymbol{V}\boldsymbol{t} \tag{10}$$

where $\boldsymbol{t}$ is the coordinate coefficients vector correspond to bases $\boldsymbol{v}_1, \boldsymbol{v}_2, \cdots, \boldsymbol{v}_s$, with $\|\boldsymbol{t}\|_2 = 1$. According to Lagrange's method, we have

$$L(\boldsymbol{t}, \lambda) = \|\boldsymbol{y} - \hat{\boldsymbol{y}}\|_2^2 + \lambda(\|\boldsymbol{y}\|_2^2 - 1) \tag{11}$$

Let $\partial L / \partial \boldsymbol{t} = 0$ and $\partial L / \partial \lambda = 0$, with substitution of Eq.10 in Eq.11, we get the following expression,

$$\boldsymbol{A}\boldsymbol{t} = \lambda \ \boldsymbol{t} \tag{12}$$

where $\boldsymbol{A} = \boldsymbol{V}^T\boldsymbol{U}\boldsymbol{U}^T\boldsymbol{V}$. The coordinate coefficients vector $\boldsymbol{t}$ is an eigenvector of the matrix **A**, and λ is the corresponding eigenvalue. The distance between two subspaces is obtained by the substitution of Eq.12 into Eq.8,

$$d = \sqrt{1 - \lambda_{\min}(\boldsymbol{A})} \tag{13}$$

Now, we prove the distance $d \in [0,1]$.

Proof. $\because \boldsymbol{A} = \boldsymbol{V}^T\boldsymbol{U}\boldsymbol{U}^T\boldsymbol{V} = (\boldsymbol{U}^T\boldsymbol{V})^T\boldsymbol{U}^T\boldsymbol{V}$,

$\therefore$ $\boldsymbol{A}$ is nonnegative definite , that is , $\boldsymbol{A} \geq 0$, $\lambda_{\min}(\boldsymbol{A}) \geq 0$.

Suppose the bases of residual subspace of fault F_i is $\tilde{\boldsymbol{U}} = [\tilde{\boldsymbol{u}}_{r+1}, \tilde{\boldsymbol{u}}_{r+2}, \cdots, \tilde{\boldsymbol{u}}_m]$. Let $\boldsymbol{E} = [\boldsymbol{U}, \tilde{\boldsymbol{U}}]$, then $\boldsymbol{E}$ is the bases of the measurement space S_{m}, with $\boldsymbol{E}^T\boldsymbol{E} = \boldsymbol{E}\boldsymbol{E}^T = \boldsymbol{I}$. $\because \boldsymbol{E}\boldsymbol{E}^T = \boldsymbol{U}\boldsymbol{U}^T + \tilde{\boldsymbol{U}}\tilde{\boldsymbol{U}}^T = \boldsymbol{I}$, and $\because \tilde{\boldsymbol{U}}\tilde{\boldsymbol{U}}^T \geq 0$, $\therefore \boldsymbol{U}\boldsymbol{U}^T \leq \boldsymbol{I}$. Thus, $\boldsymbol{A} = \boldsymbol{V}^T\boldsymbol{U}\boldsymbol{U}^T\boldsymbol{V} \leq \boldsymbol{I}$, that is, $\lambda_{\min}(\boldsymbol{A}) \leq 1$

Therefore, $0 \leq d \leq 1$, End.

Thus, we have the following three special cases:

(i) if the subspace $S_{\mathrm{i}} = S_{\mathrm{j}}$, that is , the two subspace are identical, then $\boldsymbol{U} = \boldsymbol{V}\boldsymbol{Q}$, where $\boldsymbol{Q}$ is nonsingular orthogonal matrix. With Eq.13, we can get $\lambda_{\min}(\boldsymbol{A}) = 1$, that is, d=0. In the case of this, the fault F_i, F_j can be considered as the same fault.

(ii) If the subspace $S_i \subset S_j$, that is, the subspace spanned by the model for the fault F_j contains the subspace spanned by the model for fault F_i, we can also get d=0. It means that the fault F_i is masked by fault F_j, and they can not be distinguished from each other. In fact, they are mistaken for the same fault.

(iii) If the subspace $S_i = S_j^{\perp}$, that is, they are orthogonal, then $\boldsymbol{U}^T\boldsymbol{V} = 0$. Thus, we can get $\lambda_{\min}(\mathbf{A}) = 0$, that is , d=1. It means that the fault F_i, F_j can be distinguished from each other to the most extent.

2.2 Fault Diagnosis Based on Distance

From above description, the distance between subspaces can be used to identify the different faults. We define a match function as follows,

$$p_{i,j} = (1 - d_{i,j}) \times 100\%$$

$$= 1 - \sqrt{1 - \lambda_{\min}(\boldsymbol{A}_{i,j})} \times 100\% \tag{14}$$

When a fault occurs, the loading vectors of the fault data are calculated through PCA and used to represent the bases of characteristic subspace of the fault. On the basis of that, the library of characteristic subspace of faults can be formed and represented as follows,

$$S_F = [S_1, S_2, \cdots, S_n] \tag{15}$$

Where S_i is the characteristic subspace corresponding to the fault F_i, and S_F the subspace set, and n the number of faults.

The currently monitored process measurements can then be analyzed using PCA. The calculated loading vectors form the bases of the subspace corresponding to the current observations. Denoting the current characteristic subspace by S_{cur}, the matching degree between S_{cur} and the every subspace in S_F can be measured by Eq.14 respectively after a fault is detected. If the matching degree between S_{cur} and some subspace (for example, S_i) is very close to 100%, then the current abnormal occurrence may be probably ascribed to fault F_i. On the contrary, if the matching degree is close to zero, it may be least ascribed to fault F_i. Thus, fault identification can be performed by calculating the matching degree

between the characteristic subspace of the current data and the library of subspace of known faults. As already discussed, some faults may be masked, so domain knowledge is further needed in that case to analyze the results and determine which fault has occurred on earth.

In practical application, a diagnostic threshold is required to be defined in advance. The maximum of matching degree between the current data and the faults in the library should be larger than the diagnostic threshold. Otherwise, if the maximum of matching degree is less than the diagnostic threshold, that is, the current data subspace is not well matched with any fault characteristic subspace in the library, then it is likely that a novel fault has occurred. Once the occurrence of a novel fault is confirmed, the bases of the current data subspace can be stored in the library. Through this method, diagnostic knowledge about novel faults is progressively learnt and the library updated.

3. CASE STUDY

3.1 Process Description

Fluid catalytic cracking unit (FCCU) is considered as one of the most important unit in the refinery. A simplified flow diagram is shown in Fig.1. Briefly, the fresh feed and recycle sludge oil are preheated, mixed, and then enter into the riser reactor where they contact regenerated catalyst and start the cracking reactions. The spent catalyst passes to the steam stripping section and enters the regenerator where the coke on the catalyst is burnt off with air. The heat released by the combustion of coke is supplied to the endothermic cracking reactions. The extra heat than what is required by cracking reactions is taken away by the heat exchanger outside the regenerator. The FCCU reactor–regenerator model which is used in this paper can be referred to the work done by Yang, *et al.* (1997).

To generate an instance, the simulation is running at normal mode. When all parameters become stable, a disturbance or fault is introduced and at the same time, data recording is started. Fourteen variables are chosen to be recorded, including temperature of feed preheated, flow rate of recycle oil, sludge oil, slurry oil, distillate oil and assembled feed, flow rate of air of the first regenerator and the second regenerator, outlet temperature of riser, the heat of exchanger, carbon dioxide content in the flue gas from the first regenerator, oxygen content in the flue gas from the second regenerator, the temperature in the high density bed of the first and the second regenerator. During the simulation, random noise was added to the measurement and controller outputs. Altogether ten data instances have been generated and summarized in Table 1. Sample time is 4 minutes. Each instance is simulated for 1000 minutes, and the database is a 250×14×10 matrix.

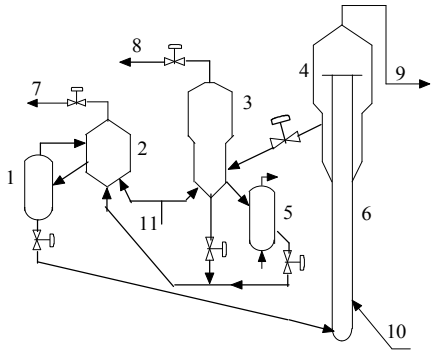

1：deaerator 2: 2nd regenerator 3: 1st regenerator 4: settler 5: heat exchanger 6: riser 7: 2nd regenerator flue gas 8: 1st regenerator flue gas 9: product 10: feed 11: air

Fig.1 FCCU Reactor-regenerator Flow Sheet

3.2 Data Analysis and Fault Identification

When the measurement data are obtained, data reconciliation is performed to validate the sensor data. Then they are normalized to zero mean and unit variance before the data of each instance is analyzed by PCA. The distance between two corresponding subspaces is calculated with Eq.13. Table 2 is the calculated results. From Table 2, it can be seen that the distance between subspaces of case 2, 3, 4 is relatively small compared with other distance, which indicates that their difference between them is relatively small. This is because they are all the flow disturbance of fresh feed, only different in the magnitude, and they have similar effect on the correlation of data. The distance between case 2,3,4 and case 5 is relatively large compared with the one

between case 2,3,4. That is because case 5 has an adverse disturbance direction. The distance between other cases is large. So we can use the distance to identify different fault or disturbance.

For online monitoring, the data matrix representing the current operating conditions is updated by moving the time-window step by step as proposed by Kano *et al* (2001). PCA is applied to the data matrix, and the distance between the subspace of current data and the one of normal operation data is calculated with Eq.13 at each step. If the distance goes beyond the given control limit, the process is judged to be out of normal operation condition. And then, the distances between the subspace of current data and the one of known faults in the library are calculated respectively, and the match degrees between them are also obtained with Eq.14. If the maximum of matching degree is larger than the diagnostic threshold, then the fault in the library corresponding to the maximum has probably occurred.

In order to verify the method for fault identification, the preheated temperature of fresh feed decreased 6K at 100 minute in the simulation. The monitoring results are shown in Fig.2, and the 95% warning limit which can be determined by statistical method is also shown.

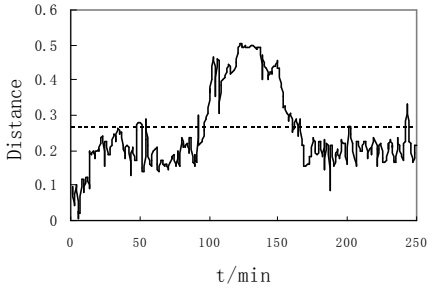

Fig 2 Monitoring results for FCCU reactor-regenerator system

When the distance is out of the control limit, the matching degrees between the current data and the faults in the historical database are calculated, and the results are shown in Fig.3. The diagnostic threshold is predefined as 0.80. It can be seen that the current case matches well with case 8 at 86.32% matching degree which is above the diagnostic threshold, and the fault is successfully identified.

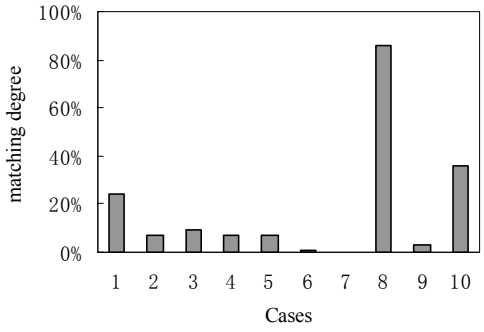

Fig 3 Matching degree of the current case with the cases in the historical database

4. CONCLUSIONS

The diagnosis of abnormal operation can be greatly facilitated if similar system performance has been recorded in the historical database. Principal component analysis is among the most popular methods for extracting information from data. Through PCA, features associated with different faults can be identified and used in fault diagnosis. The features are the characteristic subspace spanned by several loading vectors. Fault diagnosis can then be performed by calculating the distance between the subspace of current data matrix and the one of known faults in the library. It can also deal with novel faults and learn diagnosis knowledge about novel faults. This method is applied to monitoring the FCCU reactor-regenerator system. The results have shown that the method can successfully identify different faults, because it makes full use of information about several principal components. It is important to note that although the approach is well founded, there are problems to be solved in real industrial application. It is advisable to combine domain knowledge with data mining method to diagnosis fault.

5. ACKNOWLEDGEMENTS

The support from the National High Technology (863) Project (No: 2001AA413110) is gratefully acknowledged.

6. REFERRENCES

Dunia, R and Qin, S.J(1998). Subspace approach to multidimensional fault identification and reconstruction. *AIChE.J.*,**44**(8),1813-1831.

Kano, M., Hasebe,S. and Hashimoto, I.(2001). A new multivariate statistical process monitoring method using principal component analysis. *Comp.Chem.Eng*., **25**,1103-1113.

Kresta, J., MacGregor, J.F. and Marlin,T.E.(1991). Multivariate statistical monitoring of process operating performance. *Can.J.Chem.Eng*., **69**(1),35-47.

Ku, W., Storer, R.H., and Georgakis, C.(1995). Disturbance detection and isolation by dynamic principal component analysis. *Chemical Intellectual Laboratory System*, **30**,179-196.

Nomikos,P. and MacGregor, J.F.(1995). Multivariate SPC charts for monitoring batch processes. *Technometrics*, **37**(1), 41-59.

Wang, H.Q., Song, Z.H. and Wang, H.(2002). Statistical process monitoring using improved PCA with optimized sensor locations. *J. Proc. Cont.,* 6, 735-744.

Yang, M.Y, Rong, G. and Wang, S.Q.(1997). FCCU reactor-regenerator advanced control. *International Symposium on Advanced Control of Chemical Processes*, Banff, Canada, 653-657.

Zhang, J., Martin, E.B. and Morris, A.J(1996). Fault detection and diagnosis using multivariate statistical techniques. *Chemical Engineering Research and Design*, **74**(1), 89-96.

Table 1 Summary of the 10 simulated cases

Cases	Description of cases
1	normal operation
2	a step increase of 10% in fresh feed flow rate
3	a step increase of 20% in fresh feed flow rate
4	a step increase of 40% in fresh feed flow rate
5	a step decrease of 30% in fresh feed flow rate
6	a step increase of 10% in air flow rate of 1st regenerator
7	a step increase of 10% in heat of heat removal system
8	decrease of 3K in preheated temperature of fresh feed
9	increase of 3K in outlet temperature of riser reactor
10	increase of 3K in high density bed temperature of 1st regenerator

Table 2 The distance between ten different cases

d	case 1	case 2	case 3	case 4	case5	case 6	case 7	case 8	case 9	case 10
case 1	0	0.3896	0.5799	0.6619	0.5953	0.3406	0.4191	0.7596	0.5754	0.5355
case 2	0.3896	0	0.0678	0.2054	0.6251	0.9915	0.9427	0.9454	0.9998	0.9881
case 3	0.5799	0.0678	0	0.1300	0.6535	0.9991	0.9622	0.9227	0.9527	0.9555
case 4	0.6619	0.2054	0.1300	0	0.6990	0.9998	0.9653	0.9469	0.9360	0.9609
case 5	0.5953	0.6251	0.6535	0.6990	0	0.9769	0.9958	0.9359	0.9566	0.9510
case 6	0.3406	0.9915	0.9991	0.9998	0.9769	0	0.8441	0.9960	0.8684	0.9926
case 7	0.4191	0.9427	0.9622	0.9653	0.9958	0.8441	0	0.9991	0.9618	0.9998
case 8	0.7596	0.9454	0.9227	0.9469	0.9359	0.9960	0.9991	0	0.9747	0.6478
case 9	0.5754	0.9998	0.9527	0.9360	0.9566	0.8684	0.9618	0.9747	0	0.9230
case 10	0.5355	0.9881	0.9555	0.9609	0.9510	0.9926	0.9998	0.6478	0.9230	0

SOFT-SENSING OF THE DRY POINT OF BENZENE USING PCA AND DRBFN

Yuqing Chang and Fuli Wang

Dept. of Information Science and Engineering, Northeastern University
Shenyang, Liaoning Province, China

Furong Gao
Department of Chemical Engineering
Hong Kong University of Science & Technology
Clear Water Bay, Kowloon, Hong Kong

Abstract: Measurements of temperatures and flows and pressures are used to estimate the dry point of the product for the distillation column. The Problem is characterized by the model complication and the strong colinearity between the measurements. In this article, the distributed RBF neural network (DRBFN) and principal component analysis (PCA) are used to develop the soft sensor (PCA-DRBFN model), and PCA is also used for data compressing and validation. Another two models are used to compare the performance with the proposed soft sensor.

Key words: Soft Sensor, Estimation, PCA, DRBFN, Dry Point, Distillation Column

1. INTRODUCTION

A major problem in the control of product quality in chemical process is the uneasy measuring of the quality variables on-line. Although related product quality parameters (such as product composition) can be obtained by laboratory analysis off-line, this brings large measurement delays. This paper addresses the development of a soft sensor model to achieve the estimation of the uneasy measured quality parameter. The application chosen here is the use of temperature, flow and pressure parameters to estimate the product dry point.

There are many methods of developing soft sensor models and neural network is one of them being used widely because of its excellent properties (Bhat and McAvoy 1990). RBF neural network is the often-used net.

Usually, it is necessary to collect large amount of process data in order to accurately developing the soft sensor model. In this case, using one network to build model will bring a problem of long learning time. Distributed RBF network (DRBFN), which learns all the initial data using multi-nets can deal with this problem properly. However, there is usually strong colinearity among the multi-dimension variables in chemical process, and this will lead to ill-condition model, long learning time and huge model structure. Principal components analysis (PCA) technology can

compress the multidimensional collinear variables into lower dimension and guarantee the least loss of data information, so principal component regression (PCR) can be used to develop the estimation model and avoid the shortcoming from colinearity variables. However, PCR are only fit to linear regression, so this method will bring bad estimation result for the complicated nonlinear chemical process (such as distillation column).

This article proposed a new soft sensor model using PCA and DRBFN technoledges. The proposed model is of the specialties of better estimation quality and simplified structure compared with the PCR and DRBFN model.
Although it is based on a particular distillation column example, the treatment in this article is rather general.

2. DRBFN SOFT SENSOR

The objective is to obtain the best prediction $\hat{y}$ of the primary variable (product dry point in our application) using all available information. The estimation model (soft sensor model) may be written

$$\hat{y} = f(X) \tag{1}$$

where, X includes all measured secondary variables.

The structure of DRBFN soft sensor is shown in Figure 1 (Wang and Shao, 1998).

In Figure 1, RBFi (i=1,2…n) is the sub RBF network. The fuzzy classifying unit is used to classify the initial learning data into n classes using Rival Penalized Compete Learning algorithm, and the RBFi net matches the data relation of the i*th* class. The combination of all the RBF subnet is realized by the membership degree $\mu = [\mu_1, \mu_2, \cdots, \mu_n]$. μ_i is achieved by the fuzzy classifying unit in Figure 1, it can be written

$$\begin{cases} \eta_i = 1, \eta_j = 0, \quad if \quad d_i = 0, j = 1, \cdots N, j \neq i \\ \eta_i = \left(1/d_i\right) \Big/ \left(\sum_{i=1}^{N} 1/d_i\right), \quad otherwise \end{cases} \tag{2}$$

$$\mu_i = \sum_{j}^{N_i} \eta_j \text{ 。} \tag{3}$$

where, $d_i = \left\| X - X_i \right\|^2$ is the Eurlar distance between the input data X and the initial sample data $X_i (i = 1,2,\cdots,N)$, N and N_i are the total number of the sample data and the number of i*th* class sample data respectively.

The output of DRBFN can be expressed

$$Y = \sum_{i=1}^{n} \mu_i f_i(X) \tag{4}$$

Where, f_i is the output of i*th* RBF subnet, n is the number of all the RBF subnets.

The advantages of DRBFN soft sensor are that it can approximate any continuous nonlinear functions and avoid the long learning time from the large number of the sample data. However, if X is the multidimensional variable and has significant collinearity, the input of each RBF subnet will be of serious redundancy, and this will lead to ill-conditioned model, long learning time and complicated subnet structure.

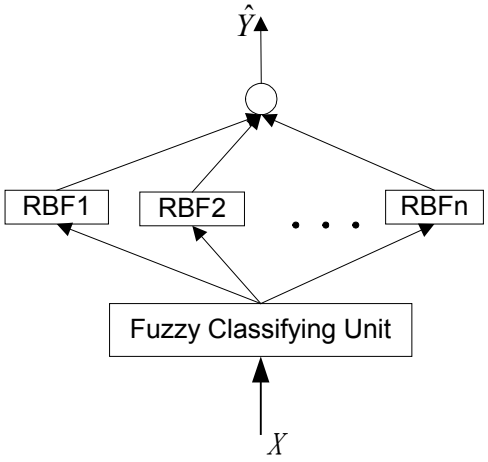

Fig.1. Soft Sensor Structure Based on the DRBF network

3. PCA-DRBFN SOFT SENSOR

3.1 DATA COMPRESSION AND VALIDATION

PCA is an extremely powerful method for data compression, and has been successfully used to a wide variety of different applications. It is at its best when applied to problems featuring both high dimensionality and a large degree of collinearity. PCA breaks data matrices $\boldsymbol{X}(N \times m)$ down into a series of abstract latent variables or principal components. Its model is given by

$$\boldsymbol{X} = \boldsymbol{T}\boldsymbol{P}^{\boldsymbol{T}} + \boldsymbol{E} = \sum_{i=1}^{l} t_l p_l^T + \boldsymbol{E} \tag{5}$$

where, $\boldsymbol{T} = [t_1, t_2 \cdots t_l]_{N \times l}$ is the score vectors, $\boldsymbol{P} = [p_1, p_2 \cdots p_l]_{m \times l}$ is the loading vectors and $\boldsymbol{E}$ is the residuals of the $\boldsymbol{X}$ blocks. In this paper, the PCA approach is adopted to compression the

original process data. Based on the above PCA method, the PCR model can be given by

$$\hat{Y} = K_{PCR} X$$

and $$K_{PCR} = \boldsymbol{Y}^T \boldsymbol{T} (\boldsymbol{T}^T \boldsymbol{T})^{-1} \boldsymbol{P}^T$$

where, Y and $\hat{Y}$ are the measurement and prediction of the primary variable respectively.

In Figure 2, the PCA demapping unit is used to regress the original variables $\hat{X}$ by the score vectors and loading vectors. This model can be expressed as

$$\hat{\boldsymbol{X}} = \boldsymbol{T}\boldsymbol{P}^T \tag{6}$$

The squared prediction error (SPE) for $\boldsymbol{x}^j$ is

$$SPE(\boldsymbol{x}^j) = \sum_{i=1}^{m} SPE_i = \sum_{i=1}^{m} (x_i^j - \hat{x}_i^j)^2 \tag{7}$$

where, $\boldsymbol{x}^j = [x_1^j, x_2^j \cdots x_m^j]$ is the sample value of the *j*th sample period, and *m* is the dimension of original variables. If one sensor fails which breaks the normal correlation, the SPE will increase significantly. Jackson and Mudholkar developed a test for SPE known as the Q-statistic. This test suggests the existence of an failure sensor when

$$SPE > Q_\alpha \tag{8}$$

where

$$Q_\alpha = \theta_1 \left[\frac{C_\alpha \sqrt{2\theta_2 h_0^2}}{\theta_1} + 1 + \frac{\theta_2 h_0 (h_0 - 1)}{\theta_1^2} \right]^{\frac{1}{h_0}} \tag{9}$$

$$\theta_i = \sum_{j=l+1}^{m} (\lambda_j)^i \quad i = 1,2,3 \tag{10}$$

$$h_0 = 1 - \frac{2\theta_1 \theta_3}{3\theta_2^2} \tag{11}$$

and C_α is the confidence limit for the $1-\alpha$ percentile in a normally distributed.
Defines the SPE contribution β_i as

$$\beta_i = SPE_i / SPE \quad i = 1,2 \cdots m \tag{12}$$

The data x_i^j is fault when

$$\beta_i > \delta \tag{13}$$

where, δ is a given value. From (6), we have

$$\hat{\boldsymbol{X}} = \boldsymbol{T}\boldsymbol{P}^T = \boldsymbol{X}\boldsymbol{P}\boldsymbol{P}^T \tag{14}$$

and

$$\boldsymbol{P}\boldsymbol{P}^T = [\overline{\boldsymbol{w}}_1, \overline{\boldsymbol{w}}_2 \cdots \overline{\boldsymbol{w}}_m] \tag{15}$$

The validation of fault data x_i^j can be expressed as

$$\hat{x}_i^j = \boldsymbol{x}^j \overline{\boldsymbol{w}}_i \tag{16}$$

In this paper, the above PCA method will be used to realize the data compression and validation.

3.2 PCA-DRBFN SOFT SENSOR

The structure of the soft sensor model based on PCA-DRBFN is shown in Figure 2, where, X and $\hat{Y}$ are the secondary variable vector and primary variable vector respectively.

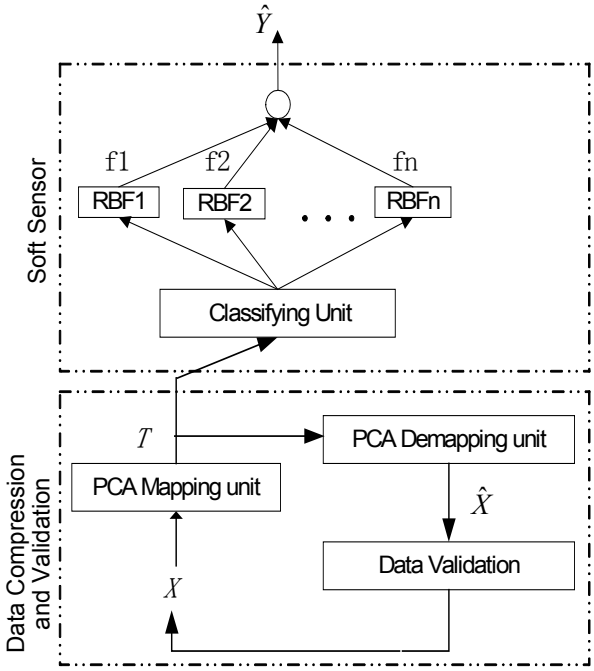

Fig. 2. Soft Sensor Structure Based on the PCA-DRBFN

In Figure 2, the Data compression and validation unit is used to compress the original higher dimensional secondary variables X into principal component variables T, and to validate the fault process data so that the process information used by soft sensor is compact and available. The relationship of T and X can be expressed by equation 5. In PCA-DRBFN model, the input of each subnet is T instead of X. By this means, the input of each subnet will be decreased from *m* to *l* (m>>*l*) if the secondary variables are collinear. So the RBF subnet structure of PCA-DRBFN can be significantly simplified by PCA method, and the learning speed of the net can also be improved.

The output of the PCA-DRBFN can be written as

$$Y = \sum_{i=1}^{n} \mu_i f_i(T) = \sum_{i=1}^{n} \mu_i f_i(XP) \qquad (17)$$

where, μ_i and f_i are designed in Section 2.

4. DRY POINT PREDICTION SIMULATION

In this paper, a benzene-distilled process is adopted as a simulation sample to test the validation of the proposed model. This column consists of 35 trays and its diameter is 1.6m. A reboiler is used to heat the raw material. A water-cooled condenser is placed in the top of the column and a small accumulator tank is used to deposit the condensate. The structure of distillation column is shown in Figure 3, and the main process variables have been marked on the sides.

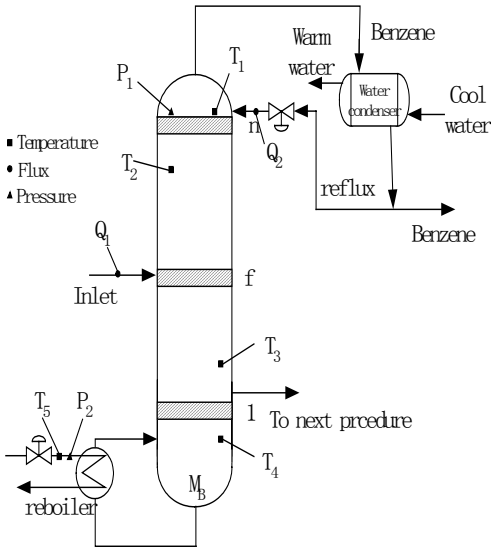

Fig.3. The Flow Chart of the Distillation Column of the Benzene

Tabel 1. Secondary variables

Index		Name of the variables
1	P_1	tower top pressure (atm)
2	T_1	tower top temperature(℃)
3	T_2	tray 28 temperature(℃)
4	T_3	tray 4 temperature(℃)
5	T_4	tower bottom temperature(℃)
6	P_2	steam pressure (atm)
7	T_5	steam temperature(℃)
8	Q_1	inlet flux(m^3/hour)
9	Q_2	reflux(m^3/hour)

The top product of this column is pure benzene. The dry point, which is achieved by sample analysis offline with a long measuring delay, is used to evaluate the quality of the product. The soft sensor based on the PCA-DRBFN is used to obtain the prediction of product dry point.

The variables that affect the dry point of the product are listed in table 1. The soft sensor model of the dry point y can be expressed as

$$y = f(P_1, T_1, T_2, T_3, T_4, P_2, T_5, Q_1, Q_2) \quad (18)$$

4.1 MODEL PREDICTION

Two hundred data points were collected from a distillation process. The variable to be predicted is the product dry point sampled by laboratory analysis. The data were collected so as to achieve the soft sensor based on the process information. In the simulation, 150 data points are used for building the PCA-DRBFN soft sensor and 50 points are used to test the generalization property of the model. After the principal component analysis for the 150 data, the contribution percent of each PC is shown in Table 2.

From Table 2, the former 4 PCs' cumulative contribution is 87.23%, so these 4 PCs can describe the information of process and filter the redundancy (Dunteman, 1989). The variables dimension is decreased from 9 to 4 after PCA. It means the net structure will be simplified significantly and the learning time of each RBFi will also be decreased.

After principal component analysis, let the compressed data input into the distributed RBF to obtain the soft sensor model. At the same time, we use the same initial sample data to develop the DRBF network soft sensor and PCR soft sensor.

50 test data are used to test the above two soft sensor. Figure 4 shows prediction results of the PCA-DRBFN soft sensor. It shows that the proposed soft sensor model can achieve the prediction value of the product dry point with a considerable precision. The estimation errors of the above three models are showed in Figure 5.

From Figure 5, we can see that the estimation quality of the DRBFN and the PCA-DRBFN is similar, but the estimation result of the PCR is deteriorated because of the higher nonlinearity of the process. Although the estimation quality of the DRBFN and the PCA-DRBFN is similar, the structure size of them is different. The biggest subnet size of DRBFN is 9×21×1(that means it has 9 nodes in input layer, 21 nodes in hider layer and 1 node in output layer), the smallest one is 9×15×1, and the biggest subnet size of PCA-DRBFN is

4×11×1, the smallest one is 4×7×1, so the structure of PCA-DRBFN is simplified. By simulation, we also find that the learning time of PCA-DRBFN is shorter than that of DRBFN.

Table 2 PC contribution percent

	Principal Component								
	t_1	t_2	t_3	t_4	t_5	t_6	t_7	t_8	t_9
Latent root	2.71	2.40	1.58	0.66	0.45	0.26	0.19	0.13	0.05
Contribution percent (%)	32.2	28.5	18.7	7.83	5.33	3.08	2.24	1.54	0.58
Cumulative Contribution percent (%)	32.2	60.7	79.4	87.23	92.56	95.64	97.88	99.42	100

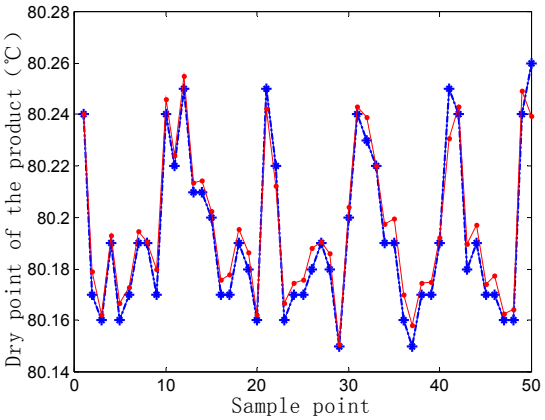

* prediction value • measured value

Fig.4. The Prediction of the Dry Point Based on the PCA-DRBF Soft Sensor

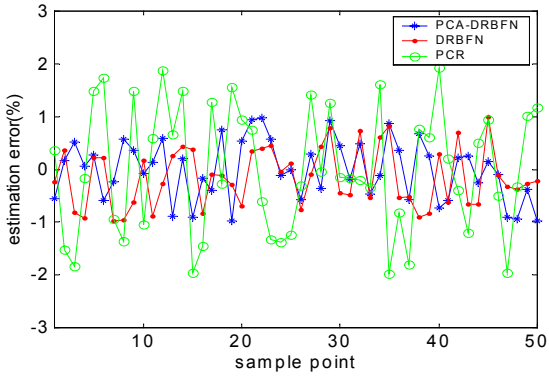

Fig.5. The Estimation Error of the Soft Sensor Model

4.2 DATA VALIDATION

Two hundred data points were collected with a bias fault introduced in the inlet flux so as to test the property of the data validation model. Based on the obtained PCA model, the SPE value of the testing data can be calculated on-line. Figure 6 shows the SPE of the data is out of the control limit after 90th sample, and Figure 7 shows the SPE contribution of the 95th sample point. From Figure 7, inlet flux Q_1 need to be reconstructed, and the SPE after data validation is shown in Figure 8. The result shows SPE returns to the normal range after the faulty data being reconstructed.

5. CONCLUSIONS

In this paper, a method of building a soft sensor model is proposed, and PCA method is used to compress the higher dimensional secondary variables, so that the soft sensor has a compact model structure. The simulation shows that the proposed soft sensor based on PCA-DRBFN can predict the uneasy measured quality variable accurately.

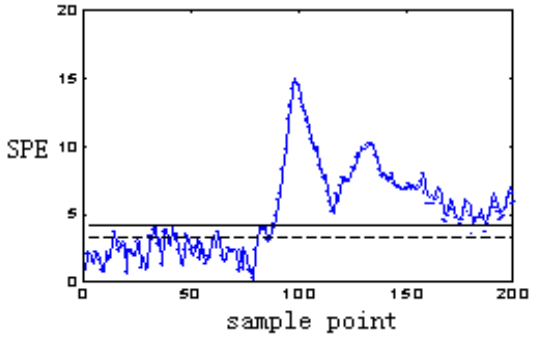

Fig.6 SPE test for faulty data

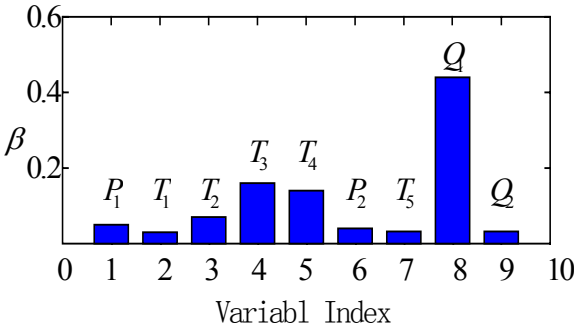

Fig.7 SPE contribution chart

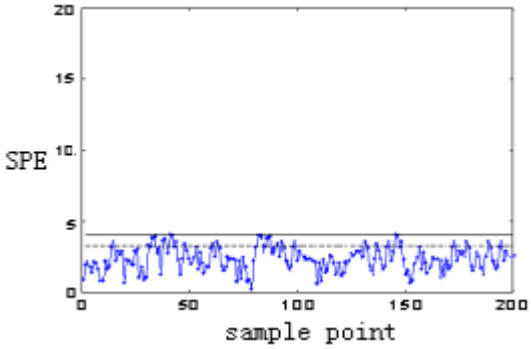

Fig.8 SPE test after data reconstruction

REFERENCES

Bhat, N. V. and T., J. McAvoy, , Use of neural nets for dynamical modeling and control of chemical process systems, Computers and Chemical Engineering, 1990, 14, 573-583

Thor Mejdell and Sigurd Skogestad, Output Estimation Using Multiple Secondary Measurements: High-Purity Distillation, AIChE J, 1993, Vol.39, No.10, 1641-1653

Xudong Wang and Huihe Shao. Distributed RBF neural network and its application in soft sensor, Control theory and application, 1998, Vol.15, No4, 558-563

Huiwen Wang, Partial Least-Squares Regression-Method and Application, National Defence Industry Publishing Company, 1999

George H. Dunteman, “Principal component analysis”, SAGE publication, 1989

Wold S., “Cross-validatory estimation of the number of components in factor and principal component models”, Technometrics, 1978, 20, 397-405

George H. Dunteman, “Principal component analysis”, SAGE publication, 1989.

Jackson, J.E., and Mudholkar, G. Control procedures for residuals associated with principal component analysis. Technometrics 1979,21,341-349

S.Joe Qin, Hongyu Yue and Ricardo Dunia, A Self-Validating Inferential Sensor for Emission Monitoring, Proceedings of the American Control Conference, 1997,473-477

A FAULT DIAGNOSIS METHOD FOR FERMENTATION PROCESS

Liling Ma, Fuli Wang, Yunbo Jiang,

P.O.Box 131
The School of Information Science and Engineering
Northeastern University, Shenyang, 110004
P.R.China
E-mail: maliling1974@yahoo.com.cn Fax:(86-24) 23890912

and

Furong Gao

Department of Chemical Engineering
Hong Kong University of Science and Technology
Clear Water Bay, Kowloon, Hong Kong

Abstract: Process fault diagnosis requires the on-line information on process state variables that are often inaccessible in real-time for the processes like a fermentation process. A composite model is proposed, combining a kinetic model of the first principles and a neural network model that models the kinetic model parameters changes, to estimate on line the states. This composite model can retain and enhance the process knowledge, at the same time, avoid the complexity of modeling the entire process by kinetics. The estimated process states from the composite model are then fed to a wavelet network for fault detection and diagnosis. The proposed system is successfully applied to a glutamic acid fermentation process, demonstrating the feasibility and effectiveness of the proposed system.

Keywords: fault diagnosis, RBF neural network, wavelet network, parameters estimation, ferment process

1. INTRODUCTION

Fault detection and diagnosis have become important tools to ensure quality, safety, and efficiency for many process industries. The detection and diagnosis reply on the analysis and identification of differences of features (or patterns) of the process, reflected by the process states. Measurement of proper process status, typically represented by as the process states, is a prerequisite for the success of a proper fault detection and diagnosis. For a fermentation process, however, there lacks proper sensors for on-line real-time measurement of key state variables. In such cases, methods have to be developed to estimate key process states for process diagnosis.

Generally, two types of models have been developed for state estimation: first-principle based model and black-box based model such as a neural network. For fermentation process, many kinetic models have been developed, based on the principles of physics, chemistry, and biology, to reflect the generation and growing courses of the process (Liu et al., 1997). One of challenge in this type of models is to obtain proper parameters used in the model, many of which are in fact changing with time and process conditions. For example, in the growing stage of a fermentation process, process perturbations can lead to significant changes in the kinetic model parameters. However, modeling of these changes in the model parameters can be a challenging task. For this reason, model parameters are often assumed to be "constants" in many cases. This, obviously, can result in deviations of the estimated states from their true values, leading to improper diagnosis. The black-box modeling approach can map an input-output relation, without using any process knowledge. Neural networks are often used to model this input-output type of black-

box relations (Zhao et al., 1999; Maki et al., 1997). Artificial neural networks (ANNs) have also been used for fault diagnosis for fermentation process (Zhang et al., 2001; Wang et al., 1997; Abhinandan et al., 2002). A black-box model relies on process input-output information only; this type of models typically can not be extended beyond to the cases where the operating conditions are not covered by the training data. Compared to a kinetic model, a black-box model can only promote limited enhancement of process knowledge.

This paper proposes a composite modeling strategy that combines a kinetic model with a neural network model to estimate on-line process states, the estimated states are fed to a wavelet network for fault detection and diagnosis. The kinetic model used can represent the true process mechanism, retaining and enhancing the process knowledge. While the complex modeling of the changes of the kinetic model parameters with the process conditions is carried with an RBF neural network. The wavelet network is developed to analyze and recognize fault patterns, based on on-line estimation of the process states from the composite model. Finally, the proposed system, consisting of the composite model for the state estimation and the wavelet network for the diagnosis, is applied to a glutamic acid fermentation process, to demonstrate the effectiveness of the proposed method.

2. THE DESIGN OF COMPOSITE MODEL

To illustrate the method proposed in this work, a fermentation process is used with the following kinetic model.

$$\begin{aligned}
\frac{dx_1}{dt} &= \mu x_1 + K_1 \\
\frac{dx_2}{dt} &= b x_1 \frac{x_3}{K_s + x_3} \\
\frac{dx_3}{dt} &= -\frac{1}{Y_G}\mu_m x_1 (1 - \frac{x_1}{x_m}) - \frac{1}{Y_p} b x_1 \frac{x_3}{K_s + x_3} - m x_1
\end{aligned} \tag{1}$$

where $x_1(t)$, $x_2(t)$, and $x_3(t)$, representing the concentrations of biomass, substrate, product respectively, can not be measured on-line for process diagnosis. μ is the growth rate of biomass, x_m is the maximum biomass concentration, b is the maximum production rate of the acid, K_s is the saturation constant of substrate, Y_G is the yield coefficient of biomass, Y_p is the yield coefficient of product, m is the maintenance coefficient of the biomass. Y_p and μ change with the degree and the conditions of the fermentation of the process.

Fermentation is a complex process, any contamination, improper medium formulation, and improper addition of the trace element can upset the normal production, leading to process faults. In correspondence, the process states, which are represented by the concentrations of biomass, substrate, product, will change differently from a normal product to reflect the process abnormality. The kinetic model parameters, such as Y_p and μ, will change as well. To predict process states correctly, these kinetic model parameters need to be updated. It is a very complex task to model the changes of the kinetic parameters, based on the first-principles. A RBF neural network is proposed to correlate the parameter changes with the process conditions, resulting in a composite model for the state estimation. The over-all scheme for the fermentation process diagnosis is illustrated as Figure 1.

Although the kinetic parameters Y_p and μ can not be measured directly either, they may be related to some measurable process variables, such as pH, dissolved oxygen (DO), and temperature (T). In other words, these kinetic parameters may be predicted from these directly measurable variables, if their relations to these variables can be established. Using the history data collected off-line, this kind of relations may be modelled via a neural network between the measurable variables and the kinetic parameters assayed. The neural network can be used online to estimate the kinetic parameters, after it is well-trained offline.

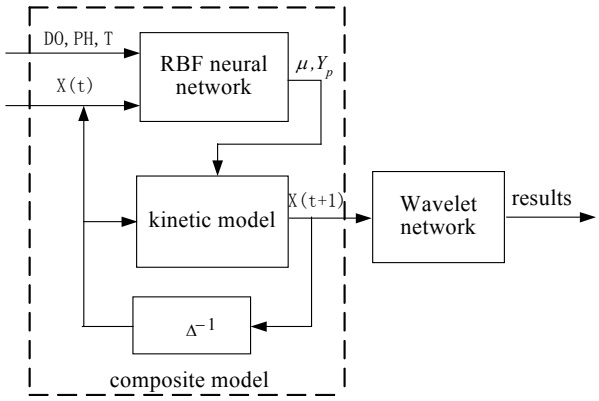

Fig. 1 Schematic of fault diagnosis strategy

Radial basis function (RBF) network, a feed forward network, is adopted for such a propose, as it has good ability of approximation and modeling (Wang , 1997; Chen, 1991). A nonlinear mapping can be realized between the input and the output of a nonlinear process as following:

$$f(X) = W_0 + \sum_{i=1}^{n} W_i * \phi(\| X - c_i \|) \tag{2}$$

where $X \in R^n$ is the vector of input, $\phi(\cdot)$ is radial basis function of $R^+ \to R$, W_i is the weights of network, c_i is the center of data, and n is the number of the center. We choose $\phi(\cdot)$ as Gauss function. Here, RBF is used to supply the estimated values of kinetic parameters for the kinetic model.

The RBF network is trained with history data consisting of pH, DO, T, the assayed values, etc. After the training, the mapping relationship has built. The composite model, composing of the trained RBF network for estimating the kinetic parameter changes and the kinetic model for estimating the states, can be used to provide state information on-line to the wavelet network for fault diagnosis as described below.

3. FAULT DIAGNOSIS

Wavelet analysis has found many applications, due its strength in analyzing transient behaviours and signal compression. It is selected here to recognize the patterns of the faults associated with the fermentation process. An evolving wavelet network (Huang et al., 2002) is chosen to capture the relationships of process states to the corresponding fault types.

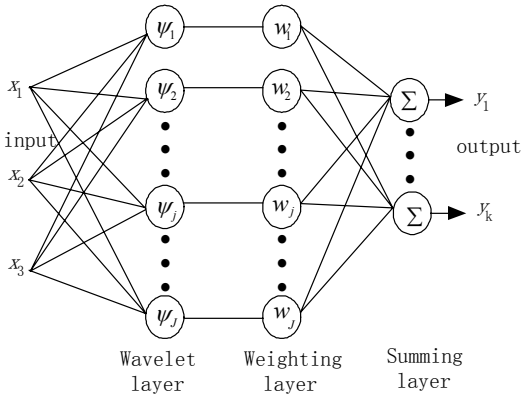

Fig. 2 Wavelet networks

The proposed wavelet networks for the fault diagnosis has a three-layer structure with a wavelet layer (input layer), weighting layer (intermediate layer), and summing layer (output layer). Each layer has one or more nodes. Figure 2 gives a schematic representation of the three-layer wavelet networks. The input data vector x, as shown in Figure 2, is the input nodes of the networks, expressed as:

$$x = [x_1, x_2, \cdots x_n]^T \quad , \tag{3}$$

where the input variables are the outputs of the composite model designed above. The activation functions of the wavelet nodes in the wavelet layer are derived from a mother wavelet $\psi(x)$. Then, the function of $\psi(x)$ can become the mother wavelet with dilation of d and translation of t

$$\psi_{d,t}(x) = 2^{d/2}\psi(2^d x - t), \qquad d, t \in Z \tag{4}$$

where Z indicates the integers. Via the operation of dilation and translation, the wavelets of (4) possess superior localization performance in both time and frequency. Since the Laplacian of the Gaussian function family meets the isotropic admissibility condition, the function of $\psi(x) = -xe^{-(1/2)x^2}$ is selected as the mother wavelet herein. Therefore, the activation function of the jth wavelet node $j = 1, 2, \cdots, J$ has the following form:

$$\psi_{d_j,t_j}(x) = -2^{d_j/2}\,(2^{d_j}x - t_j)\,e^{-0.5(2^{d_j}x - t_j)^2} \qquad d_j \;\; t_j \in Z \tag{5}$$

Each output of the weighting nodes in the weighting layer is multiplied by an appropriate weight value determined by the weighting node. In Figure 2, the weights w_{jk}, that connect the jth weighting node and the kth output node, are indicated by the weighting vectors $w_j = [w_{j1}, w_{j2}, \cdots, w_{jk}, \cdots w_{jK}]$ for $j = 1, 2 \cdots, J$ and $k = 1,2, \cdots, K$, and K is the number of the output nodes. The weighted sum of the output of J weighting nodes in the weighting layer produces the final output of the summing layer

$$y_k(x) = \sum_{j=1}^{J} w_{jk}\psi_j(x) \tag{6}$$

where $y_k(x)$ is the kth final computed output value of the networks. Note that the output $y_k(x)$ in (6) contains, implicitly, the adjustable parameters of the networks: the connection weights (w_{jk}) and the parameters, dilation (d_j), and translation (t_j) in each wavelet node.

The training algorithm for the wavelet network is as follows. The assayed data with the normal as well fault process operations are presented as the training data to the network as described above. Any output of value 1 indicates the occurrence of the fault specified by its fault type. The wavelet parameters of dilation, translation, and weighting values of the networks are determined by the evolutionary algorithm of Fogel (1994), a global-optimal approach.

4. APPLICATION EXAMPLE

The proposed diagnosis system consisting of a wavelet network for diagnosis and a composite model of on-line state estimation is put into tests with a glutamic acid fermentation process (Zhao, et al., 1999). The kinetic model of the process is described as Equation (1), where the process states of $x_1(t)$, $x_2(t)$, and $x_3(t)$ are concentrations (g / l) of biomass, glutamic acid, and glucose, respectively. They can not be measured on-line in real-time. $\mu = \mu_m x_1(1 - x_1 / x_m)$, here, $\mu_m = 0.767\ h^{-1}$ is the maximum specific growth rate, $x_m = 6.43\ (g / l)$ is the maximum biomass concentration. $b = 0.358\ h^{-1}$, $K_s = 12.04\ (g / l)$, $Y_G = 0.436$, $Y_P = 0.645$, and $m = 0.105\ h^{-1}$.

The sampling time is 45 minutes. The designed RBF network has the structure of 6-4-2. The wavelet network has three inputs and six outputs describing different process operation status (faults), the details of the wavelet outputs are described in Table 1. These outputs indicate the different fault types of the

process. During the operation, any output besides y1 with a value greater than 0.5, the corresponding process fault is assumed to have occurred.

Table 1 Definition of the output of wavelet network

output	Fault type
y1	normal
y2	poor growth
y3	thallus degradation
y4	abnormal consumption of substrate
y5	concentration abnormity
y6	contamination

The system is put into tests with a normal process operation. Figure 3 compares the estimates of the states by the composite model with the actual values obtained from the assayed data. Figure 4 is another comparison of the process states obtained by the on-line composite model with the assayed data for a poor growth operation case. In both cases, the on-line composite model can estimate the state variables well, demonstrating the application potentials of the proposed composite state estimation scheme. The fault diagnosis ability of the proposed system is also tested with these two cases. For the normal operation, the only output with a value greater than 0.5 is y1, indicating a normal operation. For the poor growth case, the only wavelet output with a value greater than 0.5 is y2, indicate the correct fault type. The time variations of the two operation cases are plotted in a single graph as Figure 5, to save the space. A comparison of the diagnoses of these two cases indicates that the proposed system can detect and make a proper diagnosis of the faults in the fermentation process.

5 CONCLUTION

A composite model combining of a neural-network model and a kinetic model has been proposed to provide on-line estimation of process states. Based on the estimation of the process states, a wavelet model has been developed for process fault detection and diagnosis. The use of the proposed composite models can avoid the complexity introduced by building a pure kinetic model for the process. At the same time, unlike a black-box model, the proposed composite model can retain the key process features as reflected by the process kinetics, this can enhance process understanding. The estimates of the process states from the composite model are fed to a wavelet network for process fault detection and diagnosis. This allows an on-line diagnosis possible, without the need of measuring on-line inaccessible state variables. The applications of the proposed system to a glutamic acid fermentation process indicate that the system can successfully recognize and discriminate faults of the process.

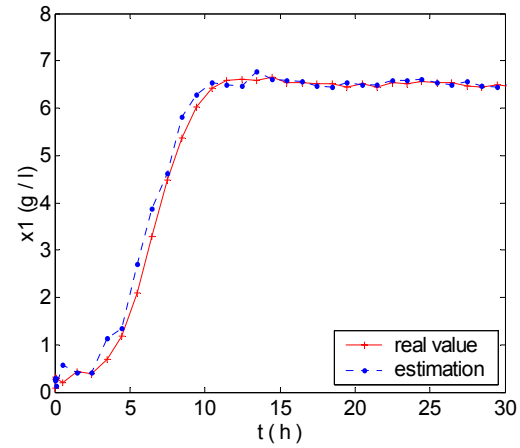

a) concentrations of biomass

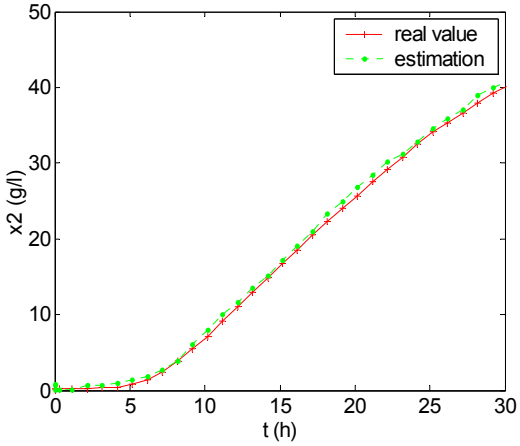

b) concentrations of glutamic acid

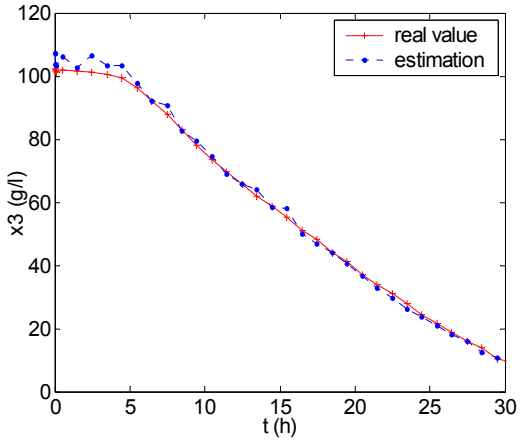

c) concentrations of glucose

Fig. 3. Comparison of state estimates and assayed values for a normal operation.

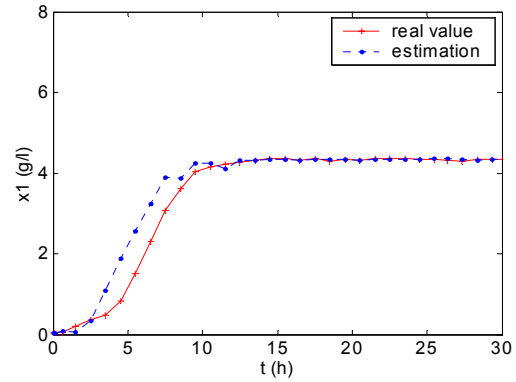

a) concentrations of biomass

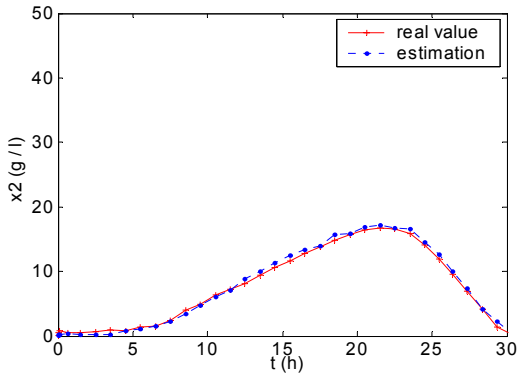

b) concentrations of glutamic acid

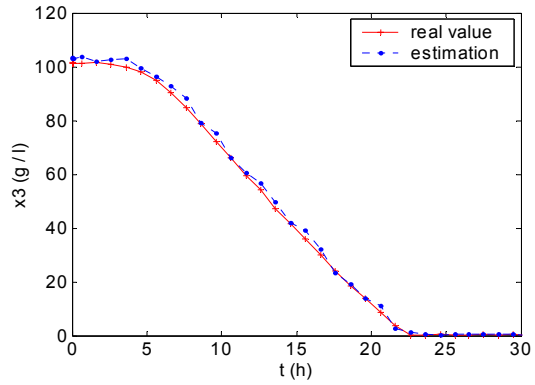

c) concentrations of glucose

Fig. 4. Comparison of state estimates with the assayed values for a faulty operation.

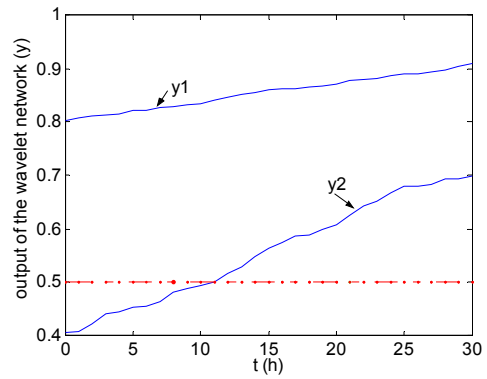

Fig. 5. The output of the diagnosis wavelet network for a normal operation (y1) and a faulty operation (y2).

REFERENCES

Abhinandan De, Nirmalendu Chatterjee (2002). Recognition of Impulse Fault Patterns in Transformers Using Kohonen's Self-Organizing Feature Map. *IEEE Transactions on power delivery*, 17(2), 489-494

Chen S.C., Cowan C.F.N., Grant P.M. (1991). Orthogonal least squares learning algorithm for radial basis function networks. *IEEE Trans. On Neural Networks*. 2(2), 302-309

D.B.Fogel (1994). An introduction to simulated envolutionary optimization. *IEEE Trans on Neural Networks*, 5, 3-14

Liu Wei, Tian Shubao (1997). A real-time method of fault diagnosis and its application to biochemical process (in Chinese). *Control and instruments in chemical industry*, 24(2), 16-21.

Hong Wang, UMIST (1997). Fault detection and diagnosis for unknown nonlinear systems: a generalized framework via neural networks. *1997 IEEE International Conference on Intelligent Processing Systems*, 1506-1510

Hua Qiang, Wang Shuqing (1996). Application of neural network model in vitamin C fermentation process (in Chinese). *Journal of Chemical Industry and Engineering*. 47(4), 433-438.

Huang Yann-Chang, Huang Chao-Ming (2002). Evolving wavelet networks for power transformer condition monitoring. *IEEE Transactions on power delivery*, 17(2), 412-416

H. Y. Zhang, C. W. Chan, K. C. Cheung, Y.J. Ye (2001). Fuzzy artmap neural network and its application to fault diagnosis of navigation systems. *Automatica*, 37, 1065-1070

Wang Xudong, Shao Huihe (1997). Modeling of nonlinear systems based on the radial basis function neural network (in Chinese). *Control Theory and Applications*. 14(1), 59-66.

Yunosuke Maki, Kenneth A. Loparo (1997). A neural-network approach to fault detection and diagnosis in industrial processes. *IEEE Transactions on control systems technology*, 5(6), 529-541.

Zhong Zhao, Xingsheng Gu, Weisun Jiang (1999). Fault detection based on wavearx neural network., *14th Triennial World Congress of IFAC*, 145-150

MULTI-PCA MODELS FOR PROCESS MONITORING AND FAULT DIAGNOSIS

Liling Ma, Yunbo Jiang, Fuli Wang

P.O.Box 131
The School of Information Science and Engineering,
Northeastern University, Shenyang, 110004, P.R.China
E-mail: maliling1974@yahoo.com.cn

and

Furong Gao

Department of Chemical Engineering
Hong Kong University of Science and Technology
Clear Water Bay, Kowloon
Hong Kong

Abstract: Multivariate statistical approaches have been proved effective for reducing the dimension of highly correlated process variables and subsequently simplifying the tasks of process monitoring and fault diagnosis. However, for the process with distinctive stages, a single statistical model is not sufficient or even incapable to map the substantive process information. In this paper, multi-PCA models are proposed for promptly detecting faults and improving the exactness of the diagnosis as well. The effectiveness of the approach is demonstrated on a complicated fermentation process.

Keywords: process monitoring; multi-PCA models; clustering technology; fault diagnosis

1. INTRODUCTION

With the ever-increasing demand of control precision, modern industrial plants become more and more complicated. As a result, the tasks of prompt detection of any abnormal process behaviour, which is caused by breakdowns or malfunctions of plant instruments or grievous working conditions, is more challenging nowadays. Traditional model-based approaches based on the assumption that the occurrence of any unexpected faults will change the physical parameters or states, are no longer applicable in most cases because of the difficulty to get the theoretical models from the control theory to setup any precise parameter estimators or state estimators (J.Zhang, et al, 1996). The knowledge-based approach known as expert system demands a deep and comprehensive understanding of the whole process (J.Zhang, et al, 1996). To setup a reasonable rule set is rather difficult and time consuming. Fortunately, with the application of modern process computers, thousands of variables can be collected and processed within a few seconds. The distributions of and correlations among these variables encapsulate precious knowledge of the plant (Theodora Kourti, et al, 1996). Thus, by analyzing the variance of the historical operating data, the characters of the plants can be learnt through multivariate statistical techniques. In recent years, data based multivariate statistical techniques, such as principal component analysis (PCA) and projection to latent structure (PLS), have received much attentions for the simplicity and practicality. Their excellent abilities in extracting the chief information of the process and casting away the noises have been fully demonstrated on many applications. By projecting the highly correlated process data onto a lower dimensional variable space without discarding any useful process information, these methods can

greatly simplify the task of process monitoring and make it easier for fault diagnosis as well (P.R.Goulding, et al ,2000). The main advantage of multivariate statistical approaches is that they are largely dependent on the historical operating data and need not have a comprehensive knowledge of the complicated process.

However, when the plant works through several different phases during a batch process, the relationships of the variables will be quite different (Svante Wold, et al, 1996). In other words, the plant will exhibit different collinear behavior in each phase. From this point, a single PCA or PLS model is not sufficient to map the whole process information. When taking different stages into consideration, the multivariate statistic confidence bounds will be inappropriately set and are always larger than needed. Consequently, the probability of failure to report the abnormal sample will be greatly increased.

The aim of this work is to overcome these annoying problems and thus improve the precision of the PCA models for prompt fault detection and diagnosis. A practical approach based on the sub-PCA models is proposed. Hyper-ellipsoid based clustering procedure is designed to categorize data. Then, supervised training approach of SOFM network is described for clustering faults features. This approach is fully demonstrated by the experiments on the fermentation process. The results show the feasibility and effectiveness of the proposed method.

2. PROCESS MONITORING AND FAULT DIAGNOSIS SCHEME

Principal components analysis was first proposed by Hotelling to analyze the correlated structures of the multi-variables. It has become one of the most popular multivariate statistical techniques and has received wide application in industrial processes. By projecting the original information onto a lower dimensional space, the principal components can summarize the chief information about the variance in the original data set (Parthasarathy Kesavan, et al, 2000). Suppose X is the original data set which is composed by m variables and k principal components are enough for summarizing the main information, X can be decomposed as the following equation:

$$X = \sum_{i=1}^{k} t_i \times p_i^{\ T} + E \qquad (1)$$

The number of proper principal components can be determined by the accumulated contributions of the principal components or cross validation. Process monitoring is based on the two statistics called T^2 and SPE (E.B.Martin, et al, 1996), which conform to F-distribution and normal distribution respectively.

$$T^2 = T_k \Lambda^{-1} T_k \qquad (2)$$

where Λ is the diagonal matrix composed of the first k eigenvalues of $X^T X$.

$$SPE = trace(R \times R^T) \qquad (3)$$

R is the residual matrix;

$$R = X - \hat{X} = X - X \times P \times P^T .$$
$$= X \times (I - P \times P^T) \qquad (4)$$

As has been discussed in Section 1， multi-PCA models are necessary for the process with distinctive stages to improve the promptness of fault detection and to ease the following fault diagnosis as well. To perform the task of the process monitoring using multi-PCA models, the data sampled from which phase should be identified first, that is, the fitness of the data to each cluster should be determined. Then the data are projected onto the related single PCA model or the combination of several PCA models and corresponding control limits are set to monitor the performance of the process. The diagram of the whole procedure is illustrated in Figure 1. This scheme is composed of three steps. At first, sampled data is classified based on hyper ellipsoid clustering technique. Then, analysing the assorted result, process monitoring is realized. If the fault is detected in this phase, the last fault diagnosis will be accomplished by SOFM network with these samples.

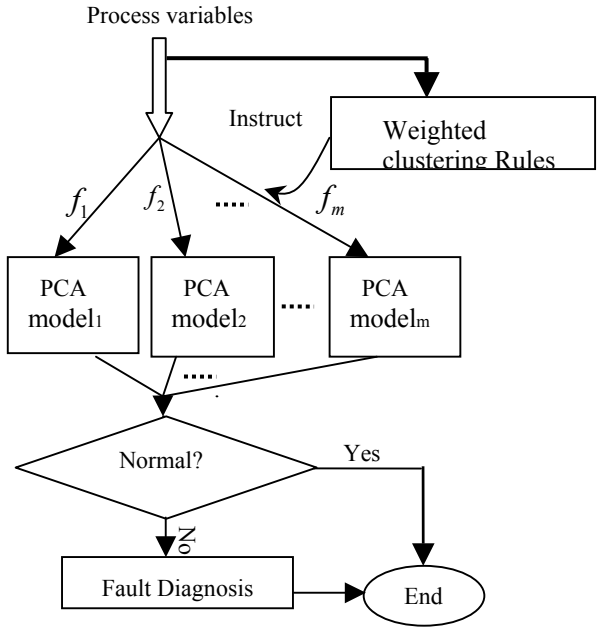

Fig1. The sketch map of the fault diagnosis

3. DESIGN OF MULTI-PCA MODELS

The core of building multi-PCA models is how to classify sampling data currently. A proper clustering technique is fundamental for reasonable decision-making. Former researches have investigated various clustering techniques ranging from simple identical sphere windows with fixed centres to intelligent approaches using neural networks, such as RBFN and SOFMN. In practical, the distribution of each group is not necessary of the same size, so the identical sphere windows will not work in most cases. Though clustering techniques using NN are powerful at processing nonlinear information and some have excellent self-learning ability in determining the numbers of the clusters, to assign the proper neurons and to train the weights of the NN are rather tough work. For example, when training the RBFN, to

select the centres of the radial basis functions of hidden neurons and to determine their widths are indeed demanding jobs (Gao Daqi, et al, 2001). Further more, the more the input variables, the more complicated of the NN structure; clustering the newly sampled data would be time-consuming because of the over-burden computing procedure.

K-means clustering approach is a well-developed technique. Currently the trial-and-error method is adopted to determine the number of the clusters. However, it is based on the Euclid distance and the data of the same cluster are confined within a hyper-sphere. Since the variance of each variable is not necessary of the same size, the bounds of the clusters should be hyper-ellipsoid rather than hyper-sphere. The traditional K-means clustering approach based on the hyper-sphere bound, improper classification of the data often happens (Johnston, et al, 1994).

To reduce the probability of the misclassification, a set of clustering rules are suggested in this paper. First, suppose the number of the clusters is known according to the knowledge of the character of the process, use K-means clustering algorithm to grossly divide the data set into several clusters. (If the number of the clusters is not known, adopt the trial-and-error method to determine the number of the clusters.) Then analyze the variance of each cluster and adjust its bound. The following procedures are detailed as follows:

Find out the direction, along which the variance is the largest, and then the next. Those directions are orthogonal to each other. Project the original data onto each direction and find the centre of the projection. In fact, the first direction contains the largest amount of the information of the process and the main information of the process can be expressed by the first few projections. The information contained in the last few projections can often be explained as noise. When there are many variables and the variances along the last few directions are small, those projections can be neglected. The whole process is similar to the procedure of subtracting principal components. The bounds of the clusters are hyper-ellipsoids whose axes are overlapped with the principal variance directions. The size of the hyper-ellipsoid can be determined according to statistical confidence level.

After finding out the directions, the fitness μ of the data X to each cluster is measured by following equation:

$$\mu = \frac{1}{S_\alpha} \times T^2 \tag{5}$$

where T^2 is Hotelling's statistic:

$$T^2: \quad T^2 = T_k \Lambda^{-1} T_k \tag{6}$$

where Λ is the diagonal matrix composed of the first k eigenvalues of $X^T X$. T_k is the first k principal components, $T^2 \in R^{1\times k}$. T^2 obeys F distribution. Define S_α based on F_α as follows:

$$S_\alpha = \frac{k(n-k+1)}{n(n-k)} \times F_\alpha(k, n-k) \tag{7}$$

where n is the size of the cluster, k is the dimension of the original data or the number of the principal components and α is the confidential level , here, $\alpha = 0.95$. $\mu = 1$ represents the hyper-elliptic bound. If $\mu < 1$, it means the data is in the inner of the bound. Any samples falling into the clustering bound can be regarded as the same type. Then reclassify the data set and adjust the chief variance directions and centres, repeat the former steps until the classification of each data will not change.

The advantages of the clustering technique based on hyper-elliptic bound are illustrated by a simple two-dimensional clustering problem in Figure1. Figure1a) demonstrates the clustering results by pure K-means and Figure1b) shows the clustering results based on elliptic bound. From the distribution of the samples, sample 125 is far away from the other samples in cluster B and it is more reasonably be classified as singularity as sample 117 and 115 etc. Sample 85 should be classified to cluster B though its Euclid distance from the centre of B is farther than that from the centre of A. From the above, the clustering based on the hyper-elliptic bound can overcome the shortcoming of the traditional K-means clustering approach.

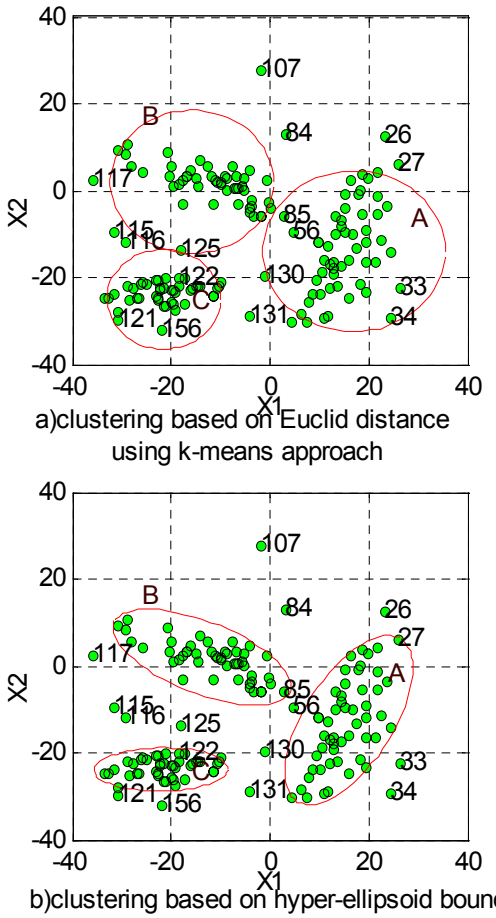

Fig 2 Comparison of the two clustering techniques

Thus, using the clustering method proposed above, multi-PCA models for process monitoring and fault diagnosis are built as follows:

$$X^{(k)} = T^{(k)} P^{(k)^T} = \sum_{i=1}^{m} t^{(k)}{}_i \; p^{(k)}{}_i{}^T + E^{(k)}{}_m \qquad (8)$$

Where k presents the kth sub-PCA model. These sub models make up the multi-PCA models.

4. PROCESS MONITORING USING MULTI-PCA MODEL

When a new sample comes during process monitoring, the data samples from which phase should be identified first, that is, the fitness of the data to each sub-PCA model should be determined. Then the data are projected onto the related single PCA model or the combination of several PCA models and corresponding control limits are set to monitor the performance of the process.

The smaller the T^2 to the cluster, the better of the fitness to that cluster. Certainly, most of the data sampled during each phase can be clearly classified. However, since the process is continuous, the transitory data are likely to contain both characters of the neighbor clusters. When the cluster bounds are rigidly set, some transitory data will be likely classified as singularities. On the other hand, the probability of misclassification will be increased. To solve this problem, fuzzy-clustering rules are proposed (Yang Yinghua, et al 2002). Two bounds of a cluster are suggested and their sizes are determined by two radius, namely, kernel radius and class radius. Here, we can also set two hyper-elliptic clustering bounds based on different confidence levels:

Class bound: $\frac{1}{S_{0.99}} \times T^2 = 1$. (9)

Kernel bound: $\frac{1}{S_{0.90}} \times T^2 = 1$ (10)

The fitness of the samples to each cluster can be computed by the following rules:

1) If T^2 statistic of the new sample falls into one of the kernel bounds, that is, $\frac{1}{S_{0.90}} \times T^2 \le 1$, the fitness of the sample to the cluster can be assigned to 1;

2) If $1 < \frac{1}{S_{0.90}} \times T^2$ and $\frac{1}{S_{0.99}} \times T^2 \le 1$, and T^2 is beyond any other class bound, the fitness of the sample to the cluster can also be assigned to 1.

3) If T^2 falls into the overlapped area of several class bounds, suppose the new T^2 statistic falls into m clusters, define

$$L_1 = \frac{1}{S_{0.99}} \times T_1^2, \ldots, L_m = \frac{1}{S_{0.99}} \times T_m{}^2 \qquad (11)$$

obviously $L_1, \ldots, L_m < 1$, the smaller the L_k, the closer of the new sample to the kernel of the cluster. The fitness of the new sample to each related cluster can be defined as follows:

$$f_i = \frac{1/L_i}{\sum_{k=1}^{m} 1/L_k} \qquad (12)$$

4) If T^2 statistic falls into neither class bounds, it can be regarded as a singularity.

If the new sample is regarded as totally subjected to one classification, the procedure of the monitoring is the same as that based on a single PCA models. When the new comer falls into the common region of several regions, the fitness to each cluster is computed according to equation (12) first. Then adjust the directions of the principal components based on its fitness to each clusters (Yang Yinghua, et al 2002):

$$P = \sum_{i=1}^{m} f_i \times p_i \qquad (13)$$

here $\sum_{i=1}^{m} f_i = 1$ and p_i is the principal components directions of each sub-PCA models. The principal components can be achieved by projecting the original data on subspace explained by P. The SPE control limit is computed as follows:

$$U_{SPE} = \sum_{i=1}^{m} f_i \times U_{SPEi} \qquad (14)$$

5. FAULT DIADNOSIS USING SOFM NETWORK

When a fault is detected by previous step, SOFM is used to diagnose the fault, dealing with the current sample data as inputs. SOFM neural network was originally developed by a Finland scientist Kohonen. It is similar to the memory mode of the human beings. Different to other kinds of neural network, the information of one pattern is not memorized by one cell in SOFM neural network, but by a set of neurons in certain region. The excited region in the network is like a Mexican Hat, with the central neuron cell being most excited when stimulated by the corresponding pattern. The excitement of the neuron nearby reduces and the neurons outside this region are restrained. Further more, the distribution of the weight vectors reflect the statistical characters of the input mode. When reminiscing, pattern classification is mainly based on the most excited neuron.

The chief advantage of the SOFM is its self-learning ability. It can automatically categorize the input mode without supervision. When the former knowledge of the clusters is not sufficient, SOFMNN is adept at extracting the character of each cluster through self-organized learning. The structure of the network is composed of two layers, input layer and output layer. The output layer is a competing layer in the form of two-dimensional array. The structure of the network is shown in Figure 3.

The training algorithm can be found in many literatures. The adjustment of the connection weights is based on the following equation:

$$W_{k+1} = \begin{cases} W_k + \eta(k)[U_k - W_k] & j \in N_k \\ W_k & j \notin N_k \end{cases} \qquad (15)$$

where N_k is the neighbor field, $\eta(k)$ is the learning factor. N_k begins with a large area and contains all the neurons from the origin, and then shrinks to only contain one to two neurons from the centre (C.W.Chan, et al, 2001):

$$N_k = int\left[N_0 \times \left(1 - \frac{k}{K}\right)\right] \quad (16)$$

The learning speed also reduces with the increase of k. It can be adjusted according to the following equation:

$$\eta(t) = \eta_0 \times exp\left(-\frac{k}{K}\right) \quad (17)$$

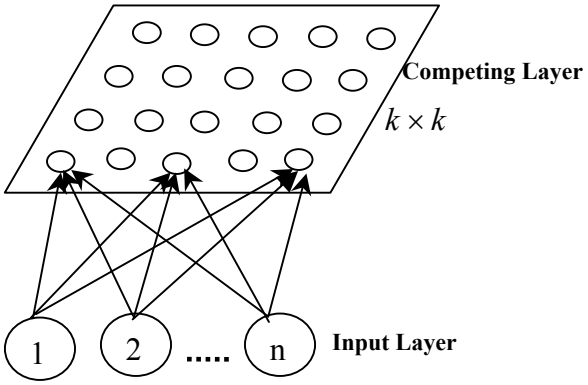

Fig 3. The structure of SOFM network

6. CASE STUDY ON FERMENTATION PROCESS

The fermentation plant for producing glutamic-acid is introduced to evaluate the approach proposed in this paper. It experiences three distinct phases, namely, the growing phase, fermenting phases and perishing phase. The acidity and the amount of dissolved oxygen have different characters in three phases. In the growing phase, the acidity increase slowly with the production of glutamic-acid. The demand for dissolved oxygen increase too. In the following fermenting phase, with a large number of glutamic-acid being produced, the PH value decrease quickly and the demand for dissolved oxygen increase markedly. When the production peak passes away, the acidity falls slightly. So in this experience, the PH value and the amount of the dissolved oxygen as well as their tendencies are used for pattern classifications(Xu Ling, et al, 1999). Three hyper-ellipsoids are defined for classification on the historical normal operating data. In this experiment, the class hyper-elliptic bound is set based on 0.99 confidence level and the kernel bound based on 0.90 confidence level. The distribution of the historical normal operating data and the clustering bounds for each clusters are illustrated in Figure4.

Based on the classification, three PCA models are developed for monitoring. Seven variables are used while analyzing the fermenting process. They are PH value, dissolved oxygen density (DO), the changing rate of DO, temperature of the fermenting environment, the inflow of the atmosphere, the position of the outlet valve and the pressure of the fermenting environment. Figure 5 and Figure 6 show the performance of the PCA models when monitoring a normal process and detecting the occurrence of the fault1 and fault2 using single PCA model and multi-PCA models respectively. Fault1 represents the failure of outlet valve. The solid line in the figures represents the control limits based on 0.99 confidence level and the dash based on 0.90 confidence level. The plus signs represent the abnormal samples identified during clustering. The diamond signs represent the samples falling into the overlapped regions of the clusters' class bounds.

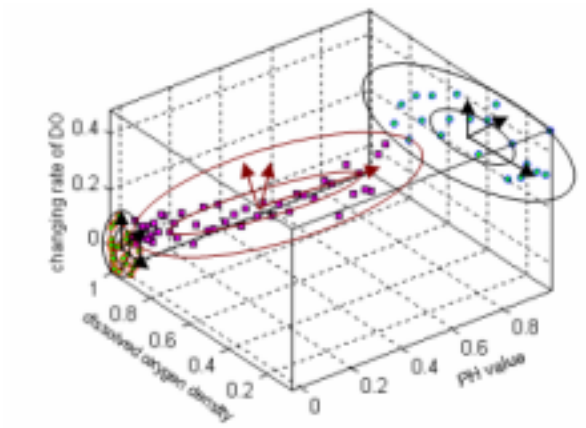

Fig. 4 Clustering illustration of fermentation plant

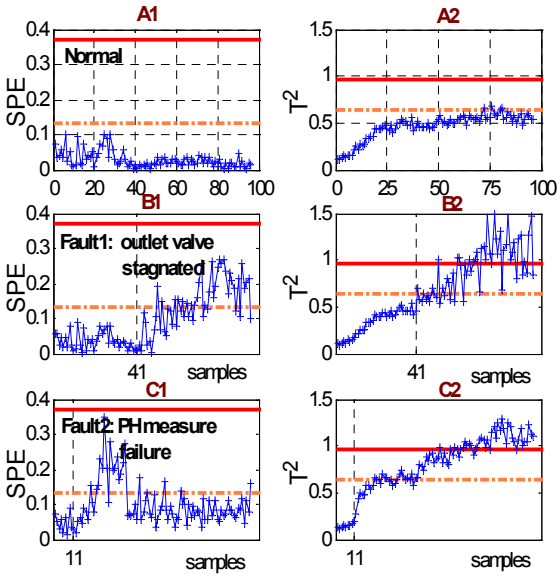

Fig.5 Process monitoring using single PCA model

When the pressure inside the fermentation is out of control, there is a contamination. As a result, the PH value will be affected too. Fault2 simulated a sensor failure, that is, the PH instrument doesn't work. When the faults occur, the correlated structure of the data will be changed, the two T^2 and SPE statistics will be out of control theoretically. However, since the fermentation plant contains three distinct phases, whose correlated variable structures are quite different, the bound of the control is difficult to be adjusted. It is obviously that the SPE control limit is lager than needed during the fermenting phases and perishing phases, which leads to the failure to report the Fault2 illustrated in the C1 sub-chart. The

T^2 control limit is also inappropriately set for the growing phase. From Figure6, the precision of the monitoring models is greatly improved when using multi-PCA models and consequently the promptness of detecting faults is improved too.

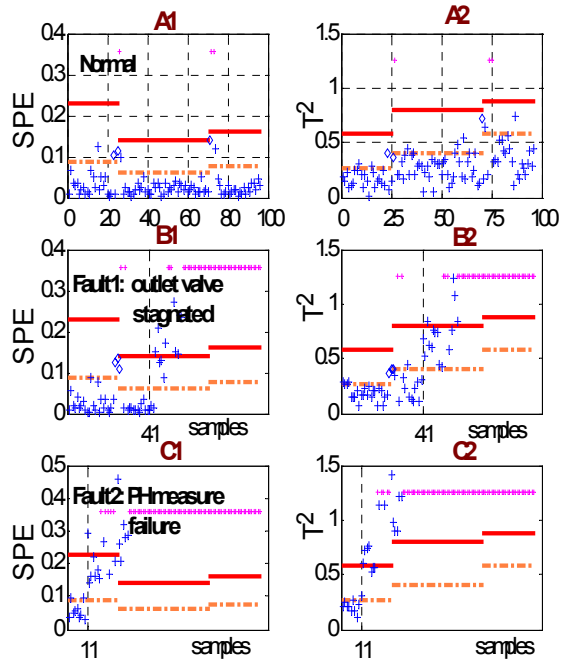

Fig.6 Process monitoring using multi-PCA models

Figure 7 shows the results of fault classification. Choose a 8×8 array of neurons to compose a competing layer and select the tendency of the PH value and DO, temperature, pressure etc. as the input of the SOFM network. After training, three regions of neurons are stimulated corresponding to three pattern inputs. When the Fault1 is detected and the current sampled data is input to the SOFM network, the 18th neuron or the neurons nearby will be the most excited according to the reminiscence. The Fault2 data will stimulate the neurons with the centre of 13th neuron. The results of Figure 7 show that the corresponding faults can be diagnosed exactly.

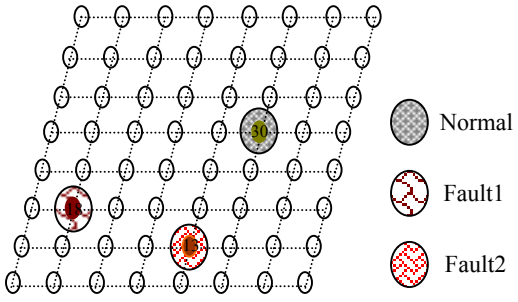

Fig.7 Illustration of faults classification on SOFMN's competing layer

6. CONCLUSIONS

Multivariate statistical approaches have received widely application for the processes rich in measurement data. However, for those the data structures are quite different in different stages, setting proper control limits is difficult. In this paper, multi-PCA models are suggested. Process monitoring is based on the combinations of related sub-PCA models and the weigh of each sub-PCA model is assigned according to the weighted clustering technique. Fault classification is realized by SOFM network. The feature of the fault can be stored in the weights of the network through self-organize learning. The effectiveness of the proposed approach is demonstrated by the experiment on fermentation process.

REFERENCES

C.W.Chan, Hong Jin, K.C.Cheung (2001) Fault Detection of Systems with Redundant Sensors using Constrained Kohonen Networks. *Automatica*. 37, 1671-1676.

E.B.Martin, A,J,Morris (1996). Process Performance Monitoring Using Multivariate Statistical Process Control. *IEE Proc-Control Theory Appl.* 143 (2), 132-144.

Gao Daqi, Yang Genxing, (2001). Basic Principles of Pattern Classification Methods Based on Improved RBF Neural Networks. *Journal of East China University of Science and Technology*. 27(6), 667-683.

Johnston, L.P.M.; Kramer, M.A. (1994). Probability Density Estimation Using Elliptical Basis Functions. *AJCHE J*. 40, 1639.

J.Zhang, E.B.Martin, A.J.Morris(1996).Fault Detection and Diagnosis Using Multivariate Statistical Techniques. *Trans IchemE*. 74, Part A, January, 89-96.

Parthasarathy Kesavan, Jay H.Lee (2000). Partial Least Squares(PLS) Based Monitoring and Control of Batch Digests. *Journal of Process Control*, 10, 229-236.

P.R.Goulding, B.Lennox, (2000). Fault Detection in Continuous Processes Using Multivariate Statistical Methods. *International Journal of Systems Science*,.31 (11), 1459-1471.

Svante Wold, Nouna Kettaneh (1996). Hierarchical Multi-block PLS and PC Models for Easier Model Interpretation and as an Alternative to Variable Selection. *Journal of Chemo-metrics*. 10, 463-482.

Theodora Kourti, Jennifer Lee (1996). Experiences With Industrial Applications of Projection Methods for Multivariate Statistical *Process Control. Computers chem. Engng*. 20, S745-S750.

Xu Ling, Xu Wenbo, (1999) The Fuzzy PID Control for Dissolved Oxygen in Fermentation Process. *Process Automation Instrumentation*.20, 3-7.

Yang Yinghua, Lu Ningyun, Wang Fuli (2002) Statistical Process Monitoring Using Multiple PCA Models. *American Control Conference (ACC02)*. 5072-5073.

A FAULT ACCOMMODATION CONTROL FOR NONLINEAR PROCESSES

Yingwei Zhang, Fuli Wang, Ge Yu
School of Information Science & Engineering, P.O.Box 135,
Northeastern University, Shenyang, Liaoning, 110004
P. R. China
Email address: zhang_yingwei2001@yahoo.com.cn
and
Furong Gao
Department of Chemical Engineering
Hong Kong University of Science & Technology
Clear Water Bay, Kowloon, Hong Kong

Abstract: An active fault accommodation control law is developed for a class of nonlinear processes to guarantee the closed-loop stability in the presence of a fault, based on a neural network representation of the dynamics due to faults. Applications of the proposed design indicate that the fault accommodation control law is effective for a typical nonlinear fermentation process.

Keyword: Neural networks, fault-accommodation, corrective control law

1. INTRODUCTION

The study of fault diagnosis and fault-tolerant control has attracted much attention recently [1-8], due to the industrial demands for safety and efficiency. For certain processes, it is important not only to detect (and identify) but also to accommodate any faults quickly. Fault-tolerant controls have been developed to keep such processes in control, in spite of the occurrence of a fault. Based on the nature of its design, a fault-tolerant control can be categorized into the passive or active two types. A passive fault-tolerant control uses the same control scheme before and after fault, without specific accommodating parameters, typically by introducing a conservative law. For an active fault-tolerant control, a control reconfiguration takes place, following the diagnosis of a fault, to counteract any dynamic changes caused by this fault.

Within the category of the passive fault-tolerant controls, reliable control is widely used. Results and scheme details can be found in references [3-5]. Robust control design is often adopted for reliable control to have the guaranteed closed-loop stability and H_∞ performance. This type control is typically conservative, without controller adjustment after detection of a fault; the tolerance comes at the cost to the control performance.

In an active fault-tolerant control, faults are accommodated, typically by a reconfiguration of the feedback control law. An excellent overview on the subject has been given by Patton [6]. Faults are typically associated with sensors and actuators failures; in correspondence, respective accommodation strategies can be so designed. For examples, sensor fault accommodations for MIMO systems have been discussed by Tortora [7]; actuator fault accommodations are given by Michael [8]. Adaptive approaches have also been used in fault tolerant controls. For examples, an adaptive compensation method for actuator fault with known plant dynamics has been formulated by Boskovic [9]; and a nonlinear adaptive fault accommodation controller has been designed by Idan [10] to make use of redundancy.

In this paper, a new fault accommodation control design is presented for a class of uncertain nonlinear processes. The dynamic changes due to faults are represented by a neural network, based on which an adaptive corrective control law is formulated to ensure the system stability.

The remainder of the paper is organized as follows. The problem statement and its assumptions are given in section 2, followed by the formulation of our controller and its relevant proofs in section 3. An illustrative example is given in section 4 to demonstrate the effectiveness of the proposed method. Finally, conclusions are drawn in section 5.

2. PROBLEM STATEMENTS

Consider a system described as:

$$\dot{x} = \zeta(x) + \Delta\zeta(x) + G(x)[u + \Delta g(x)] + \beta(t-T)f(x) \quad (1)$$

where $x \in R^n, u \in R^m$ are the state and input of the system, respectively, $\Delta\zeta(x)$ and $\Delta g(x)$ are the model uncertainty in the normal operation,

The paper was supported in part by Liaoning Natural Science Foundation of China(002013).

f characterizes the changes in the dynamics due to a failure. The normal system, in the absence of any faults, is described by

$$\dot{x} = \zeta(x) + \Delta\zeta(x) + G(x)[u + \Delta g(x)] \quad (2)$$

The nonlinear fault function f is multiplied by a switching function $\beta(t-T)$,

$$\beta(t-T) = diag\,(\beta_1(t-T), \beta_2(t-T), \cdots, \beta_n(t-T)) \quad (3)$$

where $\beta_i(t-T) = \begin{cases} 0 & if \quad t < T \\ 1 & if \quad t \geq T \end{cases}$, $i = 1, 2, \cdots, n$.

where T is the fault occurrence time. The problem considered is as follows:

Fault accommodation (FA) problem: Given system (1), design a control u_N for the normal system, and an additional control u_F for fault compensation, so that $u = u_N + u_F$ as the new control after the occurrence of a fault can guarantee the resulted closed-loop nonlinear system to be stable.

The following assumptions are used.

Assumption 1: There exists $u = u^a(x)$ and Lyapunov function $\overline{V}(x)$, such that

$$k_1|x|^2 \leq \overline{V}(x) \leq k_2|x|^2, \quad (4)$$

$$\frac{\partial \overline{V}(x)}{\partial x}\left(\zeta(x) + G(x)u^a(x)\right) \leq -k_3\left|\frac{\partial \overline{V}(x)}{\partial x}\right|^2 \quad (5)$$

$$\leq -k_4\overline{V}(x),$$

where $k_1, k_2, k_3, and\ k_4$ are positive constants.

Assumption 2: For system (1)

$$\|\Delta g(x)\| \leq \xi(x) \quad (6)$$

$$\left\|\left(\frac{\partial \overline{V}(x)}{\partial x}\right)^T \Delta\zeta(x)\right\| \leq \rho(x)$$

where $\dfrac{\rho(x)}{\left\|G^T(x)\left(\dfrac{\partial \overline{V}(x)}{\partial x}\right)\right\|}$ is continuous,

$\xi(\bullet)$ and $\rho(\bullet)$ are known and continuous.

Remark 1: From assumption 2, we have $\rho(x) = 0$, if $G^T(x)\left(\dfrac{\partial \overline{V}(x)}{\partial x}\right) = 0$.

3. FAULT ACCOMMODATION

Firstly, let's use a neural network to represent fault function $f(x)$. Where, x is the input vector to the neural network. It can be shown that there exists an optimized matrix W^* such that $\left|f(x) - W^*S(x)\right| \leq \varepsilon$ is satisfied for any given $\varepsilon > 0$. $S(x)$ is the sigmoid function. $W^*S(x)$ can approximate $f(x)$ to any degree of accuracy, with bounded W^*, $\|W^*\| \leq M_W$. With the above, system (1) can be rewritten as:

$$\dot{x} = \zeta(x) + \Delta\zeta(x) + G(x)[u + \Delta g(x)] + W^*S(x) + \varepsilon(x) \quad (7)$$

where, $\varepsilon(x) = \left|f(x) - W^*S(x)\right| \leq \varepsilon$ is the estimation error. If we denote W as the estimate of the uncertain weight matrix W^*, then

$$\dot{x} = \zeta(x) + \Delta\zeta(x) + G(x)[u + \Delta g(x)] - \widetilde{W}S(x) + WS(x) + \varepsilon(x) \quad (8)$$

where $\widetilde{W} = W - W^*$ and it has the appropriate dimension..

Theorem 1: Under assumptions 1 and 2, we can design a controller in the form of the following:

$$u = u_N + u_F \quad (9)$$

$$u_N = u^a + u^b + u^c$$

where u^a is given by assumption 1, and let

$$E = \left\{ x \;\middle|\; G(x)^T \frac{\partial \overline{V}(x)}{\partial x} = 0 \right\},$$

$$u^b = \begin{cases} -\dfrac{G^T(x)\dfrac{\partial \overline{V}(x)}{\partial x}}{\left\|G^T(x)\dfrac{\partial \overline{V}(x)}{\partial x}\right\|}\xi(x), & x \notin E \\ 0 & x \in E \end{cases}, \quad (10)$$

$$u^c = \begin{cases} -\dfrac{G^T(x)\dfrac{\partial \overline{V}(x)}{\partial x}}{\left\|G^T(x)\dfrac{\partial \overline{V}(x)}{\partial x}\right\|^2}\rho(x), & x \notin E \\ 0 & x \in E \end{cases}, \quad (11)$$

$$u_F = \frac{G^T(x)WS(x)}{\lambda[1 + \|G(x)\|^2]} + \frac{G^T(x)\Theta}{\lambda_1[1 + \|G(x)\|^2]}. \quad (12)$$

Where $\Theta \in R^{n \times L}$ and $\Theta = [\theta, 0, \cdots, 0]^T$. Then, the state x is ultimately consistently bounded by the set:

$$D = \left\{ x \in R^n : v_0(x) \leq \frac{\mu}{k_0\alpha}, \frac{\bar{k}_2}{\bar{k}_1} \leq k_0 \leq 1 \right\}, \quad (13)$$

with the following adaptive weight update law

$$\dot{W} = \begin{cases} 2k_0\dfrac{\partial v_0}{\partial x}S^T(x) & if \|W\| < M_W \\ -\beta W + 2k_0\dfrac{\partial v_0}{\partial x}S^T(x) & if \|W\| \geq M_W \end{cases}, \quad (14)$$

$$\dot{\theta} = -\gamma_1\theta + k_0\left|\frac{\partial v_0}{\partial x}\right|. \quad (15)$$

The parameters of $\lambda, \lambda_1, \bar{k}_1, \bar{k}_2, \alpha, and\ \mu$ can

be determined as in the proof. The proof of the above theorem is divided into the following two steps: step 1, we prove that there exist a nominal controller $u_N = u^a + u^b + u^c$ and a Lyapunov function $v_0(x)$ for the normal system described by $\dot{x} = \zeta(x) + \Delta\zeta(x) + G(x)[u + \Delta g(x)]$, such that the closed-loop of the normal system is stable; step 2, we prove that the state x is ultimately consistently bounded, using the control law stated in the theorem.

Proof: step 1

Substituting the controller equations of (9-12) into system （1）, we have:

$$\dot{x} = \zeta(x) + \Delta\zeta(x) + G(x)[u^a + u^b + u^c + \Delta g(x)]$$

Define a positive function $v_0(x) = \overline{V}(x)$, then we have:

$$\dot{v}_0(x) = (\frac{\partial \overline{V}(x)}{\partial x})^T(\zeta(x) + G(x)u^a) + (\frac{\partial \overline{V}(x)}{\partial x})^T G(x)(u^b + \Delta g(x)) + (\frac{\partial \overline{V}(x)}{\partial x})^T(\Delta\zeta(x) + G(x)u^c)$$

From Assumption 1, we have

$$(\frac{\partial \overline{V}(x)}{\partial x})^T(\zeta(x) + G(x)u^a) \le -k_3\left|\frac{\partial \overline{V}(x)}{\partial x}\right|^2 \quad (16)$$

From Assumption 2 and the structure of $u^b(x)$, we have

$$(\frac{\partial \overline{V}(x)}{\partial x})^T G(x)(u^b + \Delta g(x)) = (G^T(x)\frac{\partial \overline{V}(x)}{\partial x_i})^T(u^b + \Delta g(x)) = 0$$

when $x \in E$, and

$$(\frac{\partial \overline{V}(x)}{\partial x})^T G(x)(u^b + \Delta g(x))$$
$$= (\frac{\partial \overline{V}(x)}{\partial x})^T G(x)(-\frac{G^T(x)\frac{\partial \overline{V}(x)}{\partial x}}{\left\|G^T(x)\frac{\partial \overline{V}(x)}{\partial x}\right\|}\xi(x) + \Delta g(x))$$
$$= -\left\|G^T(x)(\frac{\partial \overline{V}(x)}{\partial x})^T\right\|\xi(x) + (\frac{\partial \overline{V}(x)}{\partial x})^T G(x)\Delta g(x)$$
$$\le -\left\|G^T(x)(\frac{\partial \overline{V}(x)}{\partial x})^T\right\|\xi(x) + \left\|(\frac{\partial \overline{V}(x)}{\partial x})^T G(x)\right\|\|\Delta g(x)\|$$
$$\le 0,$$

when $x \notin E$. Hence

$$(\frac{\partial \overline{V}(x)}{\partial x})^T G(x)(u^b + \Delta g(x)) \le 0 \quad (17)$$

From Assumption 2 and structure of $u^c(x)$, we have

$$(\frac{\partial \overline{V}(x)}{\partial x})^T(\Delta\zeta(x) + G(x)u^c)$$
$$= (\frac{\partial \overline{V}(x)}{\partial x})^T\Delta\zeta(x) + (G^T(x)\frac{\partial \overline{V}(x)}{\partial x_i})^T u^c$$
$$\le \left\|(\frac{\partial \overline{V}(x)}{\partial x})^T\Delta\zeta(x)\right\| \le \rho(x) = 0,$$

when $x \in E$, and

$$(\frac{\partial \overline{V}(x)}{\partial x})^T(\Delta\zeta(x) + G(x)u^c)$$
$$= (\frac{\partial \overline{V}(x)}{\partial x})^T\Delta\zeta(x) + (\frac{\partial \overline{V}(x)}{\partial x})^T G(x)(-\frac{G^T(x)\frac{\partial \overline{V}(x)}{\partial x}}{\left\|G^T(x)\frac{\partial \overline{V}(x)}{\partial x}\right\|^2}\rho(x))$$
$$\le \left\|(\frac{\partial \overline{V}(x)}{\partial x})^T\Delta\zeta(x)\right\| - \rho(x)$$
$$\le 0,$$

When $x \notin E$. Hence

$$(\frac{\partial \overline{V}(x)}{\partial x})^T(\Delta\zeta(x) + G(x)u^c) \le 0 \quad (18)$$

Thus, we obtain the results

$$\dot{v}_0(x) \le -k_3\left|\frac{\partial \overline{V}(x)}{\partial x}\right|^2 \quad (19)$$

From (19), the stability of the normal system is proven.

Proof: step 2:

Define a Lyapunov function for system 1 of the following form:

$$V(x, \widetilde{W}, \widetilde{\theta}) = k_0 v_0(x) + \frac{1}{2}tr\{\widetilde{W}^T\widetilde{W}\} + \frac{1}{2}\widetilde{\theta}^2 \quad (20)$$

with $\widetilde{\theta} = \theta - \varepsilon$,then the derivatives of V is

$$\dot{V} = k_0\frac{\partial v_0}{\partial x}\{f(x) + \Delta f(x) + G(x)[u^a + u^b + u^c + \Delta g(x)]\} + k_0\frac{\partial v_0}{\partial x}g(x)u^F - k_0\frac{\partial v_0}{\partial x}\widetilde{W}S(x) + k\frac{\partial v_0}{\partial x}WS(x) + k_0\frac{\partial v_0}{\partial x}\varepsilon(x) + tr\{\dot{W}^T\widetilde{W}\} + \widetilde{\theta}\dot{\theta} \quad (21)$$

Using (14), we obtain

$$\dot{V} = k_0\dot{v}_0 + k_0\frac{\partial v_0}{\partial x}G(x)u^F + k_0\frac{\partial v_0}{\partial x}WS(x) + k_0\frac{\partial v_0}{\partial x}\varepsilon(x) - \beta I_W tr\{W^T\widetilde{W}\} + \widetilde{\theta}\dot{\theta}$$

where I_W is the indicator function of W, and it satisfies

$$I_W = \begin{cases} 1 & if\ \|W\| \ge M_W \\ 0 & if\ \|W\| < M_W \end{cases} \quad (22)$$

As $tr\{W^T\widetilde{W}\} = \frac{1}{2}\|W\|^2 + \frac{1}{2}\|\widetilde{W}\|^2 - \frac{1}{2}\|W^*\|^2$, then

$$\dot{V} = k_0\dot{v}_0 + k_0\frac{\partial v_0}{\partial x}G(x)u^F + k_0\frac{\partial v_0}{\partial x}WS(x) + k_0\frac{\partial v_0}{\partial x}\varepsilon(x) - \frac{\beta}{2}tr\left\{\tilde{W}^T\tilde{W}\right\} + \frac{\beta}{2}(1-I_W)tr\left\{\tilde{W}^T\tilde{W}\right\} - \frac{\beta}{2}I_W\|W\|^2 + \frac{\beta}{2}I_W\|W^*\|^2 + \tilde{\theta}\dot{\theta} \quad (23)$$

By substituting u^F (λ, λ_1) into (23), from Assumption 1, the derivatives of V satisfies that

$$\dot{V} \le -k_0k_3\left|\frac{\partial v_0}{\partial x}\right|^2 + k_0\left|\frac{\partial v_0}{\partial x}\right|\frac{\|G(x)\|^2\|W\|S(x)}{\lambda[1+\|G(x)\|^2]} + k_0\left|\frac{\partial v_0}{\partial x}\right|\|W\|S(x) + k_0\left|\frac{\partial v_0}{\partial x}\right|\frac{\|G(x)\|^2|\theta|}{\lambda_1[1+\|G(x)\|^2]} + k_0\left|\frac{\partial v_0}{\partial x}\right|\varepsilon(x) + \tilde{\theta}\dot{\theta} - \frac{\beta}{2}tr\left\{\tilde{W}^T\tilde{W}\right\} + \frac{\beta}{2}(1-I_W)tr\left\{\tilde{W}^T\tilde{W}\right\} - \frac{\beta}{2}I_W\|W\|^2 + \frac{\beta}{2}I_W\|W^*\|^2 \quad (24)$$

As $\frac{\|G(x)\|^2}{1+\|G(x)\|^2} \le 1$, (24) can be rewritten as

$$\dot{V} \le -k_0k_3\left|\frac{\partial v_0}{\partial x}\right|^2 + k_0\left|\frac{\partial v_0}{\partial x}\right|\|W\|S(x)\left(1+\frac{1}{\lambda}\right) + k_0\left|\frac{\partial v_0}{\partial x}\right|\frac{|\theta|}{\lambda_1} + k_0\left|\frac{\partial v_0}{\partial x}\right|\theta - k_0\left|\frac{\partial v_0}{\partial x}\right|\theta + k_0\left|\frac{\partial v_0}{\partial x}\right|\varepsilon + \tilde{\theta}\dot{\theta} - \frac{\beta}{2}tr\left\{\tilde{W}^T\tilde{W}\right\} + \frac{\beta}{2}(1-I_W)tr\left\{\tilde{W}^T\tilde{W}\right\} - \frac{\beta_i}{2}I_W\|W\|^2 + \frac{\beta}{2}I_W\|W^*\|^2 \quad (25)$$

Let $k_3 = \bar{k}_1 + \bar{k}_2 + \bar{k}_3$, (25) is transformed into:

$$\dot{V} \le -k_0\bar{k}_1\left|\frac{\partial v_0}{\partial x}\right|^2 - k_0\bar{k}_2\left|\frac{\partial v_0}{\partial x}\right|^2 - k_0\bar{k}_3\left|\frac{\partial v_0}{\partial x}\right|^2 + k_0s\left|\frac{\partial v_0}{\partial x}\right|\|W\|\left(1+\frac{1}{\lambda}\right) + k_0\left|\frac{\partial v_0}{\partial x}\right|\theta[1+\frac{1}{\lambda_1}] - \frac{\gamma_1}{2}\tilde{\theta}^2 - \frac{\gamma_1}{2}\theta^2 + \frac{\gamma_1}{2}\varepsilon^2 - \frac{\beta}{2}tr\left\{\tilde{W}^T\tilde{W}\right\} + \frac{\beta}{2}(1-I_W)tr\left\{\tilde{W}^T\tilde{W}\right\} - \frac{\beta}{2}I_W\|W\|^2 + \frac{\beta}{2}I_W\|W^*\|^2 \quad (26)$$

Choosing

$$\lambda \ge \frac{k_0s}{\sqrt{2\bar{k}_2\beta} - sk_0}, \quad \lambda_1 \ge \frac{k_0}{\sqrt{2k_0\bar{k}_2\gamma_1} - k_0} \quad , (27)$$

and

$$\beta > \frac{s^2k_0^2}{2\bar{k}_2}, \quad \gamma_1 > \frac{k_0}{2\bar{k}_2} \quad (28)$$

yields

$$\dot{V} \le -k_0\bar{k}_1\left|\frac{\partial v_0}{\partial x}\right|^2 - k_0\bar{k}_3\left|\frac{\partial v_0}{\partial x}\right|^2 - [\bar{k}_2\left|\frac{\partial v_0}{\partial x}\right|^2 - 2\sqrt{\frac{\bar{k}_2\beta}{2}}\left|\frac{\partial v_0}{\partial x}\right|\|W\| + \frac{\beta}{2}\|W\|^2] + [(\sqrt{k_0\bar{k}_2}\left|\frac{\partial v_0}{\partial x}\right|)^2 - 2\sqrt{\frac{k_0\bar{k}_2\gamma_1}{2}}\theta\left|\frac{\partial v_0}{\partial x}\right| + \frac{\gamma_1}{2}\theta^2] + \frac{\beta}{2}\|W\|^2 + \bar{k}_2\left|\frac{\partial v_0}{\partial x}\right|^2 - \frac{\gamma_1}{2}\tilde{\theta}^2 - \frac{\gamma_1}{2}\theta^2 + \frac{\gamma_1}{2}\varepsilon^2 - \frac{\beta}{2}tr\left\{\tilde{W}^T\tilde{W}\right\} + \frac{\beta}{2}(1-I_W)tr\left\{\tilde{W}^T\tilde{W}\right\} - \frac{\beta}{2}I_W\|W\|^2 + \frac{\beta}{2}I_W\|W^*\|^2 \quad (29)$$

If $\frac{\bar{k}_2}{\bar{k}_1} \le k_0 \le 1$ is satisfied, then (29) can be changed into

$$\dot{V} \le -k_0\bar{k}_3\left|\frac{\partial v_0}{\partial x}\right|^2 - \frac{\beta}{2}\|\tilde{W}\|^2 + \frac{\beta}{2}\|W^*\|^2 + \beta(1-I_W)tr\left\{\tilde{W}^T\tilde{W}\right\} - \frac{\gamma_1}{2}\tilde{\theta}^2 + \frac{\gamma_1}{2}\varepsilon^2 + (1-I_W)\frac{\beta}{2}M_W^2 \quad (30)$$

Since

$$\beta(1-I_W)tr\left\{\tilde{W}^T\tilde{W}\right\} = \begin{cases}\beta tr\left\{\tilde{W}^T\tilde{W}\right\} & if\ |W| < M_W \\ 0 & if\ |W| \ge M_W\end{cases} \quad (31)$$

we obtain

$$\beta(1-I_W)tr\left\{\tilde{W}^T\tilde{W}\right\} \le \beta M_W^2 \quad (32)$$

Moreover, because

$$(1-I_W)\frac{\beta}{2}M_W^2 \le \frac{\beta}{2}M_W^2 \quad (33)$$

(30) can be transformed into the following form

$$\dot{V} \le -k_0\bar{k}_3\left|\frac{\partial v_0}{\partial x}\right|^2 - \frac{\beta}{2}\|\tilde{W}\|^2 + \frac{\beta}{2}M_W^2 + \beta M_W^2 + \frac{\beta}{2}M_W^2 - \frac{\gamma_1}{2}\tilde{\theta}^2 + \frac{\gamma_1}{2}\varepsilon^2 \quad (34)$$

By using (5), we have

$$\dot{V} \le -\frac{k_0\bar{k}_3k_4}{k_3}v_0(x) - \frac{\beta}{2}\|\tilde{W}\|^2 - \frac{\gamma_1}{2}\tilde{\theta}^2 + 2\beta M_W^2 + \frac{\gamma_1}{2}\varepsilon^2 \quad (35)$$

therefore $\dot{V} \le -\alpha V + \mu$,

with $\alpha = \min\left\{\frac{\bar{k}_3k_4}{k_3}, \beta, \gamma_1\right\}$,

$$\mu = 2\beta M_W^2 + \frac{\gamma_1}{2}\varepsilon^2 \quad (36)$$

Integrating both sides of (36) yields

$$V(t) \le \frac{\mu}{\alpha} + \left[V(0) - \frac{\mu}{\alpha}\right] e^{-\alpha t}, \quad \forall t \ge 0 \tag{37}$$

Due to (37), it can be deduced that $x, W(x), \theta(x)$ are bounded consistently. From (20), we have

$$k_0 v_0(x) \le V \tag{38}$$

Therefore,

$$v_0(x) \le \frac{\mu}{k_0 \alpha} + \frac{1}{k_0}\left[V(0) - \frac{\mu}{\alpha}\right] e^{-\alpha t}, \ \forall t \ge 0. \tag{39}$$

The above completes the proof that x is ultimately consistently bounded by the set D.

4. ILLUSTRATION EXAMPLE

This section takes a fermentation process as a nonlinear process example to show that the control design of section 3 can result in a stable closed-loop to ensure the system states to converge to zero in the presence of a fault.

The fermentation process is assumed to operate at a constant volume V, with the dynamics of biomass X, substrate S, and toxin concentration C_t, described by the follows:

$$\frac{dX}{dt} = \mu X - DX \tag{40}$$

$$\frac{dS}{dt} = -DS - \mu \frac{X}{y_s} \tag{41}$$

$$\frac{dC_t}{dt} = qX^{1/3} - DC_t \tag{42}$$

Where, the dilution rate, D, and the yield coefficient, y_s, are given by

$$D = \frac{F}{V}, \ y_s = \frac{y\mu}{My + \mu},$$

and the nonlinear inhibited specific growth rate is $\mu = \mu_m \left[\frac{S}{K_s + S + S^3/K_i}\right]\left[\frac{K_t}{K_t + C_t^2}\right]$.

The parameters of $y, q, \mu_m, K_s, K_i, K_t, M$ are given in Table 1 for the process.

Table 1: Fermentation model parameters

Volume	V	200[l]
Constant	y	0.417
Constant	M	0.0196
Toxin production constant	q	0.0296[l/h(g/l)$^{2/3}$]
Maximum specific growth rate	μ_m	0.0135[l/h]
Monod constant	K_s	0.05[g/l]
Substrate inhibition constant	K_i	2150[l^2/g^2]
Toxin inhibition constant	K_t	5.5[g^2/l^2]

Defining the state as $x = [X \quad S \quad C_t]^T$, and the input $u = F/V$, the equations (40-42) become:

$$\begin{bmatrix} \frac{dX}{dt} \\ \frac{dS}{dt} \\ \frac{dC_t}{dt} \end{bmatrix} = \begin{bmatrix} \mu X \\ -(M + \mu/y)X \\ qX^{1/3} \end{bmatrix} + \begin{bmatrix} -X \\ -S \\ -C_t \end{bmatrix} u \tag{43}$$

Using the data in Table 1, we can find:

$$\zeta(x) = \begin{bmatrix} 0.5x_1 \\ -1.4x_1 \\ 0.6x_1^{1/3} \end{bmatrix}, \quad G(x) = \begin{bmatrix} -X \\ -S \\ -C_t \end{bmatrix}$$

Let $\Delta g(x) = \begin{bmatrix} \theta_1 x_1 x_2 e^{x_2} \\ 2x_2^2 e^{x_2} \sin\theta_2 \\ \theta_3 x_1 e^{x_1} \end{bmatrix}$, $\Delta\zeta(x) = \begin{bmatrix} \theta_2 x_1^2 \cos\theta_1 \\ x_1^2 \sin\theta_2 \\ \theta_3 x_1^2 \end{bmatrix}$

where $x = col(x_1, x_2, x_3) = \begin{bmatrix} \frac{dX}{dt} & \frac{dS}{dt} & \frac{dC_t}{dt} \end{bmatrix}^T$,

$\theta_1 \in (-2, 2)$ and $\theta_2, \theta_3 \in (-1, 1)$ are the uncertainty parameters. In this example, a radial basis function (RBF) network is chosen to represent the dynamic changes after the fault occurrence, with 10 hidden nodes and 10 centers that are distributed uniformly in region [-1,1].

Choose $\xi(x) = 2|x|^2 e^{|x|}$, $\rho(x) = 2x_1^2$, $v_0 = x^T x = \|x\|^2$.

Then the control input is:

$$u^a = -0.4x_1^{2/3} + 0.9x_2$$

$$u^b = \begin{cases} -2|x|^2 e^{|x|} & x_1 \ne 0 \ and \ x_2 \ne 0 \ and \ x_3 \ne 0 \\ 0 & otherwise \end{cases}$$

$$u^c = \begin{cases} -\dfrac{2x_1^2}{(x_1^2 + x_2^2 + x_3^2)^{1/2}} & x_1 \ne 0 \ and \ x_2 \ne 0 \ and \ x_3 \ne 0 \\ 0 & otherwise \end{cases}$$

the unknown fault function is assumed to be $f(x) = \begin{pmatrix} 2\cos x_1 \\ 3\cos x_2 \\ \cos x_3 \end{pmatrix}$, this results in:

$$u^F = \frac{G^T(x) W S(x)}{0.005} + \frac{G^T(x)\begin{bmatrix} \theta \\ 0 \end{bmatrix}}{0.005},$$

the weight adaptive law:

$$\dot{W} = 2k_0 \frac{\partial v_0}{\partial x} S^T(x),$$

$$\dot{\theta} = -0.0025\theta + k_0 \left|\frac{\partial v_0}{\partial x}\right|, \text{ and}$$

the set $D = \left\{x \in R^n : v_0(x) \le \frac{1.6}{k_0}, 0.5 \le k_0 \le 1\right\}$

We choose $k_0 = 0.6$, the fault is introduced at $T = 1s$, the control results are shown in Figures 1-6.

Figures 1, 3, and 5 depict the control responses of the three states without using of the proposed accommodation strategy. Obviously, the states diverge from the set-point after the occurrence of the fault at T=1. Converse to the above, the results of using the proposed accommodation control law show that all states converge despite of the fault, as shown in Figures 2,4, and 6. This suggest that the proposed control is effective.

5. CONCLUSION

An active fault-accommodation control law has been developed to ensure the closed-loop stability for a class of nonlinear systems, using a neural network approach. The application of the proposed design has been shown to be effective for a fermentation process.

References

1. Michael A. Demetriou and Marios M. Polycarpou. "Incipient fault diagnosis of dynamical systems using online approximators", IEEE Trans. Automat. Contr., 1998, 43(11): 1612-1617.

2 Xiaodong Zhang, Marios M. Polycarpou and Thomas Parisini. "A robust and isolation scheme for abrupt and incipient faults in nonlinear systems", *IEEE Trans. Automat. Contr.*, 2002, 47(4) : 576-592.

3 Guanghong Yang, Siying Zhang, James Lam and Jianliang Wang. "Reliable control using redundant controllers", *IEEE Trans. Automat. Contr.*, 1998, 47(11) : 1558-1593.

4 Delin Chu and Michel Malabre. "Numerically reliable design for proportional and derivative state-feedback decoupling controller," *15 Triennial world congress of the international federation of automatic control*, Barcelona, 2002: 599-604.

5 Veillette J. R. "Reliable linear-quadratic state feedback control". *Automatica*, 1995, 31 : 137-143.

6 Patton J. R. fault-tolerant control : the 1997 situation. in Proc. *IFAC Symp. Fault detection, supervision safety for process*, 1997: 1033-1055.

7 Tortora, G., B. Kouvaritakis and D. W. Clarke. Simultaneous optimization of tracking performance and accommodation of sensor faults. *International Journal of Control*, 2002, 75(3) : 163-176.

8. Michael A. Demetriou and Marios M. Polycarpou, Incipient fault diagnosis of dynamical systems using online approach. *IEEE Trans. Automat. Contr.*, 1998, 43(11) : 1612-1617.

9. Boskovic D. J., Yu H. S. and Mehra K. R., Astable scheme for automatic control reconfiguration in the presence of actuator failures, in Proc. *Amer. Contol conf.*, 1998: 2455-2459.

10. Idan M., Johnson M., Calise J. A. and Kaneshge J., Intelligent aerodynamic /propulsion flight control for flight safety: A nonlinear adaptive approach, in Proc. *Amer. Contol conf.*, 2001: 2918-2923.

11. Proll T., Karim N. M. Nonlinear control of a bioreactor model using exact and I/O linearization. Int. J. Control, 1994, 60(4): 499-502.

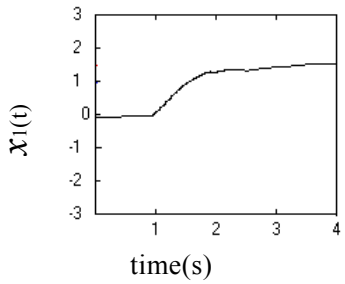

Fig.1: Control response of state $x_1(t)$ without fault accommodation.

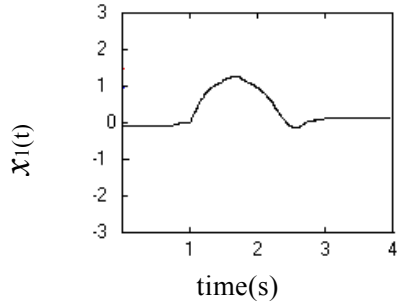

Fig.2: Control response of state $x_1(t)$ with the proposed fault accommodation.

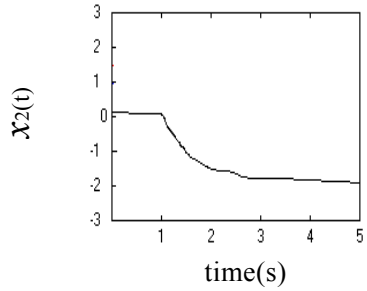

Fig.3: Control response of state $x_2(t)$ Without the fault accommodation

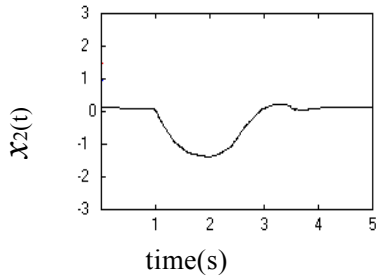

Fig.4: Control response of state $x_2(t)$ with the Proposed fault accommodation

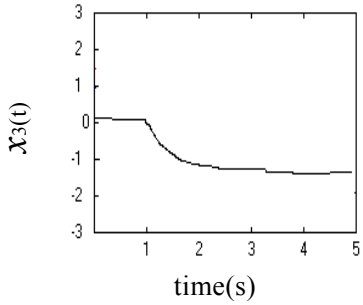

Fig.5: Control response of state $x_3(t)$ without the fault accommodation

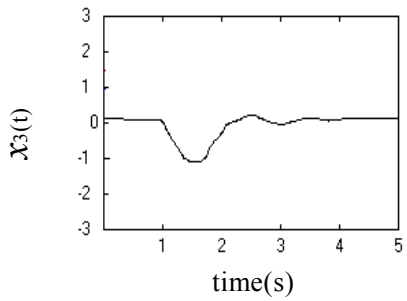

Fig.6: Control response of state $x_3(t)$ with the proposed fault accommodation.

A NOVEL DETECTION OF VESSEL LIQUID LEVEL BASED ON ECHO IDENTIFICATION[1]

Zhaohui Zhang[a], Jianmei Yuan[b], Weiyi Huang[c]

[a]*Faculty of Information Engineering, University of Science and Technology Beijing, China*
[b]*Faculty of Applied Science, University of Science and Technology Beijing, China*
[c]*Department of Instrumentation, Southeast University, Nanjing, China.*

Abstract: A novel non-invasive level detection is developed in the paper for applications to processes where high pressure, high temperature, high viscosity, strong corrosion liquid may be involved. The theoretical analysis and experiment suggest that the proposed echo method can measure level well. The key to the success of this detection is the proper extraction of the echo information from noisy waves by using a proper Wavelet Transform.

Keywords: Detecting elements, Vessel level, Non-invasion meter, Echo extraction, Wavelet Transform

1. INTRODUCTION

In situations, where high pressure, high temperature, high viscosity, or corrosive liquid or vapors are involved, the liquid level measurement can be difficult, as it is not allowed for a sensor invasion. Ultrasonic and radar level meters, which can avoid any direct contact with liquid, have to be installed inside of the vessel. They aren't adoptable for applications where high pressure or for corrosive vapors involved. Radioactive meter, which is non-invasion in nature, can not be conveniently used, as it needs special protection, storage, and encapsulation. A novel non-invasion measurement method is proposed by this paper based on proper processing of echoes for level detection.

2. PRINCIPLE OF LEVEL DETECTION

Three parts of different waves can be resulted from the striking of a vibrator against the metallic shell of the vessel. The significant part, a surface wave, propagates along the external surface of the vessel. The second part, echo, penetrates the shell and then is reflected on the internal surface, i.e, the interface of metal/liquid or metal/atmosphere. The third part, transmission wave, penetrates the shell and then is absorbed by the liquid or atmosphere. Both surface wave and echo can be sensed at a properly placed receiver, as illustrated by Fig.1.

As the thickness of the shell is much smaller than the radius of the vessel, the area around the receiver can be regarded as a plate. This helps to assess the inherent frequency to the selection of the receiver (Zhang and Huang,1999).

Now we focus on the echo. For simplification, suppose the echo is of one dimension. The

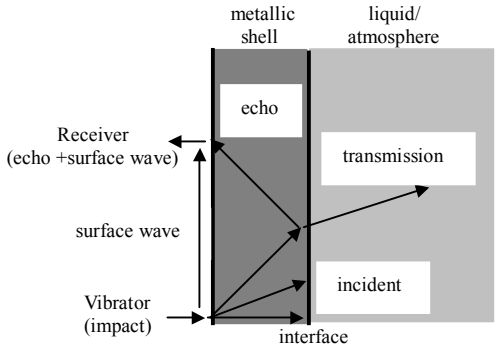

Fig.1. Vibrato rand receiver

impedance of wave conductor is defined as (Brekhovskih, 1980):

$$Z=c\rho \qquad (1)$$

Where ρ is the density and c is the sound velocity in the conductor. At the interface of conductor 1 and conductor 2, reflection coefficient is

$$C_r = \frac{Z_2/Z_1-1}{Z_2/Z_1+1} \qquad (2)$$

And the transmission coefficient is

$$C_t = \frac{2*Z_2/Z_1}{Z_2/Z_1+1} \qquad (3)$$

As an example, consider a steel vessel filled with water. The impedances of steel, water and atmosphere are

$Z_s=c_L\rho$= 5790m/s*7910Kg/m^3=4.58*10^{7}Kg/m^{2}s
Z_w=1483m/s*1000Kg/m^3=1.48*10^6 Kg/m^{2}s
Z_a=331.45m/s*1.2250Kg/m^3=4.06*10^2 Kg/m^{2}s

Thereby reflection and transmission coefficients at the interface of steel and water are

$$C_r^{s/w} = \frac{Zw/Zs-1}{Zw/Zs+1} = -0.9374$$

$$C_t^{s/w} = \frac{2*Zw/Zs}{Zw/Zs+1} = 0.0626$$

At the interface of steel and atmosphere (empty segment), the coefficients are

[1] This work was supported by UPC Grant ZX9914 and Grant BJ97026.

$$C_r^{s/a} = \frac{Za/Zs - 1}{Za/Zs + 1} = -0.99998$$

$$C_t^{s/a} = \frac{2 * Za/Zs}{Za/Zs + 1} = 0.00002$$

It can be seen that $C_t^{s/w} >> C_t^{s/a}$ and $C_r^{s/w} < C_r^{s/a}$ in their absolute values. Generally, the liquid impedance is close to that of the metallic shell, whereas the atmosphere impedance is much smaller than that of the metallic shell, i.e, $C_r^{s/l} < C_r^{s/a}$. Hence, echo exists only above the liquid level, little exists beneath the level due to attenuation. This conclusion is independent of the vessel construction, size, shell materials, and liquid types.

By moving the vibrator and receiver up or down along the vessel surface, the level can be found via echo identification.

3. SIGNAL PROCESS

The receiver signal includes two parts, surface wave and echo. It's difficult to recognize echo from the original received signals. A signal process technique is developed, next, to distinguish echo from the significant surface waves. Both signals, which are time-varying, attenuate rapidly during propagation (Breining, 1999). Therefore, Wavelet Transform is applied for their processing.

Wavelet Transform is a linear transformation that operates in time-frequency joint domains (Cohen, 1995). Its Mallat fast algorithms are

$$C_{j+1,k} = \sum_{n \in Z} \overline{h}_{n-2k} C_{j,n} \qquad (4)$$

$$D_{j+1,k} = \sum_{n \in Z} \overline{g}_{n-2k} C_{j,n} \qquad (5)$$

where h_n and g_n are constant coefficients for a specific wavelet function. For discrete signal $C_{0,k}$ (k integer), series of coefficients $C_{j,k}$ represent the jth-order approximations, i.e, the components below frequency $(\omega_c - \Delta)2^{-j}$, where ω_c and Δ are center frequency and window width determined by wavelet function. And $D_{j,k}$ represent the jth-order details.

Take the discrete receiver signal f(k) (k=1,2,…,N) as initial conditions

$$C_{0,k} = f(k) \qquad (6)$$

A simplest wavelet function, Harr, is adopted with coefficients h_0=0.707107, h_1=0.707107, g_0= -0.707107, g_1=0.707107. Harr is compactly supported (h_k , g_k =0 if k >1) so that a good computation efficiency would be achieved.

The approximations $C_{3,k}$ and details $D_{j,k}$ (j=1,2,3) can be worked out via algorithms (4) and (5) iteratively. Refer to Fig 2. The 3rd-order approximations $C_{3,k}$ are components below the frequency $(\omega_c - \Delta)2^{-3}$. All wave crests appear periodically in $C_{3,k}$, whereas a special crest appears at a phase-shift. This suggests that the special waveform segment is the echo that we are interested to identify.

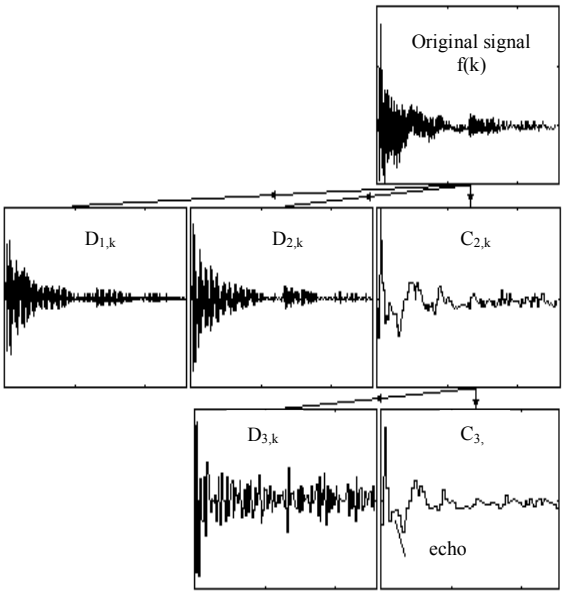

Fig.2. Receiver signal and its wavelet transforms

4. EXPERIMENT

Consider a steel vessel with 1m diameter and 1m height and being filled with 80% water. Exert a pulse strike to the shell of vessel so that a wide frequency range is excited. Touch the receiver to the shell with a little press. Move the detection point down step by step.

The 3rd-order approximations $C_{3,k}$ of the receiver signals are presented in Fig.3. Echo can be found right above the level, and disappears beneath the level.

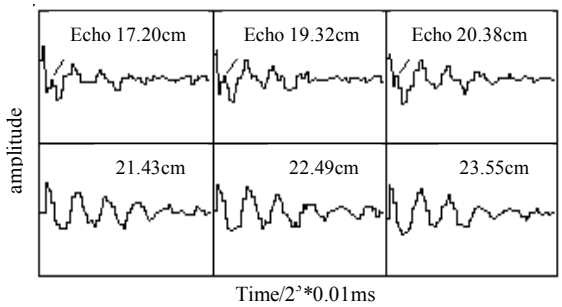

Fig.3. The 3rd–order approximations at 6 detect points

Where, the number above the line in all the four graphs represents the distance between the detect point and vessel top, the actual distance from the vessel top to the liquid surface is 20.00cm.

The level detection resolution error is less than one step, independent of the measurement span. This simple device can have high precision, particularly for large vessels.

5. CONCLUSIONS

Based on the identification of echo, a non-invasion liquid level detection system has been developed. The application of wavelet transform is the key for distinguishing the weak echo from the noisy surface waves. The authors believe such a method can be easily extended for the detection of the powder surface in vessel.

REFERENCES

Christina Breining (1999). Acoustic Echo Control. *IEEE Signal Processing Magazine*, Vol.16,No.4, pp42-69

Leon Cohen (1995). *Time-Frequency Analysis:Theory and Applications,* Prentice Hall, 1995

L.V.Brekhovskih (1980). *Waves in Layered Media*, Academic Press, New York.

Zhaohui Zhang, and Weiyi Huang (1999). A Liquid Measurement Method Based on Vibration Analysis. *Chinese Journal of Scientific Instrument,* Vol.20, No.3, pp250-253. (In Chinese)

MULTI-SITE PERFORMANCE MONITORING IN BATCH PHARMACEUTICAL PRODUCTION

C. W. L. Wong, R. E. A. Escott*, A. J. Morris and E. B. Martin

Centre for Process Analytics and Control Technology,
School of Chemical Engineering and Advanced Materials,
University of Newcastle, Newcastle upon Tyne, NE1 7RU, UK
**GlaxoSmithKline Chemical Development, Tonbridge, UK*

Abstract: A challenge facing the pharmaceutical and chemical industries is how to understand and identify differences in process behaviour where a product is manufactured at two different sites. Three approaches based on multi-group principal component analysis are investigated and benchmarked against single site models. The multi-group approach is shown to remove differences between sites such as operational scale thereby enabling the analysis to focus on identifying differences in variation between the two sites that are not a consequence of process configurations. From the analysis it is observed that the multi-group approach can assist in the understanding of manufacturing performance.

Keywords: Biotechnology, Manufacturing Processes, Performance Monitoring, Statistical Analysis

1. INTRODUCTION

Manufacturing challenges facing the chemical and pharmaceutical industries include the need to reduce the time between product development and full-scale production, the achievement of right-first-time manufacture and the manufacture of consistently high quality product with minimal environmental impact. The second and third challenges are compounded by the need to transfer the manufacture of a product to different sites around the world in a robust manner. A contribution to these challenges is to utilise the data collected from the process and to convert it into information and ultimately knowledge, thereby enabling an enhanced understanding of the process to be achieved. This approach has resulted in process performance monitoring and its associated techniques becoming an integral part of process operation.

For many industrial processes, performance monitoring systems are developed for individual process units, as opposed to the complete process. The complexity of this problem is compounded when the product is manufactured at two or more sites, where independent monitoring systems can be developed. A major disadvantage of this situation is that the sources of the differences in process operation and product variation, between the sites, cannot readily be identified. Previously it has been conjectured that process operation and scale differences are responsible for variability, and cannot be removed through modelling. In this paper the multi-group methodology of Lane *et al.* (2001) helps address this situation in terms of multi-site process performance monitoring. It is shown that scale and processing differences can be removed thereby enabling the real differences between sites to be identified. The paper focuses on empirical, i.e. data based, approaches. However alternative techniques are possible including the use of hybrid modelling, i.e. the conjunction of a reduced complexity mechanistic model and an empirical model (McPherson *et al.*, 2001).

One of the characteristics of batch operations is the variation in duration as a consequence of the process itself, down-stream processing, etc. To apply the techniques described in the paper, it is necessary to perform batch length equalisation. Multivariate Dynamic Time Warping (DTW) and the cutting of the batch process data to a minimum length are considered.

A number of approaches are considered in the paper for the development of a multi-site monitoring scheme for a drug intermediate. The benchmark approach was based on the development of an individual model for each site. The data matrices comprising the common variables from the two sites were then combined and different scaling procedures applied. The first resulted in the removal of the global mean and standard deviation of each variable (calculated from the data for the two sites) whilst for the second approach, the local mean and standard deviation for each individual variable for each site was removed. Finally a multi-group model based on the pooled sample variance-covariance matrix was developed using all the variables monitored at both sites. Fig. 1 provides an overview of the different approaches.

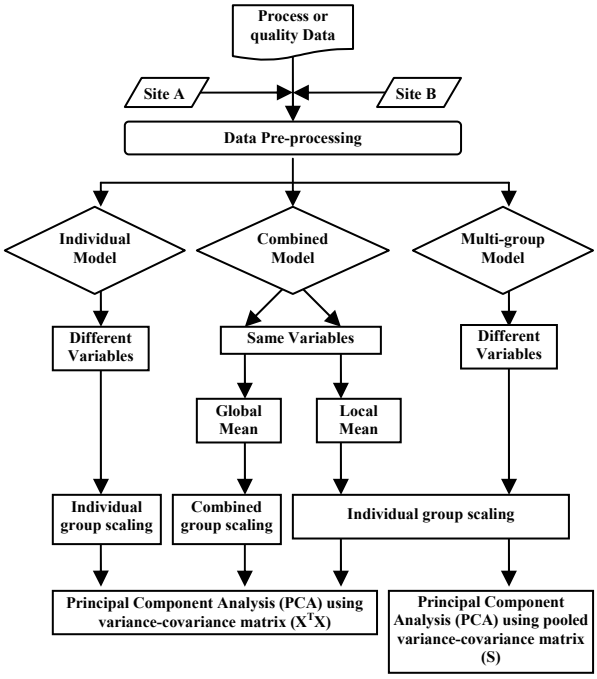

Fig. 1. Summary of different monitoring approaches.

2. PROCESS DESCRIPTION

The process interrogated is a single stage within a multi-stage synthetic route for the production of an active pharmaceutical ingredient (API). The process is carried out at two manufacturing sites by a regulated batch procedure. The process data have been acquired at both sites from reactor probes that are linked to data historians and that have been subsequently extracted for analysis. The chemistry step involves an exothermic addition that is controlled by reactant addition rate and the reactor temperature and has a duration period of approximately 4 hours. Although different plant configurations have been employed at the two sites, similar process variables are monitored, alongside coincident quality control measures. The process data variables include reactant addition rate (maturity), reactor temperature, reactor pressure, agitation rate and vapour temperature. The quality variables include input and output material activity, process yield and various impurity levels. Data from 57 batches from Site A and 152 batches from Site B were included in the analysis.

3. DATA PRE-PROCESSING

The raw data collected were initially pre-screened for missing observations, outliers, small signal to noise ratios, etc. Once data anomalies were identified, an appropriate in-filling algorithm was applied such as data deletion or linear interpolation. The next stage was to examine the resulting time series plots of the individual variables to attain good process operation understanding. It is essential that this stage is undertaken in collaboration with process personnel.

Batch process data collected on a number of batches is typically arranged in a three-way matrix, batch (I) x variables (J) x time (K). After equalisation of batch lengths, multi-way principal component analysis (MPCA) (Nomikos and MacGregor, 1994) was applied. The data matrix is first unfolded to give a two-dimensional array as shown in Fig. 2 and PCA is applied to the unfolded data matrix.

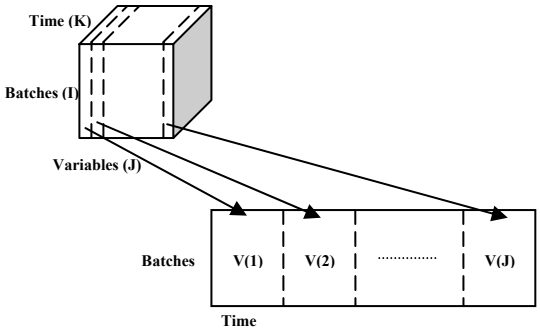

Fig. 2. Schematic representation of the unfolding of a three-way matrix.

To apply the bi-linear technique of multi-way principal component analysis illustrated in Fig. 2 batch lengths are required to be of equal duration. Two methods proposed to standardise batch length are cutting to a minimum length and multivariate Dynamic Time Warping (DTW) (Gollmer and Posten, 1996; Kassidas *et al.,* 1998). DTW is a method that matches features in a data pattern, or profile, to a reference profile. An optimal batch profile is first identified and the other batches are aligned against this reference batch. Fig. 3 illustrates the resulting synchronisation for the variables, reactor temperature and pressure for all batches at site A. Of particular note is the extraction of the underlying structure in the pressure variable that was masked prior to the application of DTW.

The second step was to remove data during periods of operation that were not deemed to be important in the subsequent analysis. For this specific application, the most important period with respect to product quality, is during the reactant addition period and hence this period defined the time period over which the data was analysed.

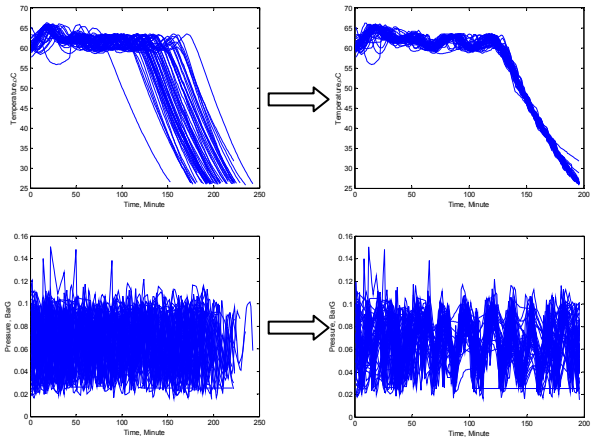

Fig. 3. Synchronisation of the time trajectories by DTW for reactor temperature and pressure for all batches at site A.

4. STATISTICAL DATA ANALYSIS

Both process and quality data were investigated but the results reported are for the process data only. A total of five process variables are monitored at site A and four at site B with three variables common to the two sites.

4.1 Individual PCA Model

Having pre-screened and equalised the duration of the batch data, the next step was to build individual multi-way PCA models for each site. By extracting the principal component score vectors, batch behaviour could be investigated. The leverage plot for the individual batches for the first two principal components, Fig. 4, clearly illustrates the impact of batch 15.

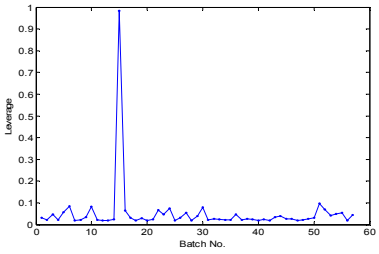

Fig. 4. Leverage for scores of principal component 1 and principal component 2.

By interrogating the data, it was observed that there had been an agitator failure during this batch run. Consequently to develop an appropriate monitoring model, it was necessary to remove batch 15 from the data matrix. From Fig. 4 it is not apparent that any other batches will have a major impact on the analysis, thus multi-way PCA was applied to the remaining 56 batches, Fig. 5. Ten principal components were retained in the subsequent analysis explaining 68% of the underlying variability. From Fig. 5 it can be observed that the scatter of the batches is random with a number lying out with the action limits. These batches were interrogated and issues relating to the data acquisition system were identified.

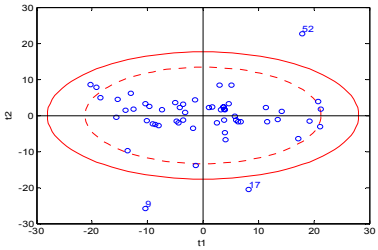

Fig. 5. Bivariate scores plot of principal component 1 and 2 after removal of batch 15.

From the loadings plot, process behaviour over time for different variables can be examined. Fig. 6 and 7 show the univariate loadings plot for principal component 1 and principal component 3, respectively. The dotted line is used to differentiate between the five variables through a batch run (reactor temperature, pressure, level, agitator speed and reactant addition rate). Variable three is observed to have a high loading throughout the duration of the batch for principal component one. It is interesting to observe from the loadings how the influence of variable changes over batch duration. This is particularly evident from principal component 3, Fig. 7.

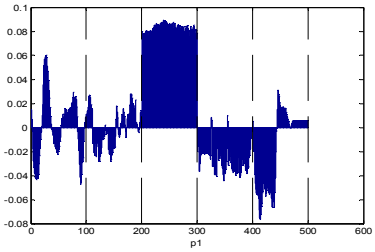

Fig. 6. Univariate loadings plot of principal component 1 for 5 process variables.

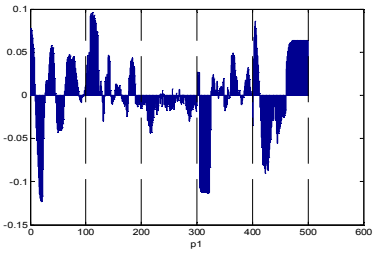

Fig. 7. Univariate loadings plot of principal component 3 for 5 process variables.

The same analysis was undertaken for site B. From examination of the leverage plot (not shown) two batches, 34 and 47, were identified as having high leverage. After the removal of these batches, a randomly scattered scores plot was obtained (Fig. 8). Retention of 10 principal components in this case resulted in 86% of the underlying variation in the data being explained. Examining the contribution plot of batch 127 (Fig. 9) for principal component one and the time series plots of the process variables it was noted

that there was an abnormal reactant addition rate for this batch. This information can be used by process personnel who can either take corrective action or else ensure that subsequent batches are not affected by a similar problem.

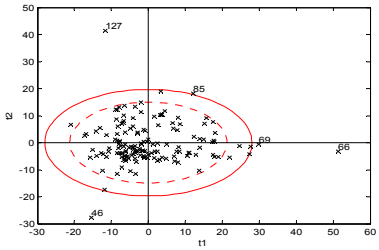

Fig. 8. Bivariate scores plot of principal component 1 and 2 after removal of batch 34 and 47.

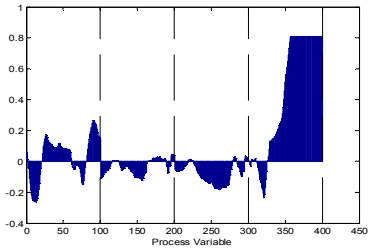

Fig. 9. Contribution plot for batch 127.

4.2 Combined PCA Model - Removal of Global Mean

The first combined model was constructed by applying multi-way PCA to the standardised data matrix based on the batch process data from the two sites. Only identical variables were selected to be included for analysis (reactor temperature, pressure and reactant addition rate). Examining Hotelling's T^2, three non-conforming batches were identified, batch 15 at site A and batches 17 and 125 at site B (not shown). It is interesting to observe that the batches from site B differed to those identified in the individual site analysis, demonstrating the potential limitation of this approach in terms of it providing conflicting information to the previous analysis. Following the removal of these batches, multi-way principal component analysis was applied to the remaining data, Fig. 10.

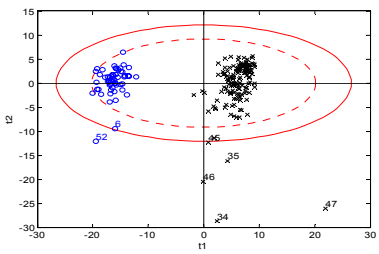

Fig. 10. Bivariate scores plot of principal component 1 and 2 after removal of batch 15 at site A and batch 17 and 125 at site B. Site A, 'o', Site B, 'x'.

From the figure, two clusters can be observed. More specifically, principal component 1 identifies the variation about the global mean for the two sites (Fig. 11) and thus both "within" and "between" group variation is captured.

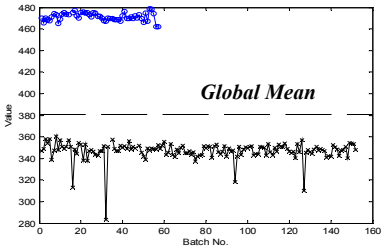

Fig. 11. Variation for one variable.

The lower order components do not exhibit this behaviour and display a more random scatter. Fig. 12 shows the bivariate scores plot of principal component 3 and principal component 4. A total of 77% of the variation was explained by the ten retained principal components.

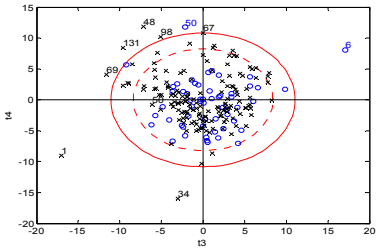

Fig. 12. Bivariate scores plot of principal component 3 and principal component 4.

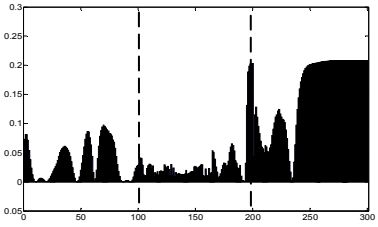

Fig. 13. Differential contribution plot between the two clusters.

Fig. 13 shows the differential contribution plot for the first principal component. The differential contribution plot calculates the difference between the contribution for a group of points from site A and a group of points from site B. From the resulting representation, it was observed that the differences were mainly related to the reactant addition rate. The rates and the total amounts of addition differ between the two sites due to operational differences, i.e. different reactor sizes and configurations. Thus it was conjectured that by removing the scale effect, a single model could realistically be developed for the two sites.

4.3 Combined PCA Model -Removal of the Local Mean

A second combined multi-way PCA model was built from the same data sets as in Section 4.2. However, the data was standardised specifically for each site. By standardising the data matrix in this way, the variation

of each variable from its mean value relative to the individual site, Fig. 14, is considered.

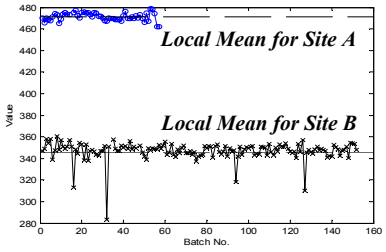

Fig. 14. Local variation for one variable.

From the bivariate scores plot of principal component 1 and principal component 2, batch 15 at site A and batch 34 and 47 at site B were again observed to have a strong influence on the process representation. Removing these batches, the subsequent analysis resulted in 75% of the underlying variation being explained following the inclusion of ten principal components.

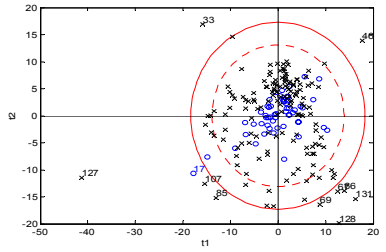

Fig. 15. Bivariate scores plot of principal component 1 and 2 after removal of batch 15 at site A and batch 34 and 47 at site B.

Examining the loadings plot, it can be observed that the key variable in terms of defining the main source of variation associated with principal component one is that of the reactant addition rate.

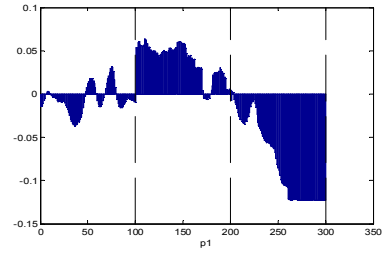

Fig. 15. Univariate Loadings plot of principal component 1.

4.4 Multi-group PCA Model

An extension to traditional multi-way PCA, multi-group multi-way PCA, was then investigated for the simultaneous monitoring of different manufacturing sites. Multi-group modelling is based on the assumption that a common eigenvector subspace exists for the sample variance-covariance matrix of individual sites. Through the pooled sample variance-covariance matrix, the principal component loadings are calculated. The pooled sample variance-covariance matrix (**S**), which forms the basis of the multi-group model is defined as a weighted sum of the g individual variance-covariance matrices $s_1, s_2, \ldots, s_g$:

$$S = \frac{(n_1 - 1)s_1 + (n_2 - 1)s_2 + \ldots + (n_g - 1)s_g}{(N - g)} \qquad (1)$$

for $i = 1, \ldots, g$. N is the total number of observations (batches), g is the number of groups and n_i is the number of observations within group i. Consider the data set for site A, containing variables 1 to 5 and data set for site B comprising variables 1, 2, 3 and 6 in which variables 1, 2 and 3 are identical. The individual variance-covariance matrices for site A and B are given in Table 1 and the pooled variance-covariance matrix is defined in Table 2.

Table 1 Variance-covariance matrix for site A and B.

Variance-covariance matrix for Site A					
Variable	1	2	3	4	5
1	**A_{11}**	**A_{12}**	**A_{13}**	**A_{14}**	**A_{15}**
2	A_{12}	**A_{22}**	**A_{23}**	**A_{24}**	**A_{25}**
3	A_{13}	A_{23}	**A_{33}**	**A_{34}**	**A_{35}**
4	A_{14}	A_{24}	A_{34}	**A_{44}**	**A_{45}**
5	A_{15}	A_{25}	A_{34}	A_{45}	**A_{55}**

Variance-covariance matrix for Site B				
Variable	1	2	3	6
1	**B_{11}**	**B_{12}**	**B_{13}**	**B_{16}**
2	B_{12}	**B_{22}**	**B_{23}**	**B_{26}**
3	B_{13}	B_{23}	**B_{33}**	**B_{36}**
6	B_{16}	B_{26}	B_{36}	**B_{66}**

Table 2 Pooled variance-covariance matrix.

Pooled variance-covariance matrix						
Variable	1	2	3	4	5	6
1	**C_{11}**	**C_{12}**	**C_{13}**	**C_{14}**	**C_{15}**	**C_{16}**
2	C_{12}	**C_{22}**	**C_{23}**	**C_{24}**	**C_{25}**	**C_{26}**
3	C_{13}	C_{23}	**C_{33}**	**C_{34}**	**C_{35}**	**C_{36}**
4	C_{14}	C_{24}	C_{34}	**C_{44}**	**C_{45}**	**C_{46}**
5	C_{15}	C_{25}	C_{35}	C_{45}	**C_{55}**	**C_{56}**
6	C_{16}	C_{26}	C_{36}	C_{46}	C_{56}	**C_{66}**

where

$$C_{11} = \frac{(n_1 - 1)A_{11} + (n_2 - 1)B_{11}}{(n_1 + n_2 - 2)} \qquad C_{33} = \frac{(n_1 - 1)A_{33} + (n_2 - 1)B_{33}}{(n_1 + n_2 - 2)}$$

$$C_{12} = \frac{(n_1 - 1)A_{12} + (n_2 - 1)B_{12}}{(n_1 + n_2 - 2)} \qquad C_{34} = A_{34}$$

$$C_{13} = \frac{(n_1 - 1)A_{13} + (n_2 - 1)B_{13}}{(n_1 + n_2 - 2)} \qquad C_{35} = A_{35}$$

$$C_{14} = A_{14} \qquad C_{36} = B_{36}$$
$$C_{15} = A_{15} \qquad C_{44} = A_{44}$$
$$C_{16} = B_{16} \qquad C_{45} = A_{45}$$
$$C_{46} = 0$$

$$C_{22} = \frac{(n_1 - 1)A_{22} + (n_2 - 1)B_{22}}{(n_1 + n_2 - 2)}$$

$$C_{23} = \frac{(n_1 - 1)A_{23} + (n_2 - 1)B_{23}}{(n_1 + n_2 - 2)} \qquad C_{55} = A_{55}$$

$$C_{24} = A_{24} \qquad C_{56} = 0$$
$$C_{25} = A_{25} \qquad C_{66} = B_{66}$$
$$C_{26} = B_{26}$$

Multi-group PCA was then applied to the pooled variance-covariance matrix. Batch 15 from site A and batch 34 and 47 from site B were removed from the analysis as they have a major influence on the model. Reapplying multi-group multi-way PCA resulted in 63% of the variation being explained by ten principal components, Fig. 16.

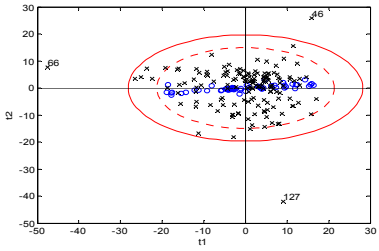

Fig. 16. Bivariate scores plot of principal component 1 and 2 of multi-group model after removal of batch 15 at site A and batch 34 and 47 at site B.

From the loadings plot, Fig. 17, variable three, reactant addition rate, was identified as the most important variable in terms of defining the main source of variation for principal component one. This variable was one of the three common to the two sites along with variable one and two, reactor temperature and pressure. Variable four and five related to those monitored only at site A, level and agitator speed, and variable six related to vapour temperature that was only monitored at site B.

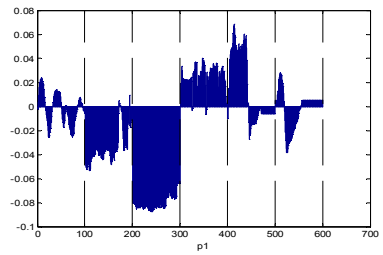

Fig. 17. Univariate loadings plot of principal component 1.

The advantage of being able to develop a single model for two, or more, sites is that it enables an enhanced understanding of the subtle differences in performance between the two manufacturing processes. In addition it can help facilitate the transfer of a process to a new site by providing a baseline monitoring model with the model being updated as new batches are manufactured. The scores plot clearly detects those batches which move outside the statistical control region for the two sites on one chart and the corresponding scores contribution plots identifies the combination of variables responsible for the out of control signal. Thus, the application has demonstrated that the multi-group model has acceptable detection and diagnostic properties though the overall sensitivity may be affected compared with those of the corresponding individual plant models.

5. CONCLUSION

The capabilities of multi-group models, to model different process configurations on two sites, based on the pooled sample variance-covariance matrix has been demonstrated by its application to data from a drug intermediate batch process. Pre-screening of the data was initially performed to remove any abnormal variability. Batch length equalisation was achieved through the application of multivariate DTW to the process data. The DTW batch data was further reduced to ensure that the analysis focused on the main area of interest. Multi-way principal component analysis was then applied to the pre-processed data. The first approach used analysed the data from each plant individually. Two combined models where the data was scaled differently were also studied. The multi-group models developed not only eliminates between cluster variations but also allows the process monitoring of two different plants by a single model. This development provides a powerful monitoring tool for understanding and hence minimising the differences in product quality and process operation across different manufacturing plants. In addition based on the proposed approach, it is possible to utilise the approach to assist in the transfer of a process to a new site.

6. ACKNOWLEDGEMENTS

Chris Wong would like to acknowledge the EPSRC, GlaxoSmithKline, the UK ORS Scheme and CPACT for financial support of his PhD.

7. REFERENCES

Gollmer, K. and C. Posten (1996). Supervision of bioprocesses using a dynamic time warping algorithm. *Control Engineering Practice* **4(9)**, pp. 1287-1295.

Jolliffe, I.T. (1986). *Principal component analysis*. Springer-Verlag, New York.

Kassidas, A., J. MacGregor and P.A. Taylor (1998). Synchronisation of batch trajectories using dynamic time wraping. *AIChE* Journal, **44(4)**, pp. 864-875.

Lane, S., E.B. Martin, R. Kooijmans and A.J. Morris (2001). Performance monitoring of a multi-product semi-batch process. *Journal of Process Control*, **11**, pp. 1-11.

Martin, E.B., A.J. Morris and C. Kiparissides (1999). Manufacturing performance enhancement through multivariate statistical process control. *Annual Reviews in Control* **23(1)**, pp. 35-44.

McPherson, L.A., E.B. Martin and A.J. Morris (2002). Super model-based techniques for batch performance monitoring, *ESCAPE-12*, pp. 523-528.

Nomikos, P. and J. MacGregor (1994). Monitoring batch processes using multiway principal component analysis. *AIChE Journal* **40(8)**, pp. 1361-1373.

PROCESS MONITORING OF AN ELECTRO-PNEUMATIC VALVE ACTUATOR USING KERNEL PRINCIPAL COMPONENT ANALYSIS

Sang-Oak Song, Gibaek Lee, En Sup Yoon

School of Chemical Engineering, Seoul National University

Abstract:. In this paper, an approach for process monitoring using a multivariate statistical technique, namely kernel principal component analysis is studied. Kernel principal analysis has recently been proposed as a new method for performing a nonlinear form of principal component analysis (PCA). The basic idea of kernel PCA is to first map the input space into a feature space via a nonlinear map and then compute the principal components in that feature space. For the process monitoring application, reconstructed input patterns can be obtained by approximating the pre-image of scores in feature space. An application study of an electro-pneumatic valve actuator in a sugar factory is described. The results show that the kernel PCA approach can detect several actuator faults earlier than linear PCA This study indicates the great potential of Kernel PCA for process monitoring.

Keywords: Kernel PCA, fault detection, actuators, control valves, process monitoring

1. INTRODUCTION

In recent process industry, on-line monitoring of process performance is extremely important for plant safety, production efficiency and product quality. As industrial systems becoming more heavily instrumented, resulting in larger quantities of data available for use in process monitoring, and modern computers are becoming more powerful, empirical modelling approaches that are basically data-driven multivariate statistical methods have attracted much interest by process engineers. These approaches are based on the theory of statistical process control (SPC), under which the behaviour of a process is modelled using data obtained when the process is operating well and in a state of control. Future unusual events are detected by referencing the measured process behaviour against this model.

Principal component analysis (PCA) is the most widely used data-driven technique for process monitoring which has been heavily studied and applied to industrial systems over the past decade. PCA is an optimal dimensionality reduction technique in terms of capturing the variance of the data, and it accounts for correlations among variables. The lower-dimensional representations of the data produced by PCA can improve the proficiency of detecting and diagnosing faults using multivariate statistics. The principal components span a low dimensional subspace used for analysis. The details of linear PCA can be found elsewhere (Jolliffe, 1986).

However, PCA is a linear technique, which ignores the nonlinearities in the process data. Industrial processes are inherently nonlinear; therefore, it may be necessary to use nonlinear methods. Kramer (1991) has generalized PCA to the nonlinear case by using autoassociative neural networks. Dong and McAvoy (1996) have developed a nonlinear PCA approach based on principal curves and neural networks that produce independent principal components (Song, 2001).

Recently, the conceptual idea of generalizing an existing linear technique to a nonlinear version by applying the kernel trick has become an area of active research. One important result in this direction is the extension of linear PCA to kernel PCA, as shown by Schölkopf, *et al*. (1998). In Kernel PCA they were not interested in principal components in input space, but rather in principal components of

variables, or features, which are nonlinearly related to the input variables. Among these are for instance variables obtained by taking higher-order correlations between input variables. To this end, the method of expressing dot products in feature space in terms of kernel functions in input space is used. Given any algorithm which can be expressed solely in terms of dot products, i.e. without explicit usage of the variables themselves, this kernel method enables to construct different nonlinear versions of it (Vapnik, 1995).

The present work studies a nonlinear version of PCA using kernel technique and an application for process monitoring of an electro-pneumatic valve actuator. We first introduce the concept of Kernel PCA and reconstruction. And then Kernel PCA based process monitoring has been illustrated on the electro-pneumatic valve actuator benchmark system and its simulation results are discussed.

2. KERNEL PRINCIPAL COMPONENT ANALYSIS

1.1 Principal Component Analysis in Feature Spaces

Given a set of N centered observations $\mathbf{x}_k$, $k = 1, \cdots, M$, $\mathbf{x}_k \in \mathbf{R}^N$, $\sum_{k=1}^{M} \mathbf{x}_k = 0$, PCA diagonalizes the covariance matrix

$$C = \frac{1}{M} \sum_{j=1}^{M} \mathbf{x}_j \mathbf{x}_j^T \tag{1}$$

To do this, one has to solve the Eigenvalue equation

$$\lambda \mathbf{v} = C\mathbf{v} \tag{2}$$

for Eigenvalues $\lambda \geq 0$ and $\mathbf{v} \in \mathbf{R}^N \setminus \{0\}$. As $C\mathbf{v} = \frac{1}{M} \sum_{J=1}^{M} (\mathbf{x}_j \cdot \mathbf{v}) \mathbf{x}_j$, all solutions $\mathbf{v}$ must lie in the span of $\mathbf{x}_1 \cdots \mathbf{x}_N$, hence (2) is equivalent to

$$\lambda (\mathbf{x}_k \cdot \mathbf{v}) = (\mathbf{x}_k \cdot C\mathbf{v}) \text{ for all } k = 1, \cdots, M . \tag{3}$$

Next, let us consider this computation in another feature space $\mathbf{F}$, which is related to the input space by a possibly nonlinear map

$$\begin{aligned} \Phi : \mathbf{R}^N &\to \mathbf{F} \\ \mathbf{x} &\to \mathbf{X} \end{aligned} \tag{4}$$

Note that $\mathbf{F}$, the feature space could have an arbitrarily large, possibly infinite, dimensionality. Here and in the following upper case characters are used for elements of $\mathbf{F}$, while lower case characters denote elements of $\mathbf{R}^N$. It is assumed that we are dealing with centered data, i.e. $\sum_{k=1}^{M} \Phi(\mathbf{x}_k) = 0$. To perform PCA in feature space, we need to find Eigenvalue $\lambda \geq 0$ and Eigenvectors $\mathbf{V} \in \mathbf{F} \setminus \{0\}$ with the covariance matrix in F,

$$\bar{C} = \frac{1}{M} \sum_{1}^{M} \Phi(\mathbf{x}_j) \Phi(\mathbf{x}_j)^T \tag{5}$$

Substituting $\bar{C}$ into the Eigenvector equation, we note that all solutions $\mathbf{V}$ must lie in the span of Φ-images of the training data. This implies that we can consider the equivalent system

$$\lambda (\Phi(\mathbf{x}_k) \cdot \mathbf{V}) = (\Phi(\mathbf{x}_k) \cdot \bar{C}\mathbf{V}) \text{ for all } k = 1, \cdots, M \tag{6}$$

and that there exist coefficients $\alpha_i \; (i = 1, \cdots, M)$ such that

$$\mathbf{V} = \sum_{i=1}^{M} \alpha_i \Phi(\mathbf{x}_i) \tag{7}$$

Combining (7) and (8), we get

$$\lambda \sum_{i=1}^{M} \alpha_i (\Phi(\mathbf{x}_k) \cdot \Phi(\mathbf{x}_i)) =$$

$$\frac{1}{M} \sum_{i=1}^{M} \alpha_i (\Phi(\mathbf{x}_k) \cdot \sum_{j=1}^{M} \Phi(\mathbf{x}_j)(\Phi(\mathbf{x}_j) \cdot \Phi(\mathbf{x}_i)) \tag{8}$$

for all $k = 1, \cdots, M$

Defining an $M \times M$ matrix K by

$$K_{ij} := (\Phi(\mathbf{x}_i) \cdot \Phi(\mathbf{x}_j)) , \tag{9}$$

this leads to

$$M\lambda K\alpha = K^2 \alpha \tag{10}$$

where α denotes the column vector with entries $\alpha_1, \cdots \alpha_M$. As K is symmetric, it has a set of Eigenvectors which spans the whole space, thus

$$M\lambda\alpha = K\alpha \tag{11}$$

gives us all solutions α of Eq. (10). Note that K is positive semi definite, which can be seen by noticing that it equals

$$(\Phi(\mathbf{x}_1), \cdots, \Phi(\mathbf{x}_M))^T \cdot (\Phi(\mathbf{x}_1), \cdots, \Phi(\mathbf{x}_M)) \tag{12}$$

which implies that for all $\mathbf{X} \in \mathbf{F}$,

$$(\mathbf{X} \cdot K\mathbf{X}) = \left\| (\Phi(\mathbf{x}_1), \cdots, \Phi(\mathbf{x}_M))\mathbf{X} \right\|^2 \geq 0 \tag{13}$$

Consequently, K's Eigenvalues will be nonnegative, and will exactly give the solutions $M\lambda$ of Eq. (10). We therefore only need to diagonalizes K. Let $\lambda_1 \leq \lambda_2 \leq \cdots \leq \lambda_M$ denote the Eigenvalues, and $\alpha^1, \cdots, \alpha^M$ the corresponding complete set of Eigenvectors, with λ_p being the first nonzero Eigenvalue. We normalize $\alpha^p, \cdots, \alpha^N$ by requiring that the corresponding vectors in F be normalized, i.e.

$$(\mathbf{V}^k \cdot \mathbf{V}^k) = 1 \text{ for all } k = p, \cdots, M \tag{14}$$

By virtue of (7) and (11), this translates into a normalization condition for $\alpha^p, \cdots, \alpha^M$:

$$\begin{aligned} 1 &= \sum_{i,j=1}^{M} \alpha_i^k \alpha_j^k (\Phi(\mathbf{x}_i) \cdot \Phi(\mathbf{x}_j)) \\ &= \sum_{i,j=1}^{M} \alpha_i^k \alpha_j^k K_{ij} \\ &= (\alpha^k \cdot K\alpha^k) \\ &= \lambda_k (\alpha^k \cdot \alpha^k) \end{aligned} \tag{15}$$

For the purpose of principal component extraction, we need to compute projections on the Eigenvectors $\mathbf{V}^k$ in $\mathbf{F}$ ($k = p, \cdots, M$). Let $\mathbf{x}$ be a test point with an image $\Phi(\mathbf{x})$ in $\mathbf{F}$, then

$$(\mathbf{V}^k \cdot \Phi(\mathbf{x})) = \sum_{i=1}^{M} \alpha_i^k (\Phi(\mathbf{x}_i) \cdot \Phi(\mathbf{x})) \quad (16)$$

may be called its nonlinear principal components corresponding to Φ.

1.2 The Algorithm of Kernel PCA

To perform kernel PCA, the following steps have to be carried out: first, we compute the dot product matrix.

$$K_{ij} = (k(\mathbf{x}_i, \mathbf{x}_j))_{ij} \quad (17)$$

Next, solve (11) by diagonalizing *K*, and normalize the Eigenvector expansion coefficients α^k by requiring Eq. (15),

$$1 = \lambda_k (\alpha^k \cdot \alpha^k) \quad (18)$$

To extract the principal components (corresponding to the kernel *k*) of a test point **x**, we then compute projections onto the Eigenvectors by

$$\beta_k = (\mathbf{V}^k \cdot \Phi(\mathbf{x})) = \sum_{i=1}^{M} \alpha_i^k k(\mathbf{x}_i, \mathbf{x}) \quad (19)$$

3. RECONSTRUCTION ORIGINAL PATTERNS BY APPROXIMATE PREIMAGE

When Kernel PCA can be considered as a natural generalization of linear PCA, this can be used for data compression, reconstruction, and de-nosing applications common in linear PCA. However this is a nontrivial task, as the results provided by kernel PCA live in some high dimensional feature space and need not have pre-images in input space. Schölkopf, *et al.* (1999) presented some ideas for finding approximate pre-images.

Being just a basis transformation, standard PCA allows the reconstruction of the original patterns from a complete set of extracted principal components by expansion in the Eigenvector basis. In Kernel PCA, this is no longer possible, the reason being that it may happen that a vector **V** in **F** does not have a pre-image in $\mathbf{R}^N$. We can, however, find a vector **z** in $\mathbf{R}^N$ which maps to a vector that optimally approximates **V**.

To reconstruct the Φ-image of a vector **x** from its projections onto the first *n* principal components in **F** (assuming that the Eigenvectors are ordered by decreasing Eigenvalues size), we define a projection operator P_n by

$$P_n \Phi(\mathbf{x}) = \sum_{k=1}^{n} \beta_k \mathbf{V}^k \quad (20)$$

If *n* is large enough to take into account all directions belongs to Eigenvectors with non-zero Eigenvalue, we have $P_n \Phi(\mathbf{x}_i) = \Phi(\mathbf{x}_i)$. Otherwise Kernel PCA still satisfies that the overall squared reconstruction error $\sum_i \|P_n \Phi(\mathbf{x}_i) - \Phi(\mathbf{x}_i)\|^2$ is minimal and the retained variance is maximal among all projections onto orthogonal directions in **F**. In common applications, however, we are interested in a reconstruction in input space rather than in **F**. To achieve this we compute a vector **z** by minimizing

$$\rho(\mathbf{z}) = \|\Phi(\mathbf{z}) - P_n \Phi(\mathbf{x})\|^2 \quad (21)$$

The hope is that for the kernel used, such a **z** will be a good approximation of **x** in input space.
In (21), replacing terms independent of **z** by Ω, we obtain

$$\rho(\mathbf{z}) = \|\Phi(\mathbf{z})\|^2 - 2(\Phi(\mathbf{z}) \bullet P_n \Phi(\mathbf{x})) + \Omega \quad (21)$$

Substituting (20) and (7) into (21), we arrive at an expression which is written in terms of dot products. Consequently, we can introduce a kernel to obtain a formula for ρ which does not rely on carrying out Φ explicitly.

$$\rho(\mathbf{z}) = k(\mathbf{z}, \mathbf{z}) - 2\sum_{k=1}^{n} \beta_k \sum_{i=1}^{M} \alpha_i^k k(\mathbf{z}, \mathbf{x}_i) + \Omega \quad (22)$$

4. CASE STUDY: ELECTRO-PNEUMATIC VALVE ACTUATOR BENCHMARK PROBLEM

To verify and illustrate the usefulness of Kernel PCA for process monitoring, data generated from the control valve actuator benchmark system were used.

The actuator benchmark problem was built by Development and Application of Methods for Actuator Diagnosis in industrial Control Systems (DAMADICS) research training network for comparing the properties of fault detection and isolation methods based on the real sugar factory (DAMADICS RNT Information Website). The benchmark actuator selected is a final control element or simply named actuator, which interacts with the controlled process. The input of actuator is the output of the process controller (flow or level controller) and the actuator modifies the position of the valve allowing a direct effect on the primary variable in order to follow the flow or level set point.

Figure I shows the actuator scheme. The actuator consists in three main components: control valve, spring-and-diaphragm pneumatic servo-motor and positioner. Control valve is the mean used to prevent and/or limit the flow of fluids. Changing the state of the control valve is accomplished by a servomotor. A spring-and diaphragm pneumatic servomotor can be defined as a compressible (air) fluid powered device

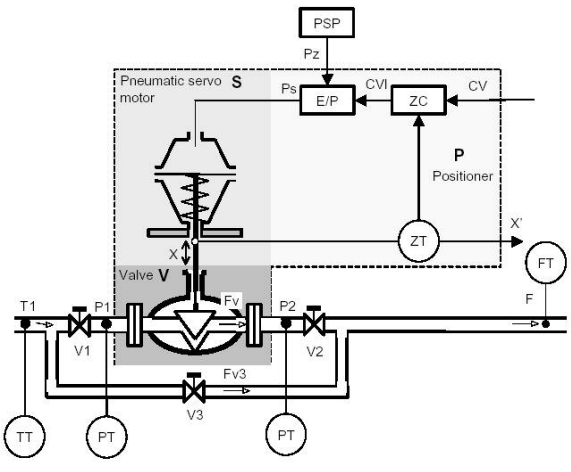

Figure. I. The actuator scheme

in which the fluid acts upon the flexible diaphragm, to provide linear motion of the servomotor system. Positioner is a device applied to eliminate the control-valve-stem miss-positions produced by the external or internal sources such as friction, pressure unbalance, hydrodynamic forces etc. It consists in a inner loop with a P controller of a cascade control structure, including the output signal of the outer loop of the flow or level controller and the inner loop of the position controller. More details are in DAMADICS RNT Information Website.

The basic measured physical values are composed of six variables: external controller output (CV), flow sensor measurement (F), valve input pressure (P1), valve output pressure (P2), liquid temperature (T1) and rod displacement (X). The Simulink library constructed by a non-linear mathematical model of the valve was used to generate faulty or fault-free data to evaluate Kernel PCA based process monitoring. All the measurement signals are normalized in the range of <0, 1> referring to the real measurement spans.

The training data for Kernel PCA model of the valve actuator system are generated without any fault for 2400 seconds. Total 2100 data except set-up zone data for initial 300s are used for building a process monitoring model.

Four kind of fault scenarios are considered for actuator monitoring in this study.

- Scenario I: Control valve faults (Valve clogging/ small abrupt fault)
- Scenario II: Control valve faults (Increased of valve or bushing friction/ incipient fault)
- Scenario III: Pneumatic servo-motor faults (Servo-motor's spring fault/ big abrupt fault)
- Scenario IV: Positioner fault (Rod displacement sensor fault/ incipient fault)

All faults are introduced at 900s of simulation time. The initial set-up zone (300s) is not also considered to avoid taking into account false detections which can occur at the beginning. Therefore, the fault situations are introduced at 600s in effect.

5. RESULTS

Two models of linear PCA and Kernel PCA are compared for verifying the potential of Kernel PCA technique. For this comparison, we define some performance indexes.

- Detection time (T_{dt}): time of detecting fault in three successions.
-True detection rate (R_{td}):

$$R_d = \frac{the\ number\ of\ \ fault\ detection}{faulty\ situation\ \ period} \times 100$$

We adopted the detection time for three successive detections in order to avoid taking into account false detection moments. One can consider false detection rate as one of performance indexes. In this study, we use 99% control limits and then false detection rate is

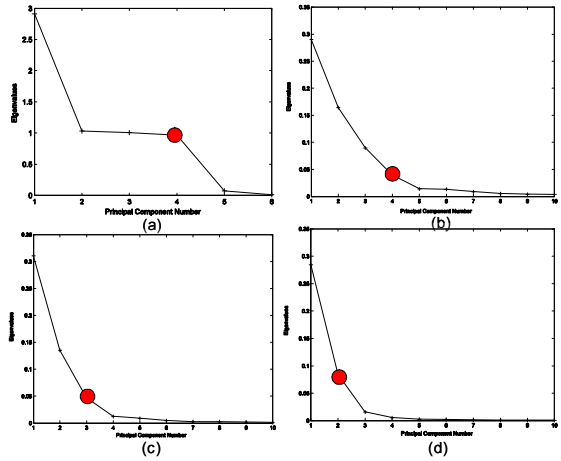

Figure. II. The eigenvalues plot

(a) Linear PCA
(b) Kernel PCA (σ^2=0.1)
(c) Kernel PCA (σ^2=0.2)
(d) Kernel PCA (σ^2=0.4)

very small (almost zero). Thus, this index is excluded for the comparison.

The number of principal components (PCs) to retain in the model should be determined for both of PCA and Kernel PCA before training. In the case of Kernel PCA, we should determine the Kernel type and corresponding parameters (e.g. bandwidthin the case of RBF Kernels). We used RBF Kernels in this work. Some research shows that RBF Kernels consistently yield good performance through an empirical assessment of Kernel type performance (Baesens, *et. al.*, 2000).

In general, the choice of the number of PCs in standard PCA is made by cross validation, a few rules of thumb and the user's knowledge of the data. 4 PCs (98.59 % variance captured) are selected from Figure. II. (a) in this work. It is generally useful to plot the eigenvalues. When looking at the plot of eigenvalues, one looks for a sudden jump in the values from the small ones. In the Kernel PCA, the problem how many principal components are used depends on the Kernel parameters determined (σ^2). Figure. II. (b)-(d) shows that the lager parameter one use, the smaller PCs one should choose. We can understand this relation intuitively from the fact that RBF Kernels with larger bandwidth can capture more complex features. By cross validation, we determined the RBF Kernels with σ^2=0.1 and 4 PCs (about 92% variance captured) to retain in the Kernel PCA model.

When using PCA, one uses primarily Q and T^2 for detecting system faults. Q statistic is a measure of the variation in the data outside the PCA model. T^2 statistic, on the other hand, is a measure of the distance from the multivariate mean to the projection of the operating point onto the hyper plane defined by the PCs, that is, a measure of the variation within the PCA model. In practice, violations of the Q and T^2 limits generally occur for different reasons. Assuming a normal value of Q, a T^2 fault indicates that the process has gone outside the usual range of operation but in a direction of variation common to

Table. 1 The comparison of performance indexes

Scenarios	Detection Time (s)		True Detection Rate (%)	
	Linear PCA	Kernel PCA	Linear PCA	Kernel PCA
I	617	611	62.73	51.60
II	2960	2959	19.60	13.79
III	-	-	3.40	0.13
IV	761	692	79.95	76.60

the process. A Q fault indicates that the process has gone in an entirely new direction-something entirely new has happened. Most process faults show up in Q. Very few faults are detected by T^2 alone (Wise, B.M., *et al*., 1999). In this work we use only Q statistics and 99% control limit for monitoring measure because T^2 statistics are under control limit about all fault scenarios.

Next Figures and Table 1 summarize the simulation results. They show that Kernel PCA outperforms linear PCA about all fault scenarios. In the case of scenario III, servo-motor's spring fault doesn't affect measured variables much and both of two models can not detect this fault well. We can not obtain the performance index of detection time in this fault scenario. However, the true detection rate of Kernel PCA model is much larger than one of linear PCA in scenario III.

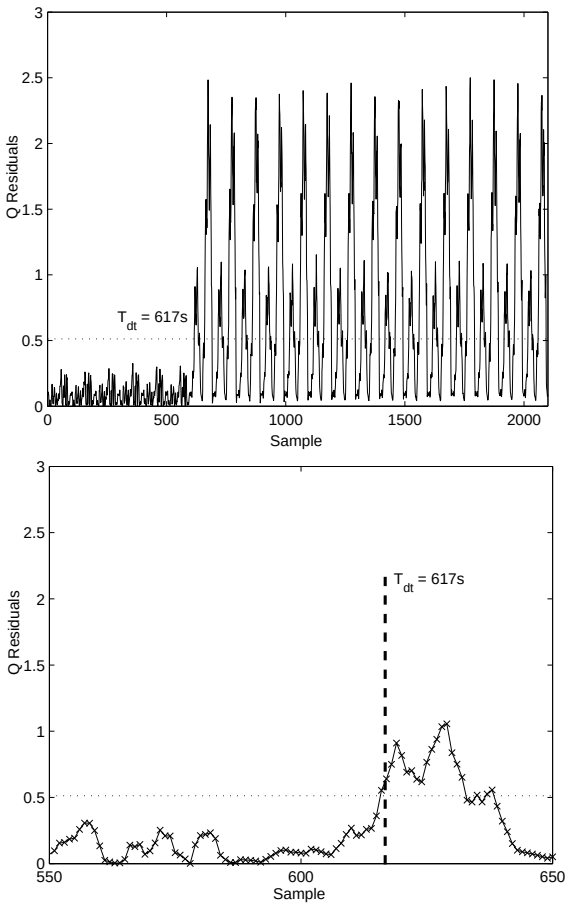

Figure. III. The PCA monitoring result of scenario I

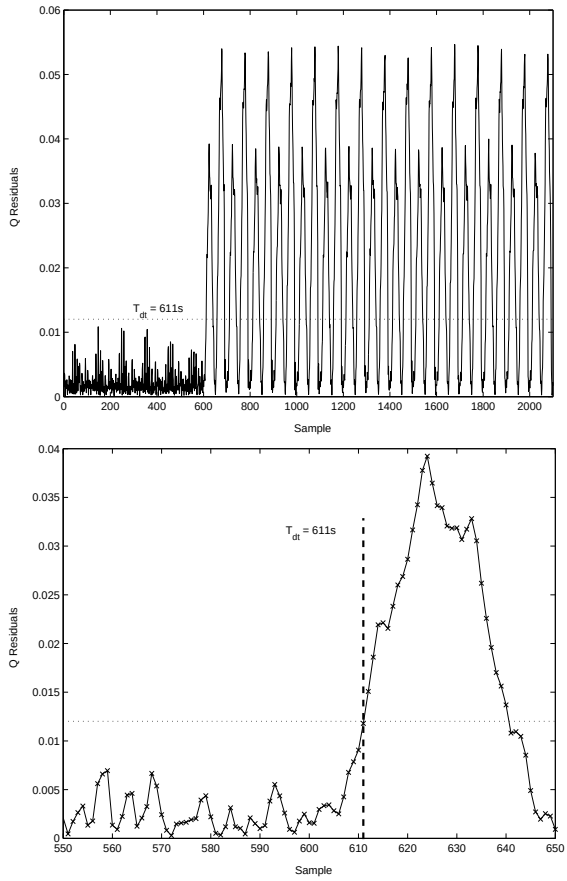

Figure. IV. The Kernel PCA monitoring result of scenario I

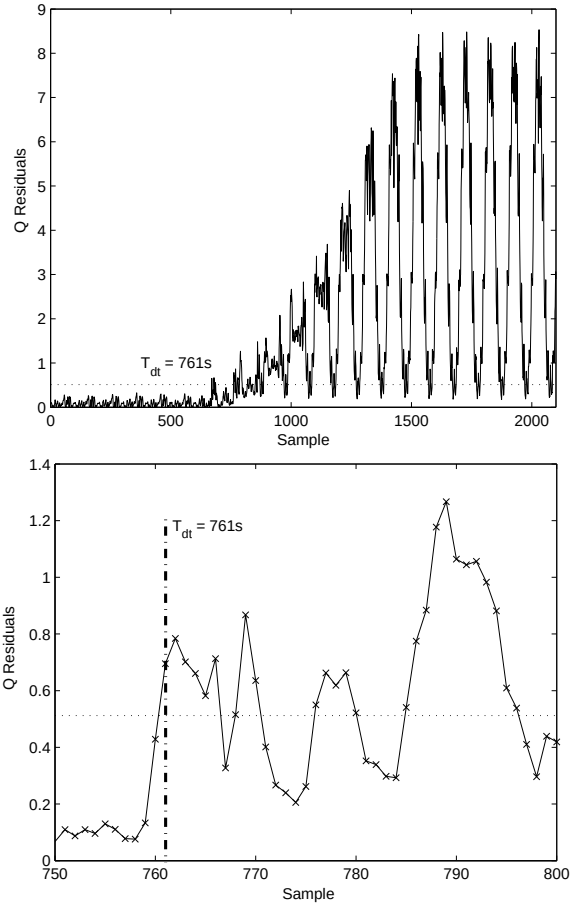

Figure. V. The PCA monitoring result of scenario IV

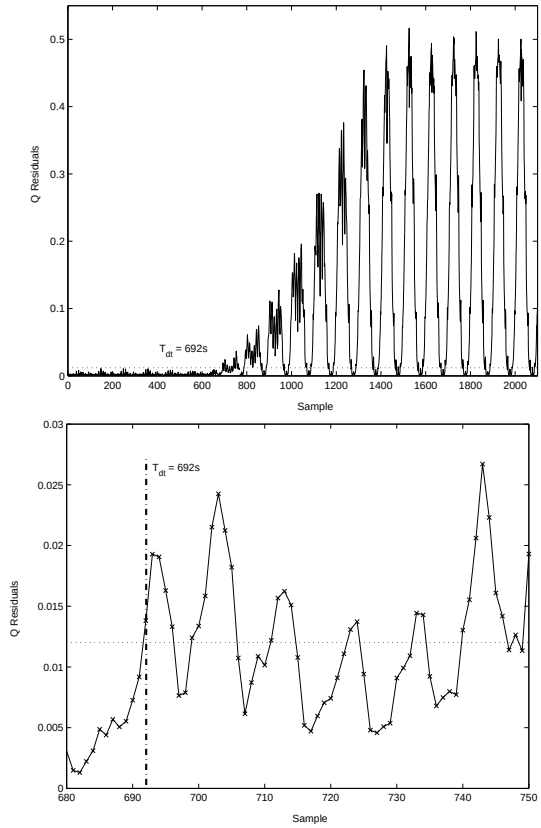

Figure. VI. The Kernel PCA monitoring result of scenario IV

4 PCs of linear PCA can captures almost 99% of variance. Thus One can assert that this actuator system can be modelled using linear PCA sufficiently and nonlinear technique such as Kernel PCA does not have great advantage against linear PCA. However Figure. VII shows the small nonlinearity in the training data. This nonlinearity makes the performance differences between Kernel PCA and linear PCA. If we apply Kernel PCA to more complex and nonlinear systems (e.g. some polymerization processes or biochemical processes), the monitoring performance will be much better.

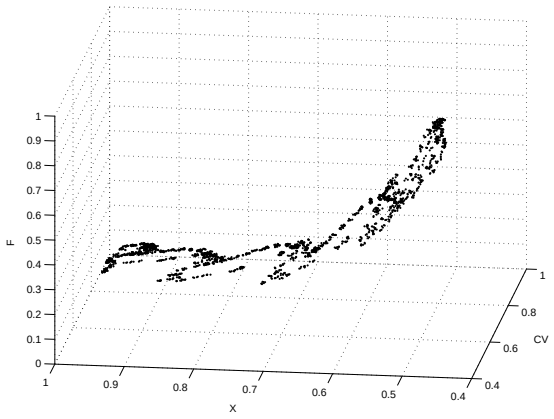

Figure. VII. The nonlinearity of normal training data

6. CONCLUSION

Kernel PCA can be considered as a nonlinear version of PCA and extract more information in nonlinear systems. However, Kernel PCA dose not provide the exact reconstructed input patterns due to implicit mapping procedure to high dimensional feature space and have some restriction on applying to process monitoring.

In this work, we reconstruct input patterns by approximating pre-images and apply to valve actuator fault monitoring. The simulation result shows that Kernel PCA based monitoring can detect several actuator faults better and earlier than conventional PCA based one. As real world industrial processes are not linear clearly, the process monitoring approach using Kernel PCA has great potential to fault diagnosis of the industrial processes.

ACKNOWLEDGEMENT

We acknowledge the financial aid for this research provided by the Brain Korea 21 Program supported by the Ministry of Education. In addition, we would like to thank the Automation & Systems Research Institute and Research Institute of Engineering Science of Seoul National University.

REFERENCES

Baesens, B., Viaene, S., Van Gestel, T., Suykens, J.A.K., Dedene, G., De Moor, B. and Vanthienen, J. (2000), An empirical assessment of Kernel type performance for least squares support vector machine classifiers, *Proceeding of 4th International Conference on Knowledge-Based Intelligent Engineering Systems & Allied Technologies*, 313-316.

Dong, D. and McAvoy, T.J. (1996), Nonlinear principal component analysis based on principal curves and neural networks, *Computers & Chemical Engineering*, **20**, 65-78.

Jolliffe, I.T. (1986), *Principal Component Analysis*, Springer Verlag, New York.

Kramer, M.A. (1991), Nonlinear principal analysis using autoassociative neural networks, *AIChe J.*, **37**, 233-243.

Schölkopf, B., Smola, A. and Müller, K. (1998), Nonlinear Component Analysis as a Kernel Eigenvalue Problem, *Neural Computation*, **10** (5), 1299-1399.

Schölkopf, B., Mica, S, Burges, C.J.C., Knirsch, P., Müller, K, Rätsch, G. and Smola, A.J. (1999), Input Space Versus Feature Space in Kernel-Basd Methods, IEEE transactions on neural networks, **10**(5), 1000-1017.

Song, S.O., Yoon, E.S. and Chang, K.S. (2001), Analysis of novelty detection properties of autoassociators, *Proceeding of '2001 China-Korea Joint Workshop on PSE*, 1-5.

Wise, B.M., Gallagher, N.B., Butler, S.W., White JR, D.D. and Barna, G.G. (1999), A comparison of principal component analysis, multiway principal component analysis, trilinear decomposition and parallel factor analysis for fault detection in a semiconductor etch process, *J. Chemometrics*, 13, 379-396.

Vapnik, V.(1995), *The Nature of Statistical Learning Theory*, Springer Verlag, New York.

REAL-TIME APPLICATION OF SCHEDULING QUASI-MINMAX MODEL PREDICTIVE CONTROL TO A BENCH-SCALE NEUTRALIZATION REACTOR

Yaohui Lu [1]

School of Chemical Engineering
Georgia Institute of Technology
Atlanta, GA 30332

Yaman Arkun [2]

Dean of College of Engineering
KOC University
Rumelifeneri Yolu, Istanbul, Turkey

Ahemet Palazoglu

Department of Chemical Engineering and Materials Science
University of California at Davis
Davis, CA 95616

Abstract: Scheduling quasi-minmax model predictive control is an MPC algorithm developed by (Lu and Arkun, 2000) initially for linear parameter varying (LPV) system, then developed for nonlinear systems in (Lu and Arkun, 2002). In this paper, real-time application of the scheduling quasi-minmax MPC algorithm onto a bench-scale pH neutralization reactor is presented. The control performance is compared with multi-linear model based MPC modified from the algorithm in (Kwon and Pearson, 1978) and scheduling IMC-PID controller in which tuning parameters are from IMC design in (Morari and Zafiriou, 1989).

Keywords: Scheduling, Quasi-min-max, Model Predictive Control (MPC), Nonlinear Systems, Ph neutralization reactor, bench-scale, Linear Matrix Inequalities (LMIs), Linear Parameter Varying (LPV)

1. SCHEDULING QUASI-MINMAX MODEL PREDICTIVE CONTROL

Scheduling quasi-minmax MPC is an MPC algorithm developed by (Lu and Arkun, 2000) initially for linear parameter varying (LPV) system, then developed for nonlinear systems in (Lu and

[1] Presently at Air Products & Chemicals Inc., Allentown, PA

[2] To whom all correspondence should be addressed, yarkun@ku.edu.tr

Arkun, 2002). In this algorithm, the system is expressed as a combination of a dynamic linear model with a linear parameter varying model. The linear dynamic model is used to express the current dynamic behavior of the nonlinear system, and the linear parameter varying (LPV) model is used to approximate the future nonlinear behavior. Linear parameter varying model has been successfully used to approximate nonlinear system (see (Johansen and Foss, 1993) and (Banerjee *et al.*, 1997)). First of all, the plant operating space is partitioned into several local descriptions by linear models that are valid at some regimes. Then a "global" model is interpolated between the regions by using a parameter vector as interpolating or model validity function. A linear parameter varying model can be written in the following form:

$$\begin{aligned} x(k+i+1|k) &= A(\rho(k+i|k))x(k+i|k) \\ &\quad +B(\rho(k+i|k))u(k+i|k), \qquad i\geq 1 \\ y(k+i|k) &= Cx(k+i|k) \end{aligned} \tag{1}$$

where

$$\begin{aligned} A(\rho(k+i|k)) &= \sum_{j=1}^{N} \rho_j(k+i|k)A_j \\ B(\rho(k+i|k)) &= \sum_{j=1}^{N} \rho_j(k+i|k)B_j \end{aligned} \tag{2}$$

$[A_j,\ B_j]$ are local models that can be obtained around different operating points. Here N is the number of the local models included in the LPV model, and $\rho_j(k+i|k)$ is the scheduling parameter reflecting the validity of the local linear models. More details of linear parameter varying model can be found in (Lu and Arkun, 2000).

In LPV model, the scheduling parameter $\rho_j(k+i|k)$ for $i\geq 1$ are generally unknown. However, the current time parameter $\rho(k|k)$ may be measured or estimated (see (Banerjee *et al.*, 1997)). Then the current nonlinear dynamics can be expressed explicitly by a current linear model.

$$\begin{aligned} x(k+1|k) &= A(\rho(k|k))x(k|k) + B(\rho(k|k))u(k|k) \\ y(k|k) &= Cx(k|k) \end{aligned} \tag{3}$$

The current linear model can also be obtained from linearization of the nonlinear model:

$$\begin{aligned} \dot{\tilde{x}} &= f(\tilde{x}, \tilde{u}) \\ \tilde{y} &= C\tilde{x} \end{aligned} \tag{4}$$

where $\tilde{x}$ is the state variable, $\tilde{u}$ is the control variable, and $\tilde{y}$ is the output variable. By using Taylor series expansion around current point k, we will have

$$\begin{aligned} \dot{\tilde{x}} \approx\ & f(\tilde{x}(k|k), \tilde{u}(k-1|k-1)) \\ & + \frac{\partial f}{\partial x}|_{\tilde{x}(k|k),\tilde{u}(k-1|k-1)}(\tilde{x} - \tilde{x}(k|k)) \\ & + \frac{\partial f}{\partial u}|_{\tilde{x}(k|k),\tilde{u}(k-1|k-1)}(\tilde{u} - \tilde{u}(k-1|k-1)) \end{aligned} \tag{5}$$

where $\tilde{x}(k|k)$ is the measured current state variable and $\tilde{u}(k-1|k-1)$ is the control action calculated from the previous point. The discrete state space model can be written as

$$\begin{aligned} x(k+1|k) &\approx A(k|k)x(k|k) + B(k|k)u(k|k) + \theta(k|k) \\ y(k|k) &= Cx(k|k) \end{aligned} \tag{6}$$

The detail derivation can be found in (Lu and Arkun, 2002).

Scheduling quasi-minmax MPC minimize an infinite horizon objective function based on the combination of linear model and linear parameter varying model. The formulation of the algorithm can be expressed as:

$$\begin{aligned} \min_{U_0^\infty} J_0^\infty = \sum_{i=0}^{\infty} & [x(k+i|k)^T Q x(k+i|k) \\ & + u(k+i|k)^T R u(k+i|k)] \\ = & x^T(k|k)Qx(k|k) + u^T(k|k)Ru(k|k) \\ & + \sum_{i=1}^{\infty} [x(k+i|k)^T Q x(k+i|k) \\ & + u^T(k+i|k)Ru(k+i|k)] \\ = & J_0^1(k) + J_1^\infty(k) \end{aligned} \tag{7}$$

where Q and R are appropriate weights, and U_0^∞ stands for all the control actions from the current time to the infinity.

$$U_0^\infty = \{u(k+i|k), i = 0, 1, 2, \cdots\} \tag{8}$$

The optimization is solved subject to the following constraints:

- Constraints on the control action that will be implemented to the plant $u(k|k)$ and the resulting output $y(k+1|k)$

$$\begin{aligned} & u^{min}(k) \leq u(k|k) \leq u^{max}(k) \\ & y^{min}(k+1) \leq y(k+1|k) \leq y^{max}(k+1) \end{aligned} \tag{9}$$

- Upper bound constraint which makes the predicted state variables varying within an invariant ellipsoid, and the objective function starting from the next step $J_1^\infty(k)$ is upper bounded by the worst case value.

$$J_1^\infty(k) \leq x^T(k+1|k)P(k)x(k+1|k) \tag{10}$$

where $P(k)$ is a positive definite matrix that will be decided from optimization.

- Lyapunov stability constraint which forces the objective function of quasi-min-max decrease monotonically:

$$\Phi(k) \leq \Phi(k-1) \tag{11}$$

where

$$\Phi(k) = J_0^1(k) + x^T(k+1)P(k)x(k+1|k)$$

Lyapunov stability is guaranteed when the algorithm is implemented in a receding horizon fashion.

The optimization can be solved by semi-definite program. Details of the LMI formulation and derivations can be found in (Lu and Arkun, 2000) and (Lu and Arkun, 2002).

2. PH NEUTRALIZATION REACTOR AND EXPERIMENTAL SETUP

The real time application of scheduling quasi-minmax is conducted at UC Davis by using a bench-scale pH neutralization experiment. An acid stream (HCL solution) and an alkaline stream ($NaOH$ and $NaHCO_3$ solution) are fed to a well-mixed tank. The pH value is measured through a sensor located in the tank. The goal of the controller is to drive the system to different pH conditions. More details about the experimental apparatus can be found in (Gálan *et al.*, 2000).

The first principle model can be written:

$$\begin{aligned}
\dot{z}_1 &= \frac{1}{\theta}(z_{1ini.} - z_1) - \frac{1}{\theta}z_1 u \\
\dot{z}_2 &= -\frac{1}{\theta}z_2 + \frac{1}{\theta}(z_{2ini.} - z_2)u \\
\dot{z}_3 &= -\frac{1}{\theta}z_3 + \frac{1}{\theta}(z_{3ini.} - z_3)u
\end{aligned} \tag{12}$$

where

$$\theta = \frac{V}{q_A} \quad u = \frac{q_B}{q_A} \tag{13}$$

z_1 is the concentration of HCL, z_2 is the concentration of $NaOH$, z_3 is the concentration of $NaHCO_3$. In the experiment, these concentrations are not measured. V is the volume of the reactor, and q_A is the flow rate of the acid, and q_B is the flow rate of the flow of base. In the experiment, the acid flow is constant with variations. The control variable is the alkaline flow while the Acid flow is considered a measured disturbance. The values of the parameters are as follows:

$$\begin{aligned}
z_{1ini.} &= 0.0012 mol HCL \ell^{-1} \\
z_{2ini.} &= 0.002 mol NaOH \ell^{-1} \\
z_{3ini.} &= 0.0025 mol NaHCO_3 \ell^{-1} \\
q_A &= 1 \ell min^{-1} \\
V &= 2.500 \ell
\end{aligned}$$

The pH value is obtained through the following nonlinear relationships:

$$\begin{aligned}
h(z,y) &= \xi + z_2 + z_3 - z_1 - \frac{K_w}{\xi} - \frac{z_3}{1 + \frac{K_x \xi}{K_w}} \\
&= 0
\end{aligned} \tag{14}$$

and

$$\xi = 10^{-y} \tag{15}$$

where y is the pH value, and

$$\begin{aligned}
K_x &= 10^{-7} mol \ell^{-1} \\
K_w &= 10^{-14} mol^2 \ell^{-2}
\end{aligned}$$

From the first principle model, it is observed that the pH value is in a strong nonlinear relationship with the input ($u = \frac{q_B}{q_A}$). The steady state curve is shown in figure 1.

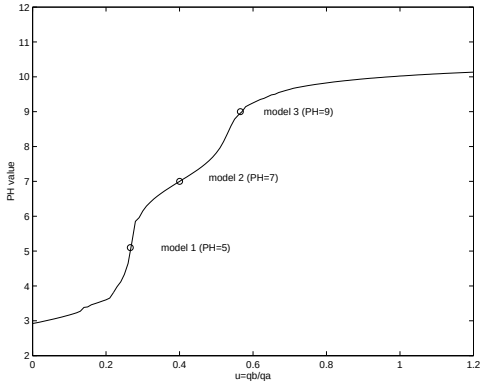

Fig. 1. Steady state curve of pH value versus the input $u = \frac{q_B}{q_A}$

The first step is to build up a state space model based on the nonlinear model. If we apply the first order Taylor expansion onto equation 12, we will have

$$A = \begin{bmatrix} -\frac{1}{\theta}(1+u_{ss}) & 0 & \\ 0 & -\frac{1}{\theta}(1+u_{ss}) & 0 \\ 0 & 0 & -\frac{1}{\theta}(1+u_{ss}) \end{bmatrix} \tag{16}$$

and

$$B = \begin{bmatrix} -\frac{1}{\theta}z_{1ss} \\ \frac{1}{\theta}(z_{2ini.} - z_{2ss}) \\ \frac{1}{\theta}(z_{3ini.} - z_{3ss}) \end{bmatrix} \tag{17}$$

Notice that A is a diagonal matrix with all the elements in diagonal are the same. From the

knowledge of $h(z,y)=0$, we can have a certain function of η that

$$y=\eta(z) \tag{18}$$

and the first-order Taylor expansion can be used again to linearize the function η

$$y-y_{ss}=\begin{bmatrix}\frac{\partial\eta}{\partial z_1} & \frac{\partial\eta}{\partial z_2} & \frac{\partial\eta}{\partial z_3}\end{bmatrix}\begin{bmatrix}z_1-z_{1ss}\\ z_2-z_{2ss}\\ z_3-z_{3ss}\end{bmatrix} \tag{19}$$

where

$$\frac{\partial\eta}{\partial z_i}=\frac{\frac{\partial h}{\partial z_i}}{\xi ln(10)\frac{\partial h}{\partial\xi}} \quad i=1,2,3 \tag{20}$$

then we have

$$\begin{aligned}\dot{y}&=\frac{\partial\eta}{\partial z_1}\dot{z}_1+\frac{\partial\eta}{\partial z_2}\dot{z}_2+\frac{\partial\eta}{\partial z_3}\dot{z}_3\\ &=\frac{\partial\eta}{\partial z_1}[(-\frac{1}{\theta}(1+u_{ss})z_1-\frac{1}{\theta}z_{1ss}u]\\ &\quad+\frac{\partial\eta}{\partial z_2}[(-\frac{1}{\theta}(1+u_{ss})z_2+\frac{1}{\theta}(z_{2i}-z_{2ss})u]\\ &\quad+\frac{\partial\eta}{\partial z_3}[(-\frac{1}{\theta}(1+u_{ss})z_3+\frac{1}{\theta}(z_{3i}-z_{3ss})u]\\ &=-\frac{1}{\theta}(1+u_{ss})[\frac{\partial\eta}{\partial z_1}z_1+\frac{\partial\eta}{\partial z_2}z_2+\frac{\partial\eta}{\partial z_3}z_3]\\ &\quad+\sum_{i=1}^{3}B_i\frac{\partial\eta}{\partial z_i}u\\ &=-\frac{1}{\theta}(1+u_{ss})y+\sum_{i=1}^{3}B_i\frac{\partial\eta}{\partial z_i}u\\ &=a_py+b_pu\end{aligned} \tag{21}$$

where

$$a_p=-\frac{1}{\theta}(1+u_{ss}) \qquad b_p=\sum_{i=1}^{3}B_i\frac{\partial\eta}{\partial z_i}$$

Equation (21) is a state space model, and the state variable is the pH value itself. In summary, the state space model can be written

$$\begin{aligned}\dot{x}&=a_px+b_pu\\ y&=x\end{aligned} \tag{22}$$

The state space model is time varying and depends on the operating conditions. a_p is the function of u_{ss}, and B_is in b_p depends on $z_{1ss}, z_{2ss}, z_{3ss}$ and z_{2i}, z_{3i}. These terms do not need to be updated on line. The term that needs to be updated is $\frac{\partial\eta}{\partial z_i}$ which is a function of concentrations z. However, these variables are not measured from the plant, more information needs to be obtained from the first principle model.

In order to have the current linear model updated in real time, the calculated control actions u is submitted to the first principle nonlinear model when it is sent to the plant. From the plant measurement, we can get the actual pH value which is y_{plant} and then calculate the value of ξ_{plant} based on equation (15). When the same control action is submitted into the first principle model (12), and calculate the state variables, z_{model}. These state variables are updated based on the value of ξ_{plant} by using equation (14) to cover any mismatches between the plant and model and any measurement noises. Since we have to calculate three variables from one equation, it is assumed that two of the state variables such as z_2, z_3 take the values from the model (z_{2model}, z_{3model}), and only update one state value such as $z_{1update}$. Then the compensated state variable would become

$$z_{update}=\{z_{1update}, z_{2model}, z_{3model}\} \tag{23}$$

This updating strategy is also used to get local linear models around different operating conditions and formulate the LPV model. The strategy is shown in the following diagram.

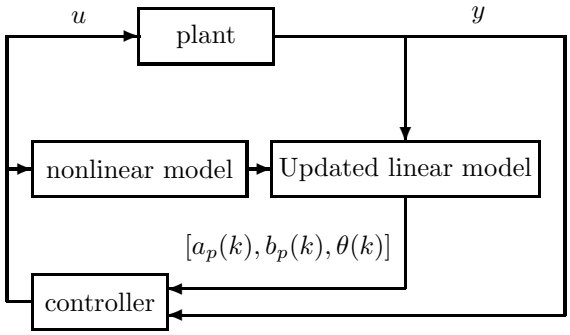

3. EXPERIMENTAL RESULT ANALYSIS

In the experiments, three pH values are selected, $Ph=5, Ph=7$, and $Ph=9$. Local models are obtained around these three points by using the strategy discussed in section 2. From the locations of these three points in figure 1, it is noticed that these three conditions have very different dynamic behaviors. The goal of the control is to track the pH value changing which is shown in figures 2 and 3. The experiments may start at any initial pH values while the setpoint is $pH=7$. Then the setpoint changes from $pH=7$ to $pH=9$, from $pH=9$ back to $pH=7$, from $pH=7$ to $pH=5$, and finally from $pH=5$ to $pH=9$. In addition to the scheduling quasi-min-max MPC, another two scheduling control algorithms are also tested.

These two controllers are scheduling IMC-PID controller and multi-linear model based (scheduling) MPC controller.

The algorithm of scheduling IMC-PID controller can be written as

$$u = u_{ss} + K_1(y - y_{ss}) + K_2 \int (y(\xi) - y_{ss}) d\xi \quad (24)$$

where

$$K_1 = \sum_{j=1}^{L} \phi_j K_{1,j} \quad K_2 = \sum_{j=1}^{L} \phi_j K_{2,j} \quad (25)$$

and $K_{1,j}, K_{2,j}$ are obtained from the formulations of IMC (Morari and Zafiriou, 1989). Around the chosen three setpoints, state space model (22) can be easily converted into the first order model

$$y(s) = \frac{k}{\tau s + 1} u(s) \quad (26)$$

where $k = -\frac{b_p}{a_p}$ and $\tau = -\frac{1}{a_p}$. Based on the tuning rules of IMC, the gain and integral parameter can be obtained

$$K_{1j} = \frac{\tau}{\lambda k} \qquad K_{2j} = \frac{1}{\lambda k} \quad (27)$$

where λ is the tuning parameter which stands for the closed-loop dynamics. At high-sensitivity regions, $PH = 5$, and $Ph = 9$, the best tuned values of λ are 100 seconds, and at low-sensitivity region, $Ph = 7$, the optimized value is found to be 10 seconds. ϕ_j is the normalized gaussian function (see (Brown *et al.*, 1997)) and can be calculated from

$$\phi_j = \frac{exp[-(\frac{x_j(k|k) - x_{measurement}(k)}{2\sigma_j})^2]}{\sum_{i=1}^{L} exp[-(\frac{x_i(k|k) - x_{measurement}(k)}{2\sigma_i})^2]} \quad j = 1, 2, \cdots, L \quad (28)$$

σ_j are the covariance of the measured signals, and they were 0.25 in the controller tuning. The multi-linear model based MPC algorithm is modified from the algorithm in (Kwon and Pearson, 1978). It was based on one single linear model, and now it is designed based on multi-linear model. The formulation is as follows:

$$\min_{u(k+i|k)|_{i=1}^{N}} J(k) = \sum_{i=1}^{N} [x(k+i|k)^T Q x(k+i|k) + u(k+i|k)^T R u(k+i|k)] \quad (29)$$

subject to

$$u^{min}(k) \leq u(k+i|k) \leq u^{max}(k) \quad i = 1, 2, \cdots, N \quad (30)$$

and the terminal constraint

$$x(k+N|k) = 0 \quad (31)$$

and

$$x(k+i+1|k) = \sum_{j=1}^{L} \phi_j(k)[A_j x(k+i|k) + B_j u(k+i|k)], \; i = 1, 2, \cdots, N \quad (32)$$

where the normalized weights are also from equation (28). In the experimental test, the control and prediction horizon was $N = 10$ which is long enough for the system dynamics. The state variable and input variable weights are the same with the weights used in scheduling quasi-minmax MPC algorithm.

Comparison of scheduling quasi-minmax MPC versus scheduling IMC-PID is shown in figure 2. The upper plot shows the setpoint tracking of the pH value, and the lower plot shows the calculated input variable which is the alkaline flow rate. From the plots, it is clear to see that scheduling quasi-minmax MPC has a much better control performance – the pH value reaches the setpoint in shorter time while the calculated control action is larger and quicker. The response of scheduling IMC-PID controller is slow, and more than that, even though integral action is included in the IMC-PID controller design, it fails to reach the targeted pH values especially at $pH = 5$ and $pH = 9$ where the pH value is highly sensitive to the input variable. Because of its intrinsic limitation, the scheduling IMC-PID controller fails at these high-sensitivity regions when the measurement is noisy.

Comparison of scheduling quasi-minmax MPC versus multi-linear model based MPC is shown in figure 3. Faster response and better tracking of the setpoint can be observed also for scheduling quasi-minmax MPC. In multi-linear model based MPC algorithm, even though multiple linear models are considered and a model is obtained by interpolating among those models, this one model is used to predict all the next N steps. The prediction based on this linear time invariant model cannot cover the future system dynamic changes even with a very long prediction horizon. However, in scheduling quasi-minmax MPC algorithm, the model contains two parts, the current linear model to express the current behavior, while the linear parameter varying model covers the possible future nonlinear behaviors. Because of the better prediction and accurate expression of the current behavior, the scheduling quasi-minmax MPC can generate a quicker and larger movement. This can be seen clearly when the pH changes from 7 to 5, the input variable of scheduling quasi-minmax

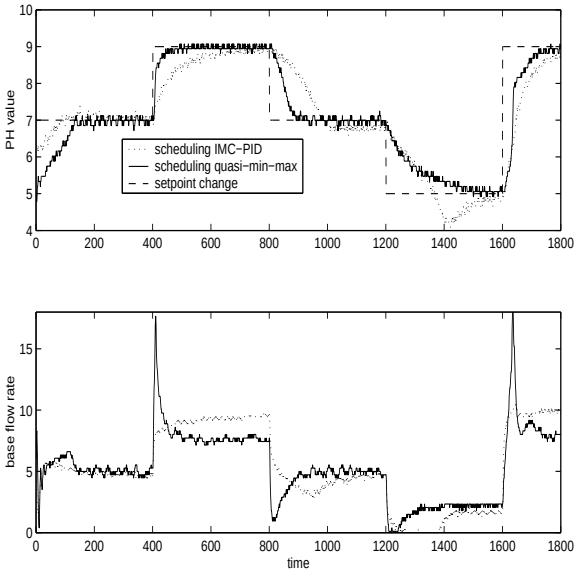

Fig. 2. Comparison between scheduling IMC-PID controller and scheduling quasi-minmax MPC controller

MPC reaches the lower limit while the action of multi-linear model based MPC never reaches the limit.

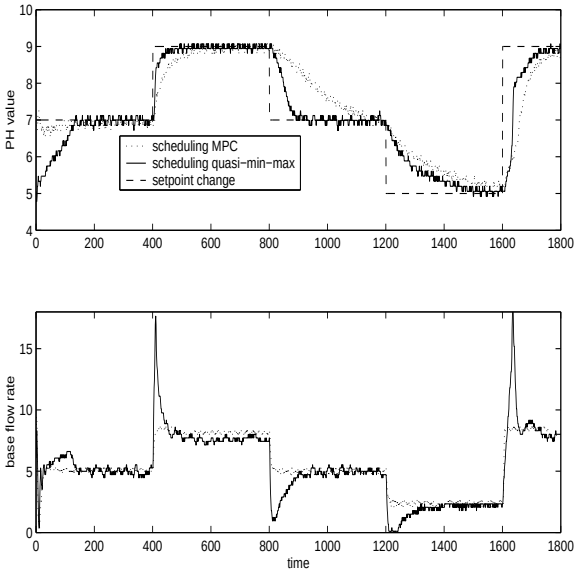

Fig. 3. Comparison between scheduling MPC controller and scheduling quasi-minmax MPC controller

4. CONCLUSION

In this paper, real-time application of scheduling quasi-minmax MPC algorithm on a bench-scale pH neutralization reactor is discussed. State space model on the pH neutralization reaction is built based on the first principle nonlinear model, and an updated strategy of the state space model is developed based on the plant measurement and model calculations. Two other control algorithms are also tested for comparison, one is scheduling IMC-PID controller in which parameters are obtained from IMC design, and the other one is multi-linear model based MPC with terminal constraint. From the experimental results analysis, scheduling quasi-minmax MPC has a better control performance due to its unique model handling approach: a current linear model which is updated on-line to capture the current dynamics while a linear parameter varying model to cover the possible future nonlinear behaviors. By having this model structure, the current step prediction can be made precisely while the future predictions belong to a range. Therefore a quasi-worst-case of infinite horizon objective function can be minimized in the algorithm.

5. REFERENCES

Banerjee, A., Y. Arkun, B. Ogunnaike and R. Pearson (1997). Estimation of nonlinear systems using linear multiple models. *AICHE Journal* **43**(5), 1204–1226.

Brown, M. D., D. Lightbody and G.W. Irwin (1997). Nonlinear internal model control using local model networks. *IEE Proceddings: Control Theory and Applications* **144**(6), 505–514.

Gálan, Omar, José A. Romagnoli and Ahmet Palazoglu (2000). Robust H_∞ control of nonlinear plants based on multi-linear models: an application to a bench-scale ph neutralization reactor. *Chemical Engineering Science* **55**, 4435–4450.

Johansen, T. A. and B. A. Foss (1993). State-space modeling using operating regime decomposition and local models. *12th IFAC World congress, Sydney, Australia* **1**, 431–434.

Kwon, W. H. and A. E. Pearson (1978). On feedback stabilizion of time–varying discrete linear systems. *IEEE Transactions on Automatic Control* **AC–23**(3), 479–481.

Lu, Yaohui and Yaman Arkun (2000). Quasi-minmax MPC algorithms for LPV systems. *Automatica* **36**(4), 527–540.

Lu, Yaohui and Yaman Arkun (2002). Scheduling quasi-minmax MPC algorithms for nonlinear systems based on combination of linear model and linear parameter varying model. *Journal of Process Control* **12**(5), 589–604.

Morari, M. and E. Zafiriou (1989). *Robust Process Control*. Prentice-Hall. Englewook Cliffs.

FAULT-TOLERANT CONTROL OF PROCESS SYSTEMS: INTEGRATING SUPERVISORY AND FEEDBACK CONTROL OVER NETWORKS

Nael H. El-Farra, Adiwinata Gani and Panagiotis D. Christofides

Department of Chemical Engineering
University of California, Los Angeles, CA 90095-1592

Abstract: This work proposes a methodology for the design of fault-tolerant control systems for nonlinear processes with actuator constraints. The proposed approach is predicated upon the idea of integrating supervisory and feedback control over networks. Initially, a family of candidate control configurations, characterized by different manipulated inputs, are identified. For each control configuration, a bounded nonlinear feedback controller, that enforces asymptotic closed-loop stability in the presence of constraints, is designed, and the constrained stability region associated with it is explicitly characterized. A switching policy is then derived, on the basis of the stability regions, to orchestrate the activation/deactivation of the constituent control configurations in a way that guarantees closed-loop stability in the event of control system failures. The switching laws are implemented by a higher-level supervisor that constantly monitors the process and communicates with the various control configurations over a network. The effects of delays in fault-detection, network communication and actuator activation are taken explicitly into account in executing the switching logic. The efficacy and implementation of the proposed approach are demonstrated through a chemical process example.

Keywords: Hybrid control, Switching laws, Constraints, Communication delays, Process systems.

1. INTRODUCTION

One of the central problems in the design of any practical process control system is the issue of fault-tolerance. Present-day process control systems are highly automated and therefore vulnerable to faults such as defects in control actuators, defects in measurement sensors, failures in the controllers or in the control loops. Such failures can cause a host of undesired reactions and consequences, if not appropriately accounted for in the control system design. Examples include degradation of the control system performance, instability, damage to technical parts of the plant, jeopardizing personnel and environmental safety, increasing downtime for process operation, increasing raw material waste, and resulting in significant production losses. As efficient and profitable process operation becomes more dependent on automated control systems, there is a greater need to design and implement advanced fault-tolerant control systems that can minimize the crippling effects of control system failures on process operation.

These considerations have consequently motivated many research studies on the problem of fault-tolerant control, particularly for linear and/or unconstrained processes (e.g., see (Willsky, 1998; Yang *et al.*, 1998; Bao *et al.*, 2002)). Many chemical processes, however, are inherently nonlinear and subject to hard constraints on the control actuators. In addition, the ability of the process control system to deal with failure situations requires, *inter alia*, inherent structural flexibility that allows the control system to safely transition from the failed control configuration to an alternative, well-functioning configuration. To this end, classical process control schemes, whereby a fixed controller

structure is used to achieve the desired control objectives, are in general not adequate for dealing with the problem because they are not properly equipped to cope with the discrete structural changes that these failures induce in the closed-loop system.

The necessary flexibility of the control system in dealing with failure situations requires consideration of hybrid control instead. Hybrid control refers to control structures that integrate lower-level continuous controllers together with higher-level logic-based supervisors that orchestrate switching between the constituent controllers. These structures have provided a natural setting for addressing a wide range of problems that cannot be addressed using classical control approaches, including fault-tolerant control of distributed systems (e.g., see (El-Farra and Christofides, 2003*b*)) and control of hybrid processes whose intrinsic dynamics exhibit switchings between multiple modes of operation (e.g., see (Bemporad and Morari, 1999; El-Farra and Christofides, 2002; El-Farra and Christofides, 2003*a*)).

In this work, we propose a methodology for the design of fault-tolerant process control systems for nonlinear processes with actuator constraints. The basic idea is that of integrating feedback control and logic-based switching between multiple constrained control configurations, each characterized by a different manipulated input and a different region of closed-loop stability. The switching policy, which is based on the stability regions, is implemented by a higher-level supervisor, that receives and transmits information to the feedback system over a network and activates/deactivates the appropriate control configuration accordingly in a way that ensures actuator fault-tolerance. The effects of delays in fault-detection, delays in network communication between the supervisor and the control loops, and delays in actuator activation are handled explicitly in designing the switching logic. Finally, the efficacy and implementation of the proposed approach are demonstrated through a chemical process example.

2. PRELIMINARIES

2.1 *System description - problem formulation*

We consider the class of continuous-time, single-input nonlinear processes with constraints on the manipulated input, represented by the following state-space description:

$$\begin{array}{rcl} \dot{x}(t) & = & f_{k(t)}(x(t)) + g_{k(t)}(x(t))u_{k(t)} \\ |u_{k(t)}| & & u^k_{max} \\ k(t) & \in & \mathscr{K} = \{1, \quad ,N\},\ N < \infty \end{array} \tag{1}$$

where $x(t) \in \mathbb{R}^n$ denotes the vector of process state variables and $u_k(t) \in [\ \ u^k_{max}, u^k_{max}] \subset \mathbb{R}$ denotes the constrained manipulated input associated with the k-th control configuration. $k(t)$, which takes values in the finite index set $\mathscr{K}$, represents a discrete state that indexes the vector fields $f_k(\ )$, $g_k(\ )$ as well as the manipulated input $u_k(\ )$. For each value that k assumes in $\mathscr{K}$, the process is controlled via a different manipulated input which defines a given control configuration. Switching between the available N control configurations is controlled by a higher-level supervisor that monitors the process and orchestrates, accordingly, the transition between the different control configurations in the event of control system failure. This in turn determines the temporal evolution of the discrete state, $k(t)$. The supervisor ensures that only one control configuration is active at any given time, and allows only a finite number of switches over any finite interval of time.

It is assumed that the origin is the equilibrium point of the nominal process (i.e. $f_k(0) = 0$) and that the vector functions $f_k(\ )$ and $g_k(\ )$ are sufficiently smooth, for all k, on $\mathbb{R}^n$. The control objective is to stabilize the process of Eq.1 in the presence of actuator constraints and faults in the control system. The basic problem is how to coordinate switching between the different control configurations (or manipulated inputs) in a way that respects actuator constraints and guarantees closed-loop stability in the event of faults. To simplify the presentation of our results, we will focus only on the state feedback problem where measurements of all process states are available for all times.

2.2 *Motivating example*

To motivate our fault-tolerant control system design methodology (presented in section 3), we introduce in this section a benchmark chemical reactor example that will be used throughout the paper to illustrate the design and implementation of the fault-tolerant control system. To this end, consider a well-mixed, non-isothermal continuous stirred tank reactor where three parallel irreversible elementary exothermic reactions of the form $A \xrightarrow{k_1} B$, $A \xrightarrow{k_2} U$ and $A \xrightarrow{k_3} R$ take place, where A is the reactant species, B is the desired product and U, R are undesired byproducts. The feed to the reactor consists of pure A at flow rate F, molar concentration C_{A0} and temperature T_{A0}. Due to the non-isothermal nature of the reactions, a jacket is used to remove/provide heat to the reactor. Under standard modeling assumptions, a mathematical model of the process can be derived from material and energy balances and takes the following form:

$$\begin{array}{rcl} \dfrac{dT}{dt} & = & \dfrac{F}{V}(T_{A0} \quad T) + \displaystyle\sum_{i=1}^{3} R_i(C_A, T) + \frac{Q}{\rho c_p V} \\ \dfrac{dC_A}{dt} & = & \dfrac{F}{V}(C_{A0} \quad C_A) \quad \displaystyle\sum_{i=1}^{3} k_{i0} e^{\dfrac{E_i}{RT}} C_A \\ \dfrac{dC_B}{dt} & = & \quad \dfrac{F}{V} C_B + k_{10} e^{\dfrac{E_1}{RT}} C_A \end{array} \tag{2}$$

where $R_i(C_A, T) = \frac{(-\Delta H_i)}{\rho c_p} k_{i0} e^{\frac{-E_i}{RT}} C_A$, C_A and C_B denote the concentrations of the species A and B, T denotes the temperature of the reactor, Q denotes rate of heat

input/removal from the reactor, V denotes the volume of the reactor, ΔH_i, k_i, E_i, $i = 1,2,3$, denote the enthalpies, pre-exponential constants and activation energies of the three reactions, respectively, c_p and ρ denote the heat capacity and density of the reactor. The values of the process parameters and the corresponding steady-state values can be found in (El-Farra and Christofides, 2001). It was verified that under these conditions, the process of Eq.2 has three steady-states (two locally asymptotically stable and one unstable at $(T_s, C_{As}, C_{Bs}) = (388\ K, 3.59\ mol/L, 0.41\ mol/L)$).

The control objective considered here is the typical one of stabilizing the reactor at the (open-loop) unstable steady-state. Operation at this point is typically sought to avoid high temperatures, while simultaneously achieving reasonable conversion. To accomplish this objective in the presence of control system failures, we consider the following manipulated input candidates (see Fig.1):

(1) Rate of heat input, $u_1 = Q$, subject to the constraints $|Q| \quad u^1_{max} = 748\ KJ/s$.
(2) Inlet stream temperature, $u_2 = T_{A0} \quad T_{A0s}$, subject to the constraints $|u_2| \quad u^2_{max} = 100$ K.
(3) Inlet reactant concentration, $u_3 = C_{A0} \quad C_{A0s}$, subject to the constraints $|u_3| \quad u^3_{max} = 4$ mol/L.

Each of the above manipulated inputs represents a unique control configuration (or control-loop) that, by itself, can stabilize the reactor. The first loop involving the heat input, Q, will be considered as the primary configuration. In the event of some failure in this configuration, however, the plant supervisor, will have to activate one of the other two backup configurations in order to maintain closed-loop stability. The main question, which we address in the next section, is how can the supervisor determine which control loop to activate once failure is detected in the active configuration.

3. INTEGRATING SUPERVISORY AND FEEDBACK CONTROL OVER NETWORKS

3.1 *Fault-tolerant design methodology*

Having identified the candidate control configurations that can be used, we outline in this section the main steps involved in the fault-tolerant control system design procedure. These include: 1) the synthesis of a stabilizing feedback controller for each control configuration, 2) the explicit characterization of the constrained stability region associated with each configuration, and 3) the design of a switching law that orchestrates the re-configuration of control system in a way that guarantees closed-loop stability in the event of failures in the active control configuration. Below is a brief description of each step as applied to the chemical reactor example introduced in section 2.2.

(a) *Constrained feedback controller synthesis:*

In this step, we synthesize, for each control configuration, a feedback controller that enforces asymptotic closed-loop stability in the presence of actuator constraints. This task is carried out on the basis of the process input/output dynamics. While our control objective is to achieve full state stabilization (and not output tracking), process outputs are introduced only to facilitate transforming the system of Eq.2 into a form more suitable for explicit controller synthesis. In the case of Eq.2, a further simplification can be obtained by noting that C_B does not affect the evolution of either T or C_A, and therefore the controller design can be addressed on the basis of the T and C_A equations only. A controller that stabilizes the (T, C_A) system will automatically stabilize the full system.

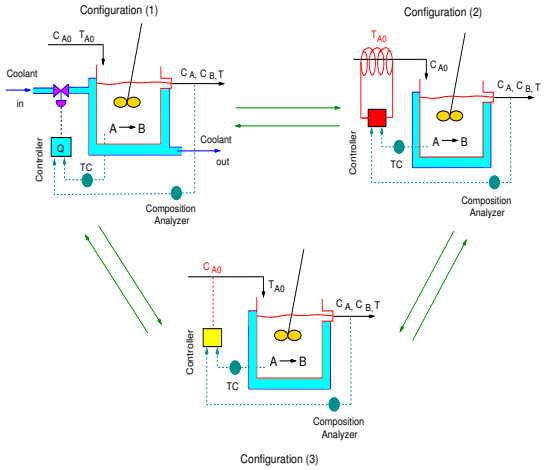

Fig. 1. Switching between multiple control configurations, each characterized by a different manipulated input

1. For the first configuration with $u_1 = Q$, we consider the output $y_1 = C_A \quad C_{As}$. This choice yields a relative degree of $r_1 = 2$ for the output with respect to the manipulated input. The coordinate transformation (in error variables form) takes the form: $e_1 = C_A \quad C_{As}$, $e_2 = \frac{F}{V}(C_{A0} \quad C_A) \quad \sum_{i=1}^{3} k_{i0} e^{\frac{-E_i}{RT}} C_A$.

2. For the second configuration with $u_2 = T_{A0} \quad T_{A0s}$, we choose the output $y_2 = C_A \quad C_{As}$ which yields the same relative degree as in the first configuration, $r_2 = 2$, and the same coordinate transformation.

3. For the third configuration with $u_3 = C_{A0} \quad C_{A0s}$, we choose the output $y_3 = T \quad T_s$ which yields a relative degree of $r_3 = 2$ and a coordinate transformation of the form: $e_1 = T \quad T_s$, $e_2 = \frac{F}{V}(T_{A0} \quad T) + \frac{Q}{\rho c_p V} + \sum_{i=1}^{3} R_i(C_A, T)$.

Note that since our objective is full state stabilization, the choice of the output in each case is really arbitrary. However, to facilitate our controller design and subsequent stability analysis, we have chosen in each case an output that produces a system of relative degree 2. For each configuration, the corresponding state transformation yields a system, describing the input/output dynamics, of the following form

$$\begin{aligned} \dot{e} &= Ae + l_k(e) + b\alpha_k u_k \\ &:= \bar{f}_k(e) + \bar{g}_k(e) u_k \end{aligned} \tag{3}$$

where $A = \begin{matrix} 0 & 1 \\ 0 & 0 \end{matrix}$, $b = \begin{matrix} 0 \\ 1 \end{matrix}$, $l_k(\ ) = L^2_{f_k} h_k(x)$, $\alpha_k(\ ) = L_{g_k} L_{f_k} h_k(x)$, $h_k(x) = y_k$ is the output associated with the k-th configuration, $x = [x_1\ x_2]^T$ with $x_1 = T \quad T_s$, $x_2 = C_A \quad C_{As}$, and the functions $f_k(\ )$ and $g_k(\ )$ can be obtained by re-writing the (T, C_A) model equations in Eq.2 in the form of Eq.1. The explicit forms of these functions are omitted for brevity. Using a quadratic Lyapunov function of the form $V_k = e^T P_k e$, where P_k is a positive-definite symmetric matrix that satisfies the Riccati inequality $A^T P_k + P_k A \quad P_k b b^T P_k < 0$, we synthesize, for each control-loop, a bounded nonlinear feedback control law (see (Lin and Sontag, 1991; El-Farra and Christofides, 2001)) of the form:

$$u = \quad r(x, u^k_{max}) L_{\bar{g}_k} V_k \tag{4}$$

where $r(x, u^k_{max}) =$

$$\frac{L^*_{\bar{f}_k} V_k + \sqrt{(L^*_{\bar{f}_k} V_k)^2 + \left(u^k_{max} |L_{\bar{g}_k} V_k|\right)^4}}{(|L_{\bar{g}_k} V_k|)^2 \quad 1 + \sqrt{1 + (u^k_{max} |L_{\bar{g}_k} V_k|)^2}} \tag{5}$$

and $L^*_{\bar{f}_k} V_k = L_{\bar{f}_k} V_k + \rho |e|^2$, $\rho > 0$. The scalar function $r(\ )$ in Eqs.4-5 can be considered as a nonlinear controller gain. This Lyapunov-based gain, which depends on both the size of actuator constraints, u^k_{max}, and the particular configuration used is shaped in a way that guarantees constraint satisfaction and asymptotic closed-loop stability within a well-characterized region in the state space. The characterization of this region is discussed in the next step.

(b) *Characterization of constrained stability regions*

Given that actuator constraints place fundamental limitations on the initial conditions that can be used for stabilization, it is important for the control system designer to explicitly characterize these limitations by identifying, for each control configuration, the set of admissible initial conditions starting from where the constrained closed-loop system is asymptotically stable. As discussed in step (c) below, this characterization is necessary for the design of an appropriate switching policy that ensures the fault-tolerance of the control system. The control law designed in step (a) provides such a characterization. Specifically, using a Lyapunov argument, one can show that the set

$$\Theta(u^k_{max}) = \{x \in \mathbb{R}^n : L^*_{\bar{f}_k} V_k \quad u^k_{max} |L_{\bar{g}_k} V_k|\} \tag{6}$$

describes a region in the state space where the control action satisfies the constraints and the time-derivative of the corresponding Lyapunov function is negative-definite along the trajectories of the closed-loop system. Note that the size of this set depends, as expected, on the magnitude of the constraints. In particular, the set becomes smaller as the constraints become tighter (smaller u^k_{max}). For a given control configuration, one can use the above inequality to estimate the stability region associated with this configuration. This can be done by constructing the largest invariant subset of Θ, which we denote by $\Omega(u^k_{max})$. Confining the initial conditions within the set $\Omega(u^k_{max})$ ensures that the closed-loop trajectory stays within the region defined by $\Theta(u^k_{max})$, and thereby V_k continues to decay monotonically, for all times that the k-th control configuration is active (see (El-Farra and Christofides, 2001) for further discussion on this issue).

(c) *Supervisory switching-logic*

Having designed the feedback control laws and characterized the stability region associated with each control configuration, the third step is to derive the switching policy that the supervisor needs to employ to activate/deactivate the appropriate control configurations in the event of failures. The key idea here is that, because of the limitations imposed by constraints on the stability region of each configuration, the supervisor can only activate the control configuration for which the closed-loop state is within the stability region at the time of control system failure. Without loss of generality, let the initial actuator configuration be $k(0) = 1$ and let T be the time when this configuration fails, then the switching rule given by

$$k(T) = j \ if \ x(T) \in \Omega(u^j_{max}) \tag{7}$$

for some $j \in \{2, 3, \quad , N\}$ guarantees asymptotic closed-loop stability. The implementation of the above switching law requires monitoring the closed-loop state trajectory with respect to the stability regions associated with the various actuator configurations. This idea of tieing the switching logic to the stability regions was first proposed in (El-Farra and Christofides, 2002) for the control of switched nonlinear systems.

3.2 *Implementation over communication networks*

Figure 2 is a schematic representation of the structure and implementation of the fault-tolerant control system over a communication network. In this setting, the multiple control loops or configurations (with their sets of sensors and actuators) are connected to the process unit (e.g., the reactor) through a network cable that transmits information to and from the plant supervisor which is physically located far from the process unit (e.g., a computer in a distant control room).

The use of a network introduces additional time-delays (e.g., see (Zhang *et al.*, 2001)) between the supervisor and the constituent control configurations due to the time sharing of the communication medium as well as the computing time required for the physical signal coding and communication processing. The characteristics of these time delays depend on the network protocols adopted as well as the hardware chosen. For our purposes here, we will consider an overall fixed time-delay (which we denote by τ_{max}) that includes the contribution of several delays, including: (1) the time for fault detection and transmission of the information to the supervisor, (2) the decision time

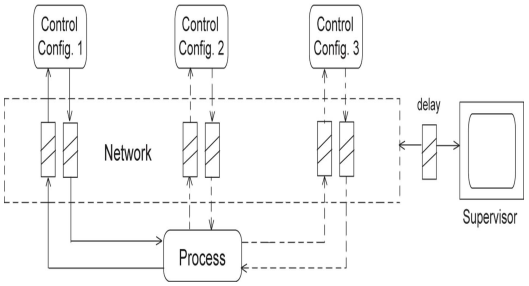

Fig. 2. Fault-tolerant control structure integrating supervisory and feedback control over network

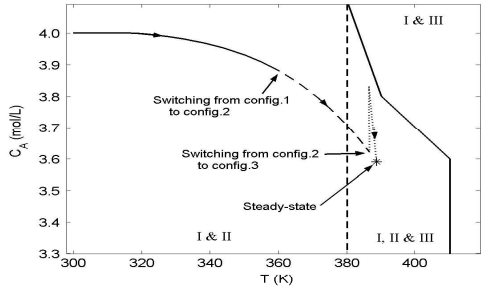

Fig. 3. Stability regions for the three control configurations (I, II, III).

for the supervisor, (3) the time it takes the supervisor's decision to reach and activate the target control configuration, and (4) the inherent time delays associated with the various actuators and sensors. Failure to take such delays into account can result in activating the wrong control configuration and subsequent instability. For example, even though failure of a given loop may take place at $t = T$, the backup configuration will not be switched in before $t = T + \tau_{max}$, where τ_{max} is the overall delay. If the delay is significant, then the switching rule of Eq.7 should be modified such that the supervisor activates the configuration for which $x(T + \tau_{max}) \in \Omega(u^j_{max})$. The implementation of this rule requires that the supervisor be able to predict where the trajectory will be at $t = T + \tau_{max}$ and choose, accordingly, the appropriate configuration. This can be accomplished by running fast simulations, on-line, using the available process model.

4. SIMULATION RESULTS

In this section, we illustrate, through computer simulations, the implementation of the proposed fault-tolerant control methodology to the chemical reactor example introduced in section 2.2. We have already described in section 3.1 how the feedback controllers can be designed and the stability regions characterized for each of the three control configurations. Figure 3 depicts the stability region, in the (T, C_A) space, for each configuration. The stability region of configuration 1 includes the entire area of the plot. The stability region of configuration 2 is the entire area to the left of the solid line, while the stability region of configuration 3 covers the area to the right of the dashed vertical line. The desired steady-state is depicted with an asterisk that lies in the intersection of the three stability regions. We consider first the case where no delays are present and the supervisor can switch immediately between the different control-loops in the event of failures. To this end, the reactor is initialized at $T(0) = 300\ K$, $C_A(0) = 4.0\ mol/L$, $C_B(0) = 0.0\, mol/L$, using the Q-control configuration, and the supervisor proceeds to monitor the evolution of the closed-loop trajectory. Due to space limitations, we present only the state profiles. As shown by the solid parts of the closed-loop trajectory in Fig.3 and the state profiles in Fig.4, the controller proceeds to drive the closed-loop trajectory towards the desired steady-state, up until the Q-configuration fails after 2.0 hr of reactor startup. From the solid part of the trajectory in Fig.3, it is clear that the failure of the primary control configuration occurs when the closed-loop trajectory is within the stability region of the second control configuration, and outside the stability region of the third control configuration. Therefore, on the basis of the switching logic of Eq.7, the supervisor immediately activates the second configuration (with T_{A0} as the manipulated input). The result is shown by the dashed parts of the closed-loop trajectory in Fig.3 and the state profiles in Fig.4 where it is seen that, upon switching to the T_{A0}-configuration, the corresponding controller continues to drive the closed-loop trajectory closer to the desired steady-state. Before reaching the steady-state, however, we consider the case when a second failure occurs (this time in the T_{A0}-configuration) at $t = 15.0$ hr (which is simulated by fixing T_{A0} for all t 15.0 hr). From the dashed part of the trajectory in Fig.3, it is clear that the failure of the second control configuration occurs when the closed-loop trajectory is within the stability region of the third configuration. Therefore, the supervisor immediately activates the third control configuration (with C_{A0} as the manipulated input) which finally stabilizes the reactor at the desired steady-state (see the dotted parts of the closed-loop trajectory in Fig.3 and the state profiles in Fig.4).

To demonstrate the effect of delays on the implementation of the switching logic, we consider an overall delay, between the supervisor and the constituent control configurations, of $\tau_{max} = 8.0$ min (accounting for delays in fault-detection, transmission and actuator activation). In this case, the reactor is initialized at $(T(0), C_A(0), C_B(0)) = (300\ K, 4.0\ mol/L, 0\ mol/L)$ under the first control configuration (with Q as the manipulated input). The actual failure of this configuration occurs at $t = 10$ hr, which, as can be seen from Fig.5, is a time when the state trajectory is within the intersection of all stability regions. In the absence of delays, this suggests that switching to either configuration 2 or 3 should preserve closed-loop stability. We observe however from Fig.6 that, when the delay is present, activation of configuration 3 leads to instability (dotted profile) while activation of configuration 2 achieves stabilization at the desired steady-state (dashed profiles). The reason is the fact that, for

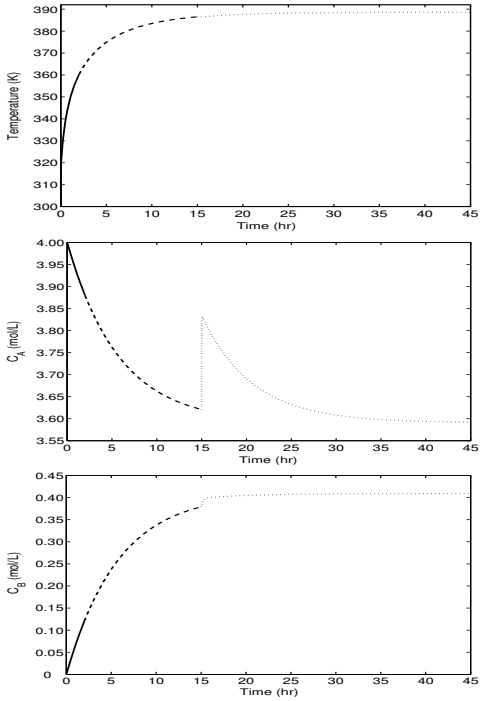

Fig. 4. Evolution of closed-loop state profiles under repeated control system failures and subsequent switching from configuration 1 (solid lines) to 2 (dashed lines) to 3 (dotted lines).

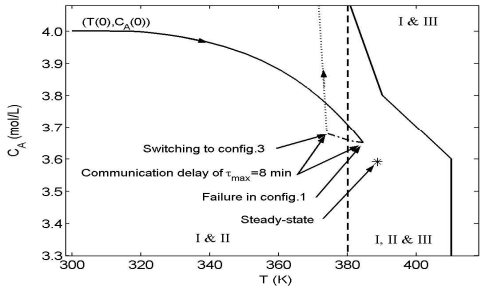

Fig. 5. A phase plot showing the closed-loop state trajectory leaving the intersection zone (I,II & III) during the delay period (dashed-dotted lines) rendering configuration 3 destabilizing (dotted trajectory).

the time period between the actual failure ($t = 10$ hr) and the activation of the backup configuration ($t = 10.13$ hr), the process evolves in an open-loop fashion leading the trajectory to move out of the intersection zone, such that at $t = 10.13$ hr, the state is within the stability region of configuration 2 and outside that of configuration 3. This is shown in Fig.5. To activate the correct configuration in this case, the supervisor needs to predict where the state trajectory will be at the end of the communication delay period.

5. REFERENCES

Bao, J., W. Z. Zhang and P. L. Lee (2002). Passivity-based decentralized failure-tolerant control. *Ind. & Eng. Chem. Res.* **41**, 5702–5715.

Bemporad, A. and M. Morari (1999). Control of systems integrating logic, dynamics and constraints. *Automatica* **35**, 407–427.

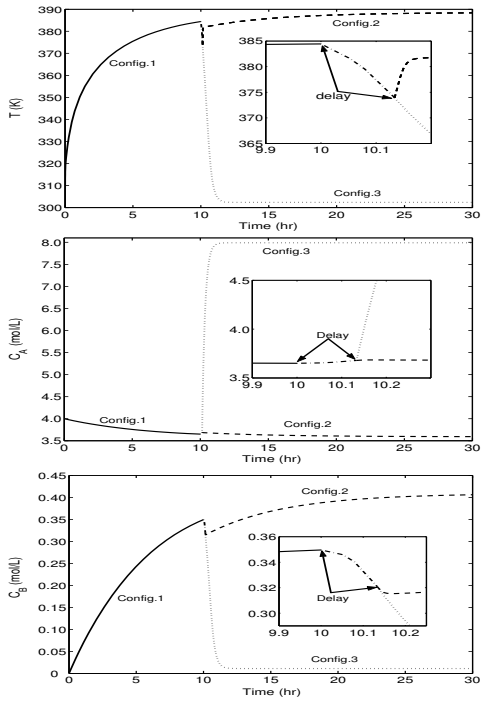

Fig. 6. Closed-loop state profiles when configuration 1 (solid lines) fails at $t = 10$ hr and an overall delay of $\tau_{max} = 8.0$ min elapses before the backup configuration is activated.

El-Farra, N. H. and P. D. Christofides (2001). Integrating robustness, optimality, and constraints in control of nonlinear processes. *Chem. Eng. Sci.* **56**, 1841–1868.

El-Farra, N. H. and P. D. Christofides (2002). Switching and feedback laws for control of constrained switched nonlinear systems. In: *Lecture Notes in Computer Science Series*. Vol. 2289. Tomlin, C. J. and M. R. Greenstreet (Eds.), Berlin, Germany: Springer-Verlag. pp. 164–178.

El-Farra, N. H. and P. D. Christofides (2003*a*). Coordinating feedback and switching for control of hybrid nonlinear processes, to appear. *AIChE J.*

El-Farra, N. H. and P. D. Christofides (2003*b*). Hybrid control of parabolic PDEs: Handling faults of constrained control actuators. In: *Lecture Notes in Computer Science Series*. Vol. 2623. Maler, O. and A. Pnueli (Eds.), Berlin, Germany: Springer-Verlag. pp. 172–187.

Lin, Y. and E. D. Sontag (1991). A universal formula for stabilization with bounded controls. *Systems & Control Letters* **16**, 393–397.

Willsky, A. S. (1998). A survey of design methods for failure detection in dynamic systems. *Automatica* **12**, 601–611.

Yang, G. H., S. Y. Zhang, J. Lam and J. Wang (1998). Reliable control using redundant controllers. *IEEE Trans. Autom. Contr.* **43**, 1588–1593.

Zhang, W., M. S. Branicky and S. M. Phillips (2001). Stability of networked control systems. *IEEE Control Systems Magazine* **21**, 84–99.